On model materials designed by atomic layer deposition for catalysis purposes

Dissertation for the degree of Philosophiae Doctor

Madeleine Diskus

Department of Chemistry
Center for Materials Science and Nanotechnology
Innovative Natural Gas Processes and Products

Faculty of Mathematics and Natural Sciences
University of Oslo

September 2011

Dedicated to my cousin

Alexandre

Preface

The thesis *"On model materials designed by atomic layer deposition for catalysis purposes"* was carried out from October 2007 to September 2011 in the Group of Inorganic Chemistry, Department of Chemistry, University of Oslo. This work forms a part of the InGAP Centre of Research-based Innovation, which receives financial support from the Norwegian Research Council under (NFR).

At first, I would like to express my sincere gratitude to my main supervisor professor Helmer Fjellvåg for giving me the opportunity to accomplish this PhD, for believing in my work and for his outstanding pedagogical skills; to my second supervisor Ola Nilsen for contributing with valuable suggestions throughout the project and his precious help when writing the papers.

I would like to thank Professor Bert M. Weckhuysen who gave me the opportunity to enlarge my perspective by working in his group for two weeks and there by perform experiments unavailable at the University of Oslo. Moreover, I am grateful to Clare Harvey and Evelien van Schrojenstein Lantman first for introducing me to the combined AFM/Raman technique, on the other hand for providing an enjoyable stay in Utrecht.

I also would like to thank Michael Brorson, Stig Helveg and Jens Sehested, first for being interested in my work and thereby making the collaboration project with the company Haldor Topsøe possible. I am thankful to everyone at Topsøe for providing a great environment and making me feeling part of the team, especially Birgitte, Aino, Kirstine, Sylvain, Marie, Annette and Christophe. I will always remember Sven Ullman saying *" You have made such nice samples. So beautiful, so easy to handle and to study as compared with the real catalysts I am use to get"*, which was the aim of my work and made me feel successful.

I am grateful to my colleagues from InGAP and the Inorganic Group at the Department of Chemistry for creating a nice working environment and being always available for skiing and partying. Special thanks go to my office mates Mahsa and Francesca and to my close friends Mari and Sandrine, who have been supporting me during the whole process and have always been available for sharing my pains and joys. Special thought to Erik and Jon who made me feel part of the Norwegian team even though I am so French.

I can not find the words to express how much I am thankful to Jean-Baptiste Mitschler who has chosen to move to Norway and made this adventure possible; who has never given up believing in me; who has always known how to take care of me and how to make me smile during the worst times; and who proposed me to share his name forever.

A special thought to my family in France who were supportive and present despite the distance. Last but not least, this thesis is dedicated to my cousin Alexandre who young made me choose studying Sciences rather than Literature or Art and who left us too early.

Oslo, September 2011

Madeleine Diskus

Table of contents

The author´s contribution

Article I: "Growth of thin films of molybdenum oxide by atomic layer deposition"

The author has planned and performed all the experiments and analysis of the samples. The author has prepared the manuscript and was strongly involved in the interpretation of the results.

Article II: "Combination of characterization techniques for ALD MoO_3 coatings: from the amorphous to the orthorhombic alpha-MoO_3 crystalline phase"

The author has planned all the experiments and analysis of the samples and has performed all the characterizations with the exception of the combined AFM/Raman and the XPS measurements. The author has prepared the manuscript and was strongly involved in the interpretation of the results.

Article III: "Thin films of cobalt oxide deposited on high aspect ratio supports by atomic layer deposition"

The author has planned and performed all the experiments and analysis of the samples. The author has prepared the manuscript and was strongly involved in the interpretation of the results.

Article IV: "Influence of the precursors chemistry on the ALD growth of cobalt-molybdenum oxide films"

The author has planned and performed all the experiments and analysis of the samples. The author has prepared the manuscript and was strongly involved in the interpretation of the results.

Unpublished results: Two collaboration projects with the company Haldor Topsøe "Cobalt molybdenum oxides coating of alumina carriers by atomic layer deposition for the hydrodesulfurization process" and "*Ex situ* and *in situ* Transmission Electron Microscopy imaging investigation of copper, zinc and aluminum oxides multilayered thin films obtained by ALD"

The author has planned all the experiments and analysis of the samples and has performed all the characterizations with the exception of the TEMand microprobe measurements, and the catalytic testing. The author has prepared the manuscripts and was strongly involved in the interpretation of the results.

1 Scope

Nowadays about 90 % of the industrial chemical products are obtained by catalytic processes. Catalysts are essential in the production of fine chemicals, fuels and in the pollution prevention. The catalyst accelerates the chemical reaction by offering an alternative pathway, energetically more favorable, for the reaction to occur. The reactants bond with the catalyst, react together and form the product, which detaches from the catalyst and leaves the catalyst unaltered and available for the next molecules bonding.

The catalysts technology has been used industrially since early 20th century. However at that time, the fundamental understanding of the catalysts and catalytic processes were not available due to lack of investigation tools. The development of catalysts was mainly based on trial experimentations. Later in the century, the new environmental legislations and wide energy demand induced an increasing interest in research in catalysis in order to enhance the catalytic activity and optimize the catalytic processes. Thanks to the modern research tools, the catalysts have been improved to a very large extend by studying and understanding the active structures, the reaction mechanisms, the origin of a catalyst deactivation and the importance of a catalyst preparation on its performances. The fundamental research in catalysis today tends to solve the mysterious complexity of the catalysts and understand the processes and kinetics involved, while research is applied industrially in order to improve the performances. In this work we have put our effort on the study of the structure and material aspect of catalysts rather than on the catalytic processes aspect.

Motivation for our work

An industrial catalyst is generally made of nanoparticles supported on an inert porous structure called carrier. The coated carriers constitute the bed of the catalyst reactor. The amount, shape and size of the catalyst particles are naturally determinant of the catalyst efficiency, but the porous structure has a strong impact on the catalytic performances of the material as well. As examples of the pores geometry influence on the catalytic processes, their diameter selects the size of the molecules entering the pores and their obstruction is often a cause of deactivation of the catalyst. It is thus of high interest to study the catalytic activity for a specific process as function of the size and shape of the supports pores as of the particles. The complexity of the industrial catalysts cumbersomes such investigations, but model materials can be designed as close to the catalyst as possible to enable alike studies.

The main objective of this work was to design model materials for catalysis by a thin film deposition technique called atomic layer deposition (ALD). A first idea was to tune the diameter of the pores of a porous substrate by coating the inside structure with the same material by ALD. Then the catalyst oxide phase would be deposited into the porous structure, reduced and finally activated in order to enable the investigation of the catalytic activity as function of the diameter of the pores. A schematic representation of the process is shown at the end of this scope (Figure 1.1).

The principal material of interest was a molybdenum based catalyst promoted with cobalt. The primary challenge was to develop a new process to deposit molybdenum oxide by ALD as this was never achieved before. Then, a simple and convenient process to design and grow thin film model materials of MoO_3 polymorphs and subsequent characterisation is proposed. This includes studies of the amorphous as-deposited films, studies of crystallization pathways, and characterization of annealed MoO_3 thin films. In a second time, the ALD cobalt covering of a systematic porous structure was investigated in order to confirm the possibility of coating porous materials with our ALD technology. The next step was to combine the two processes in order to grow the ternary oxide of interest, and to test the catalytic activity of our materials in the ammonia decomposition process at the laboratory scale.

Finally, the catalytic activity of our materials was studied at the industrial research scale in the hydrodesulfurization process as function of the thickness and composition of the ALD grown films. Eventually, a last study consisted in the design of multilayered thin films models of copper-zinc based catalysts for the methanol synthesis in order to image *in situ* the reduction of copper oxide into metallic copper particles. This last piece of work consisted in two industrial collaboration projects with the company Haldor Topsøe.
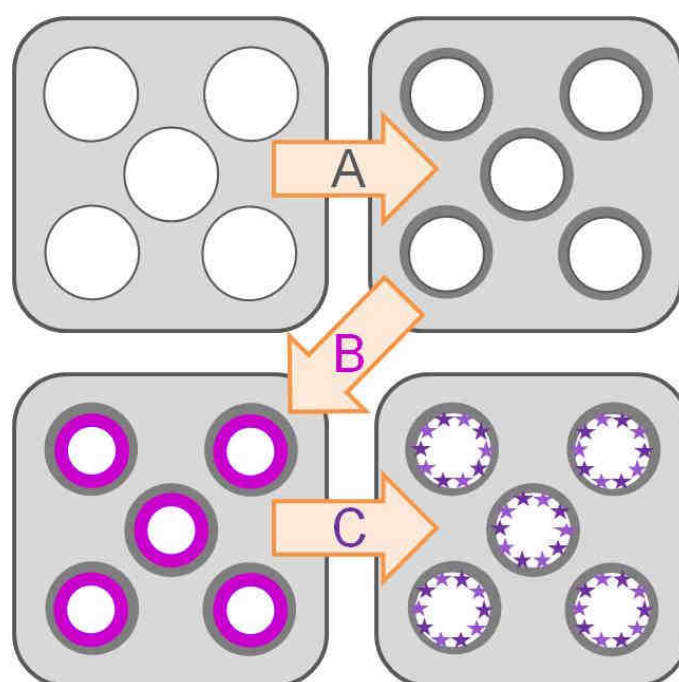

Figure 1.1 Schematic representation of the processed model materials: A) ALD deposition of an oxide layer of the same material as the substrate in order to tune the diameter of the pores, B) ALD deposition of the catalyst in its oxide phase, C) reduction and activation of the catalyst in order to investigate the catalytic activity of the material as function of the diameter of the pores.

2 Introduction to materials and catalytic processes relevant to this work

This chapter will give an introduction to the materials of interest in this work and the catalytic processes they will take part in.

2.1 Materials

In a heterogeneous catalyst assisted process, the chemical reaction takes place on the surface of the catalyst. The surface area and number of active sites per surface area of the catalyst must therefore be maximal for an optimal efficiency. This is one of the reasons why catalysts are shaped as nanoparticles on porous substrate, in order to increase the active surface area. In this case, the first step in the catalyst synthesis is to impregnate the porous structure by adsorption of a precursor, into the pores. This stage determines the loading of the metal in the porous carrier. Next, the material is calcined in order to obtain the oxide precursor of the catalyst. The catalyst is activated afterwards by annealing under different atmospheres depending on the active phase for a specific reaction. In our case, the catalyst active phases will be the sulfides or nitrides. The oxide phase is therefore determinant to a certain extend of the catalysts efficiency as it determines the final catalysts structure and shape. Moreover, today's research in catalysis focuses on the oxidic stage of the catalysts as most of the active phases are sensitive to ambient conditions and therefore difficult to study *ex situ*. In this work, we propose to obtain directly by atomic layer deposition the oxide phases of the catalysts of interest in the ammonia decomposition and the hydrodesulfurization processes: molybdenum oxide, cobalt oxide and the resulting ternary oxide.

2.1.1 Molybdenum oxide

Molybdenum oxides are the main catalysts for the hydrotreating processes [1]. In industry, the molybdenum based catalyst is synthesized by salt impregnation of a thin layer on the support, followed by a calcination at 400 °C before the final activation upon sulfidation to MoS_2. It has been shown that the calcined layer containing molybdenum holds numerous dispersed phases with well defined ionic species like $[MoO_4]^{2-}$, $[MoO_2]^{2+}$, aluminamolybdate phase

Al$_2$(MoO$_4$)$_3$, metallic molybdenum Mo(tetrahedral) and Mo(octahedral), however the main phase of interest being molybdenum oxide. The presence of all those species and phases in the unpromoted catalyst remains also when the promoters are added, leading to a very complex catalyst structure. It is consequently of high interest to be able to deposit pure molybdenum oxide phases for model materials investigations.

The Mo-O chemistry is very complex, ranging from Mo$_3$O to MoO$_3$ including numerous mixed valence compounds in the MoO$_2$ – MoO$_3$ range. Molybdenum trioxide (MoO$_3$) is of interest not only for its catalytic activity in hydrotreating processes, but also for wide applications in electrochromic devices [2] and gas sensors [3]. Moreover, molybdenum oxides are used as catalysts in the oxidation of alkenes where the catalytic mechanism proceeds *via* a redox mechanism of the catalyst. Therefore reduction of MoO$_3$ and oxidation of MoO$_2$ has attracted considerable attention [4, 5].

In this work we are particularly interested in the molybdenum trioxide polymorphs. MoO$_3$ can be found in an amorphous state and crystallizes under calcination to the metastable β-MoO$_3$ and stable α-MoO$_3$ phase [6]. The β to α phase transition appears at 400 °C in the bulk material state, as well as in the thin film form as presented later in the discussion. The structures of the orthorhombic α-MoO$_3$ and the monoclinic β-MoO$_3$ crystalline phases are represented Figure 2.1, with the molybdenum atom in the center of the octahedron.

The difference in catalytic activity between the α- and β-MoO$_3$ polymorphs is still not fully understood. For instance in the synthesis of formaldehyde, metastable β-MoO$_3$ has higher catalytic activity than the stable α-MoO$_3$ phase [7]. Furthermore, β-MoO$_3$ forms lithium molybdenum bronzes as active electrode materials in lithium batteries while α-MoO$_3$ may prevail as impurity [8, 9]. Therefore, one of the motivations to have access to well defined model materials of MoO$_3$ polymorphs in pure form is to be able to establish improved structure - property relationships.
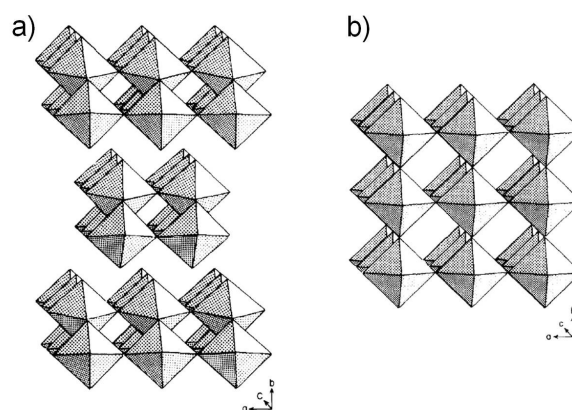

Figure 2.1 The a) α-MoO$_3$ and b) β-MoO$_3$ structures (adapted from [6]).

2.1.2 Cobalt oxide

Three different types of crystalline cobalt oxides have been reported: cobalt monoxide (CoO), cobalt(II) oxide (Co_2O_3) and cobalt (II)(III) oxide (Co_3O_4). The Co_3O_4 is of interest in this work. This oxide exhibits a spinel type structure with the Co^{2+} in tetrahedral coordination and Co^{3+} in octahedral coordination as represented Figure 2.2. In catalysis, cobalt plays an important role. Cobalt oxides are often used in catalysis to promote molybdenum oxide based catalysts as seen later in the chapter. Cobalt nanoparticles are known as the main catalyst in the Fischer-Tropsch synthesis process [10] and for their activity in the ethanol steam reforming reaction for hydrogen production [11]; they are also recognized as efficient catalysts for combustion of methane [12], combustion of volatile organic compounds [13, 14] and catalytic degradation of organic dyes [15]. They are generally obtained by impregnation of the substrate with an aqueous cobalt nitrate solution followed by a calcination. The effect of the cobalt nanoparticles size on the catalytic activity towards the different processes has been a large topic of investigation [11]. It is thus of main concern to be able to deposit cobalt oxide on porous support by ALD in order to control the deposited film thickness on the pores walls and consequently control the size of the reduced nanoparticles.
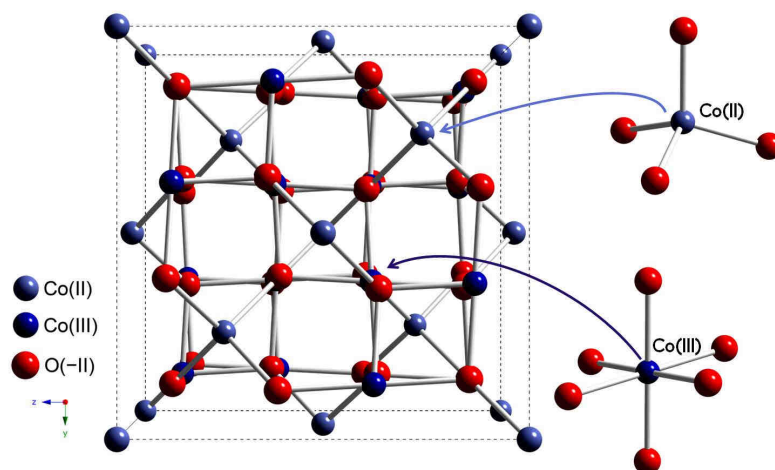

Figure 2.2 The Co_3O_4 structure.

2.1.2 The Co-Mo-O system

Two stable phases in the ternary system Co-Mo-O are identified as $Co_2Mo_3O_8$ and $CoMoO_4$ [16]. In this work we are interested in the latter ternary oxide. $CoMoO_4$ crystallizes in α- and β-$CoMoO_4$ polymorphs. The α-$CoMoO_4$ phase is the stable form at standard temperature and

pressure, while the β-CoMoO$_4$ phase corresponds to the high-temperature modification [17, 18]. Both structures are isotypic. Both cations are in octahedral coordination in the case of the α-phase, while molybdenum is in tetrahedral coordination and cobalt remains octahedrally coordinated in the β-phase [19]. The octahedra share edges to form chains parallel to each other. Each chain is joined to four chains by sharing corner oxygen atoms. Two packs of filled chains are separated by an unfilled octahedra chain as represented in Figure 2.3 [20]. Cobalt molybdate is employed industrially as catalyst in the hydrotreating processes, but it is also know to be active in the ammonia synthesis/decomposition processes after nitridation. As catalyst it is generally obtained by coprecipitation of aqueous solutions of molybdenum and cobalt, followed by a calcination step. It has been shown that the β-phase of the cobalt molybdate leads to higher activity of the final catalyst in the hydrodesulfurization process as compared with the α-phase [19]. It is proposed in this thesis to grow CoMoO$_4$ thin films by ALD for further study of the materials catalytic activity in the ammonia decomposition and the hydrodesulfurization processes.
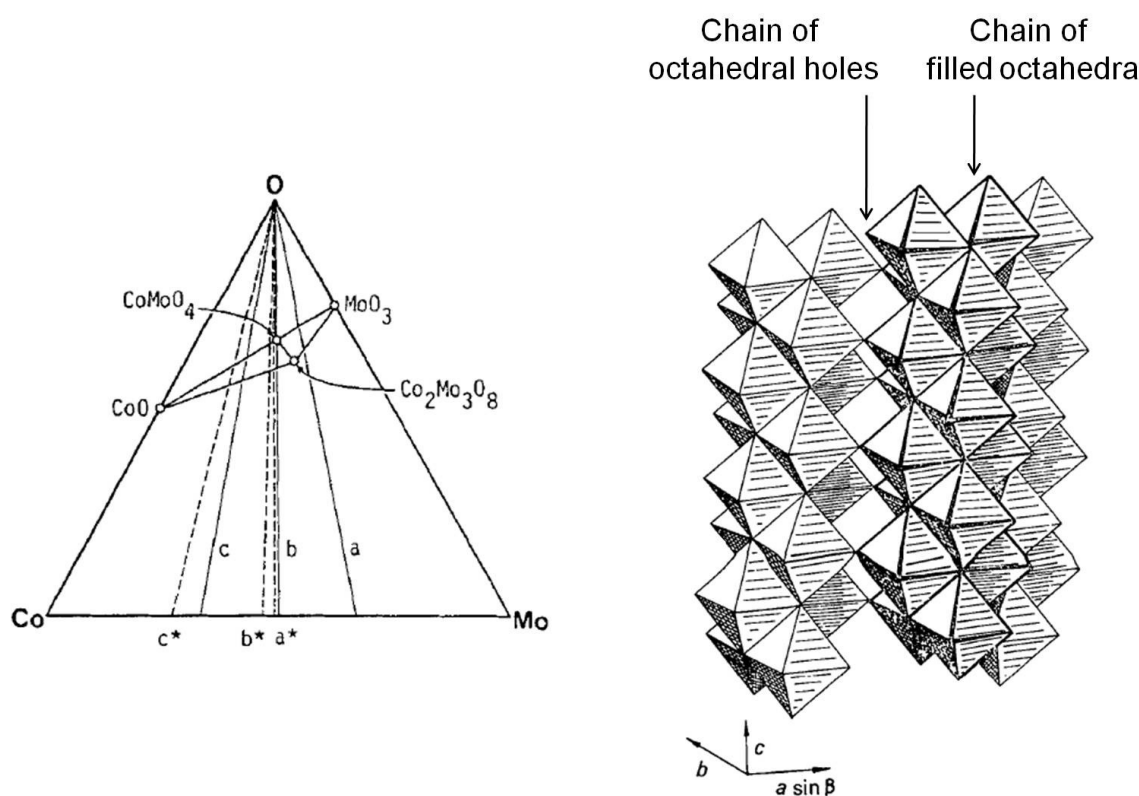

Figure 2.3 Schematic isothermal section for the Co-Mo-O phase diagram at 700 °C on the left ([16]) and representation of the cobalt molybdate CoMoO$_4$ structure on the right (adapted from [20]).

2.2 The catalytic processes of interest

2.2.1 The Ammonia Synthesis / Decomposition

A little bit of history

Haber and Bosch obtained the Nobel Prize in 1918 and 1931 respectively; Haber for finding a way to produce ammonia at the laboratory scale and Bosch for developing the technology to scale up the ammonia synthesis to the industrial scale. The ammonia synthesis process is nowadays the second largest industrial chemical process after the production of sulfuric acid. Ammonia is produced for fertilizers, nitrogen containing polymers and explosives. Originally, the catalysts were made of osmium and ruthenium for the ammonia synthesis process until an inexpensive iron-based catalyst was discovered. This catalyst is still used industrially today, but investigations of other possible catalysts showed a combined CoMo-based catalyst to be of high interest for the ammonia synthesis process [21]. The catalyst is generally prepared following the conventional route by impregnation of precursors, calcination and nitridation, leading to the bimetallic nitride active phase Co_3Mo_3N [22].

A new type of solid oxide fuel cells

A catalyst does not only improve the reaction rate forward, but it also accelerates the backward reaction. Therefore CoMo-based catalysts are active as well in the ammonia decomposition process. This reaction is of high interest today as it may be the key reaction for a new type of solid oxide fuel cell (SOFC) with ammonia as fuel. The SOFC principle elaborated by Leung et al. is presented in Figure 2.4. Ammonia is introduced in the anode and is catalytically decomposed in order to produce hydrogen. The process is however limited by the need of high temperatures for the decomposition of ammonia, catalysts are thus under investigation in order to decrease the process temperature to a functional temperature range for the SOFC technology [23-25].
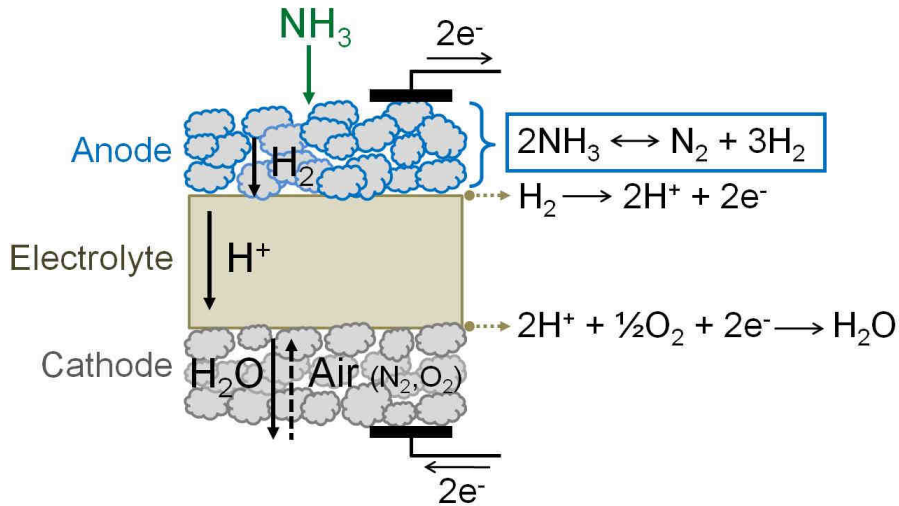
Figure 2.4 Working mechanisms of the NH$_3$-fed SOFC-H (adapted from [23]).

2.2.2 The hydrodesulfurization process

The hydrodesulfurization process is known as one of the most important industrial hydrotreating process and consists in the removal of sulfur from various fuel fractions [1]. The new environmental legislations toughening and the daily fuel needs increasing explain the crucial role of the hydrotreating catalysts today. Therefore, the high attention in improving the catalysts efficiency rises. For instance, the world wide concern on the reduction of the motor vehicle emissions induces drastic reduction in the allowable sulfur in the transport fuels. Consequently, finding effective catalysts to remove sulfur is essential to reach the latest environmental requirement. Most countries are today obliged to reduce the maximum sulfur content to less than 50 ppm and the content has been even reduced to 10 ppm in some eastern European countries and in Oceania [26]. The first use of an industrial catalyst for hydrodesulfurization was reported in 1943 and was already made of molybdenum disulfide supported on an alumina carriers and promoted with nickel or cobalt. Numerous species from the fuels are desulfurized under the catalytic process following various pathways. In order to understand the principle of catalytic desulfurization reaction, a representation of the simple process for the ethane thiol (C$_2$H$_5$SH) hydrodesulfurization is shown Figure 2.5. First, the sulfur of the C$_2$H$_5$SH molecule adsorbs on the molybdenum disulfide (MoS$_2$) sulfur vacancy. Then, the carbon sulfur (C-S) bond breaks and ethylene (C$_2$H$_4$) is released. Finally, hydrogen sulfide (H$_2$S) is formed and leaves the catalyst unaltered ready for the next sulfur containing

hydrocarbon to adsorb. One can suggest here that the number of sulfur vacancies on the metal sulfide crystallite is a key parameter in controlling the activity of the catalyst.
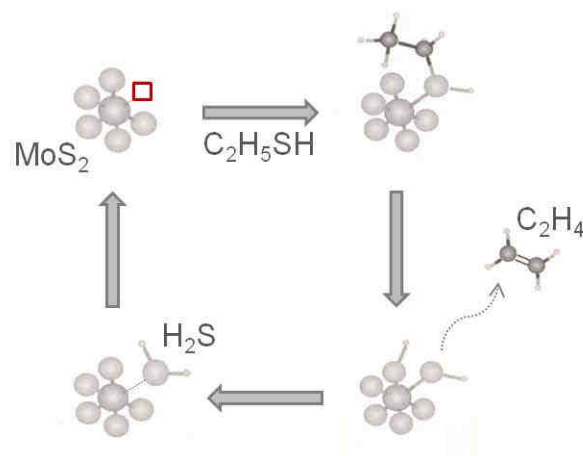

Figure 2.5 Schematic representation of the catalytic cycle for the hydrodesulfurization of ethane thiol by a sulfur vacancy on MoS_2 (adapted from [21]).

In order to enable the localization of the active sites on real catalysts, the detailed morphology of the S-Mo-S layer in MoS_2 nanostructures has been investigated by studying *in situ* sulfidation of MoS_2 model materials. It has been shown by scanning transmission electron microscopy (STEM) investigations that MoS_2 clusters display a truncated triangular morphology as represented Figure 2.6. STEM investigations of the promoted catalyst with cobalt or nickel showed a change in morphology of the MoS_2 clusters towards a more hexagonal shape. The cobalt or nickel atoms were proven to be located at the truncated edges of the MoS_2 clusters as confirmed by density functional theory (DFT) calculations (Figure 2.6) [27, 28]. It is of high interest to see how the promotion influences the morphology of the catalyst and such insight are taken into account for the study of the hydrodesulfurization reaction at the molecular level. The Co-Mo-S model considers not only the sulfur deficiency to be the reactive sites, but also the modification of the electronic and geometric structure at the MoS_2 nanoparticles edges. Therefore, the catalytic activity is dependent on the Co-S interactions at the edges of the clusters [28]. Today, the nature of the active metal generators is still under investigations in order to get closer to the real catalyst and processes conditions.

On top of the numerous molybdenum phases present in the industrial catalyst, it has been shown that many different cobalt structures exist in the calcined promoted catalyst. One counts cobalt in its oxides and metallic phases, cobalt in the alumina lattice and in cobalt

molybdate. As discussed earlier, the structures present in the calcined catalyst are determinative of the activity of the sulfided catalyst. It has been seen that the highly active Co-Mo-S structure originates from octahedral cobalt species present in the Co-Mo-O calcined phase. The other cobalt species are present in the forms of tetrahedral cobalt (in the alumina lattice and in Co_3O_4) and transform into Co_9S_8 under sulfidation. This sulfide exhibits a much lower activity than Co-Mo-S.

Despite a better fundamental understanding of this catalyst system today, it remains one of the most disputed topic in catalysis research. Furthermore, the increasing environmental demand of harmful emissions reduction implies non ending enhancement of hydrodesulfurization (HDS) catalysts efficiency.
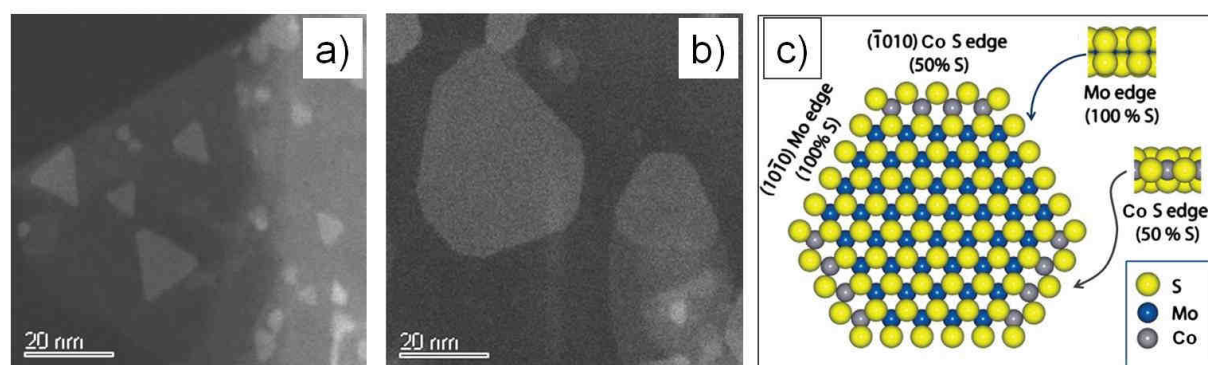

Figure 2.6 HAADF-STEM images of a) MoS_2 clusters supported on a thin graphite sheet and b) MoS_2 promoted with Co [27]; c) Ball model of a Co-Mo-S nanocluster [28].

2.2.3 The methanol synthesis

Methanol is produced industrially for use as a solvent but also as a starting reactant for producing formaldehyde and acetic acid. The methanol synthesis operates by processing a mixture of hydrogen and carbon dioxide over a $Cu/Zn/Al_2O_3$ catalyst, where the copper particles are the active catalyst while the ZnO serves as support. The carbon dioxide adsorbs on the copper nanoparticle surface and reacts with adsorbing hydrogen molecules until the methanol molecule (CH_3OH) is formed and desorbs from the copper surface. The size and shape of the copper particles has thus a large effect on the process efficiency [21]. Furthermore, the sintering of the copper particles into the support causes the overall deactivation of the catalyst. The sintering is caused by the strong influence of the environment

on the morphology and state of the particles during the process. Consequently, it is of high interest today to study *in situ* the morphology of the copper nanoparticles on the zinc oxide matrix in order to understand the effect of the gases on the Cu particles. However, Cu and ZnO nanoparticles exhibit a very similar size and mass-thickness contrast which cumbersomes the distinction between the two materials during transmission electron microscopy investigation (Figure 2.7) [29, 30]. Furthermore, the complexity of industrial $Cu/Zn/Al_2O_3$ catalysts makes their TEM imaging study challenging. In this work, we propose a new type of model materials to facilitates these studies, by designing $CuO/ZnO/Al_2O_3$ materials by ALD and perform *in situ* imaging of the reduction of copper oxide to metallic copper nanoparticles.
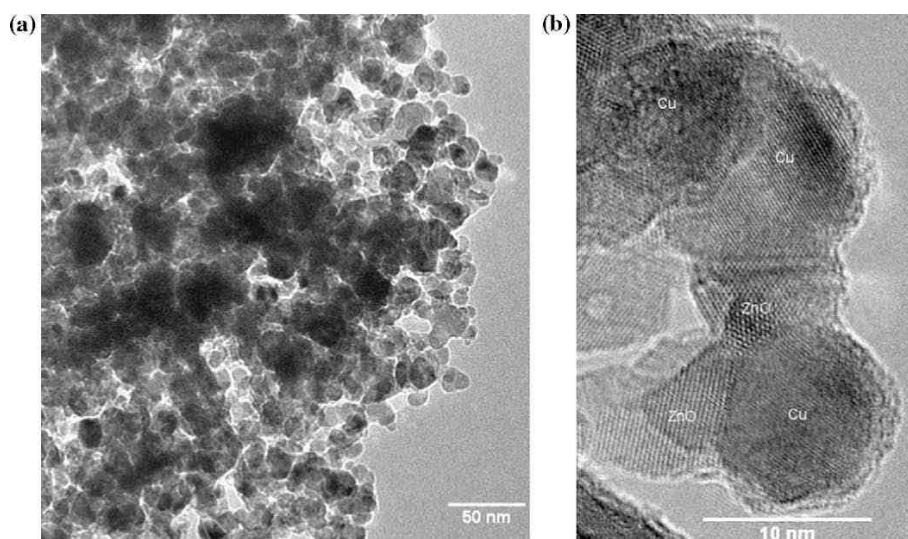

Figure 2.7 TEM images showing the difficulty to differentiate copper from zinc oxide in a reduced binary Cu/ZnO catalyst with a Cu:Zn ratio of 70:30 [31].

3 The atomic layer deposition technique

There exists numerous methods to deposit a catalyst on its porous substrate. Most of the methods are based on a liquid phase such as suspension, sol-gel deposition, electrochemical deposition and impregnation [32]. In general, a thin layer of catalyst is deposited by one of these techniques directly on the carriers. The atomic layer deposition technique is a valuable tool for growth of such thin films as it offers good control over composition and thickness of the films. At first, a description of the ALD principle and technology introduces this chapter, followed by two paragraphs on the potential use of ALD in catalysis and the ability to coat porous materials by this technique. Finally the specific ALD precursors used in this work will be described.

3.1 Description of the technique

The atomic layer deposition (ALD) technique exploits self-limiting reactions between gaseous precursors and surfaces. To illustrate the technique proceeding, consider having two precursors (A) and (B) supposed to react to form the product (P). First gaseous precursor (A) is introduced into the reaction chamber, adsorbs on the surface by creating a chemical bond with the surface. Once the surface is saturated, the excess of precursor is purged by an inert gas before the second precursor (B) is introduced and reacts with the precursor (A) to form the layer of the desired material (P). This process is repeated as many time as needed in order to achieve the intended thickness of the film. A schematic representation of the molybdenum oxide growth process is simplified and described Figure 3.1 in order to illustrate the ALD growth principle. The molybdenum hexacarbonyl molecules bond with hydroxyl groups present at the surface of the sample, then a mix of water and ozone is introduced in the chamber and reacts with the carbonyls to form the MoO_3 structure and new reactive hydroxyl groups on the surface. In this case, we are representing the carbonyl precursor to bond with only one hydroxyl group so that the model of the process is clear. Possible reaction pathways for this process will be described later in the thesis.
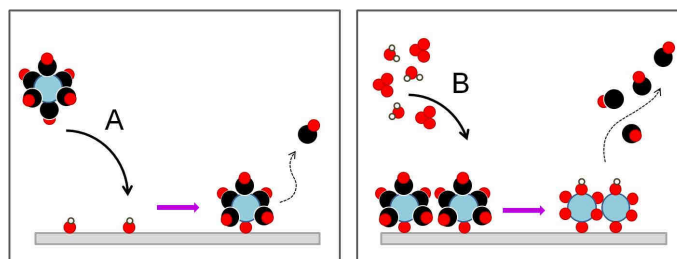
Figure 3.1 Principle of the molybdenum oxide ALD growth.

It is important for our study to differentiate the distinct types of reactors. Two principal types of ALD reactors are available commercially: the close type reactor and the flow type reactor. Hybrid reactors combining both types are designed at a laboratory scale today. In the case of a close type reactor, the reaction chamber is closed and the pressure increases when the precursor is introduced into the chamber. This type of reactor is particularly efficient for the coating of 3D structures because it forces the reactant to enter into pores and adsorb on their walls. However, the coating of flat surfaces is less homogeneous in a close type than in a flow type reactor where a constant flow is kept by applying an inert gas flow in the reactor. All our depositions have been performed in a commercial F-120 Sat flow type reactor and the ability to coat porous structures in this reactor will be discussed later in the thesis.

3.2   Why ALD in catalysis

The compounds possibly to be grown by atomic layer deposition cover almost the whole periodic table. ALD processes have been developed for metals, oxides, sulphides, nitrides, fluorides, organic and hybrid materials. Consequently, numerous materials used in catalysis have already been obtained by ALD. In addition to various types of materials deposited, the ALD technique offers uniformity and conformality of the grown films on complex surfaces; moreover it provides the control of film thickness at the atomic level [33-36].

From a technological point of view, as used for catalysts depositions on carriers, ALD would ensure a good control of the amount and composition of the catalyst in its oxide layer stage. Therefore the metal loading in the porous structure would be precise. The metal loading step is one of the most critical step in the catalyst synthesis. High loadings generally lead to waste metals as inactive structure species and low activity species, which are undesired. Furthermore, the metal loading in an industrial catalyst reactor bed differs from the bottom of

the bed reactor to the top, because the processes parameters such as pressure and temperature are uneven in the bed reactor. Differing metal loadings are thus required to compose the active catalysts for the specific parameters in the catalytic reactor bed location.

Also, as described earlier in this work (p. 9-11), the industrial catalysts compositions are very complex and only few species present in the catalyst are actually catalytically active. The atomic layer deposition technique guarantees the uniformity and conformality of the deposited materials nature and structure, which could lead to a deposition of a highly active catalyst in its pure phase, homogeneously distributed all over the support surface.

From a scientific point of view, ALD would be a useful tool to make model materials as close as possible to the real catalysts for the same reasons as mentioned above. Furthermore, the homogeneity and good distribution of the materials made by ALD facilitate their detailed characterization as compared with industrial catalysts. Finally, the control of the catalyst deposition process to the atomic scale is of high interest in the study of interactions between the elements in the nanoparticles and the support, which is the key factor for the catalytic activity.

In most of the cases, at the early stage of film nucleation by ALD, the precursor adsorbs on specific sites present on the surface of the substrate. It has frequently been stated that the adsorption sites can be hydroxyl groups, defects, ions, or specific sites generated by a pretreatment of the substrate [37, 38]. Therefore, in the subnanometric growth stage of the film, depending on the distance between the adsorption sites, the material grows as nanoparticles well distributed all over the surface (Figure 3.2). Various catalysts nanoparticles have been obtained by ALD. For instance, the formation of nanoparticles of platinum on a strontium titanate support by ALD was investigated, this catalyst being active in the oxidative dehydrogenation catalysis besides of high interest in photocatalysis and in catalytic converters [39]. Also, highly dispersed palladium nanoparticles on a mesoporous silica gel have been obtained by ALD and it has been shown that the density and size of the nanoparticles were controlled by varying the precursor exposure times or substrate pretreatment. Such catalysts are attractive for their activity in the methanol decomposition at low temperature to produce H_2 required in the hydrogen fuel cell technology [40]. Recent studies tend also to deposit thin films of zinc oxide and cobalt oxide by ALD in a porous alumina matrix, followed by spinel formation under heating treatment in order to functionalize the surface of the porous substrate [41].

The main limitation today in the use of ALD for the deposition of catalysts is about the feasibility to coat uniformly the interior surface of the catalyst support porous structure.
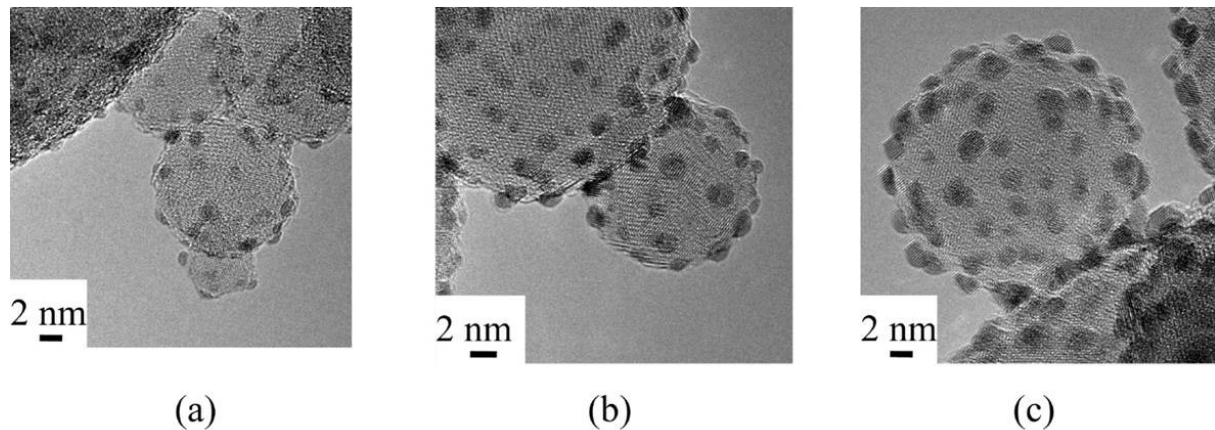

Figure 3.2 TEM images of one to three cycles of Pt ALD at 300 °C on Al_2O_3 with O_2 treatment as prepared: (a) one cycle Pt, (b) two cycles Pt, and (c) three cycles Pt [42].

3.3 ALD coating of porous materials

Many technologies require conformal deposition of ultrathin films. In microelectronics, thin films are grown in trenches and holes with large aspect ratio [43-45], additionally ultra thin films are used to fabricate nanostructures [46] and are deposited on metal nanoparticles for their passivation [47]. Atomic layer deposition is known as an excellent technique to be used for conformal coating. However, the process parameters must be optimized in order to enable full coverage of high aspect ratio supports. Therefore, experimental investigations of ALD coating of high aspect ratio features have been performed towards process optimization. In many of these studies, anodic aluminum oxide (AAO) membranes have been used as support.
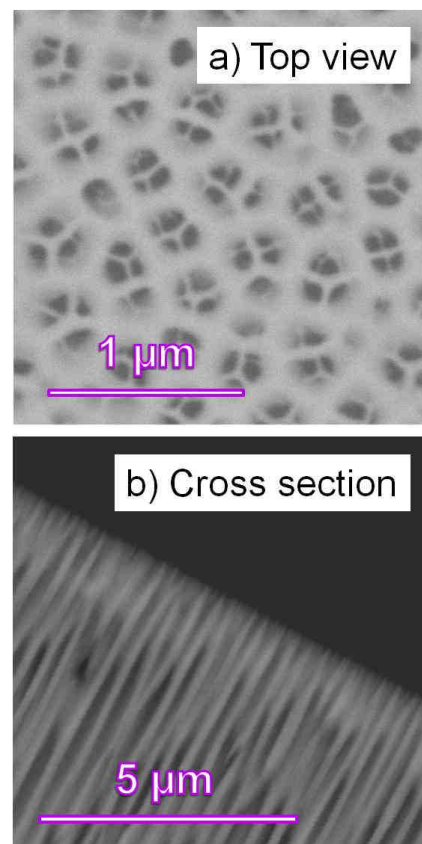

Figure 3.3 SEM image of an AAO membrane with pore diameter of 200 nm and 75 μm long.
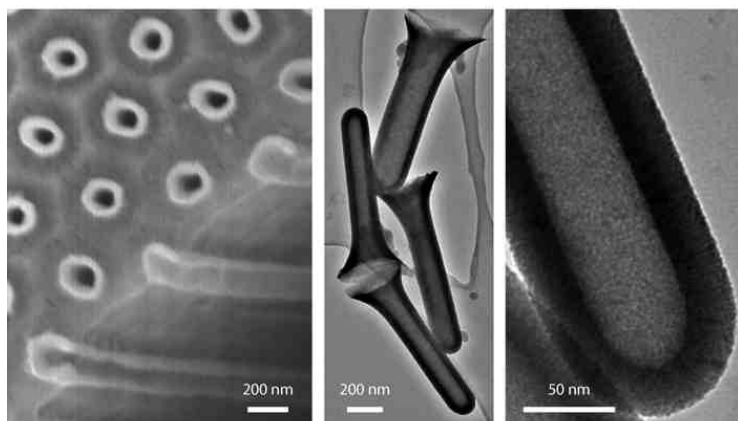
Figure 3.4 Electron micrographs of iron oxide nanotubes obtained by ALD. Left: scanning electron micrograph of an array of parallel ZrO_2 / Fe_3O_4 / ZrO_2 tubes embedded in the alumina matrix. Center and right: transmission electron micrographs of isolated short Fe_3O_4 tubes [48].

They are also known as used for the ALD synthesis of nanoarrays and nanotubes [48-51], because they offer a conformal porous structure with pores parallel to each other and a diameter available from 20 to 200 nm for a length about 70 μm (Figure 3.4) [48]. The AAO discs are commonly called anodiscs.

Offering a well defined porous structure, the membranes have often been used as model materials for high aspect ratio architecture in order to investigate the coating profile of the pores. SEM images of the anodiscs used in our work are represented Figure 3.3. The coating profile of Al_2O_3 and ZnO deposition into the anodiscs porous structure was studied by Elam et al. [52] proving the conformality to be dependent on the precursor pulse time and showing for short pulse times the pores to be uniformly coated only at their open extremities. This study, as well as Perez et al. [51] investigation of the AAO nanopores coating with HfO_2 by ALD, revealed a slope of decreasing thickness in the coverage profile. Theoretical kinetic models have been proposed in order to describe the diffusion and deposition inside the AAO membrane pores. Dendooven et al. suggested a model relating the coating thickness gradual slope to the increasing aspect ratio during the deposition and the sticking probability of the precursor [53]. The theoretical model confirmed the experimental observations of a decreasing thickness slope of the coating inside the pores. A comparison between the theoretical and experimental coverage of pores according to their model is represented Figure 3.5.

The conformality of the pores coating can be improved by combining the ALD technology with other techniques, for instance by coupling atomic layer deposition with electroosmotic flow micropumps [54]; additionally, investigations of conformal coating of high aspect ratio supports by using plasma enhanced ALD have been performed to that end [55-58].

The difficulty to coat mesopores uniformly is increased with the decrease of the diameter of the pores and raises when the mesoporous structure is made of complex channels. Recent studies showed the feasibility to coat the inside of such mesoporous structure during the first ALD cycles until the pores are not accessible anymore. From that stage, the film grows at the outer surface of the frame only [59].

As being of high importance in catalysis, the conformal coating of mesoporous materials defines in one of the biggest challenges in our work and will be discussed later.
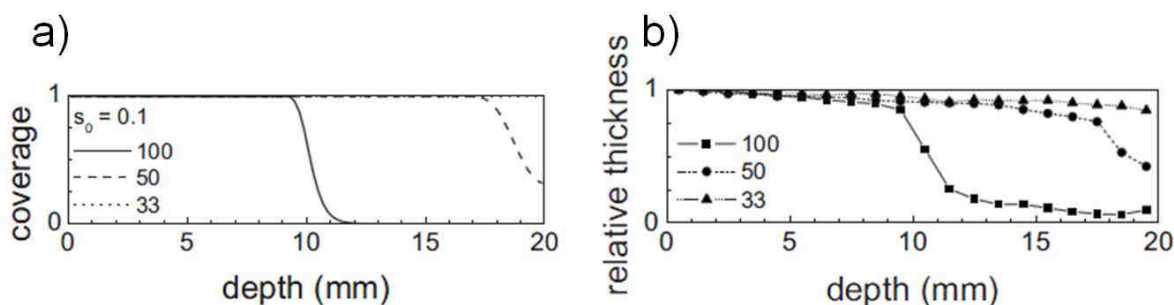

Figure 3.5 a) Simulation results of the atomic layer deposition of Al_2O_3 into holes with aspect ratios of 33, 50, and 100 using the proposed model [53] for the coverage as a function of depth inside the holes; b) Related experimental results for the relative thickness as a function of depth inside the test structure for thermally ALD grown Al_2O_3 [53].

3.4 Our precursors

The effect of the precursors chemistry on the ALD process constitutes a large field of investigation and of high relevance today. The choice of the precursors is thus of high importance for a selected ALD process. This paragraph describes our metal precursors and the reason for their selection. Concerning the oxidant, the main oxygen precursors used in ALD are oxygen, ozone and water. Despite numerous investigations, the study of their effect on the related oxide growth processes remains of high interest. In our work we have studied the contribution of ozone and water, mixed and individually, on the growth of the target oxides as summarized in the synopsis of the results.

3.4.1 Molybdenum hexacarbonyl

Previously, molybdenum nitrides and elemental molybdenum have been grown by ALD using a combination of molybdenum precursors such as molybdenum pentachloride ($MoCl_5$), bis(tert-butylimido) or bis(dimethylamido)molybdenum together with ammonia [36, 60-62]. However, the most common molybdenum precursor, $MoCl_5$ [36], was unable to provide oxides due to an etching process connected with formation of stable oxychlorides.

We will present later the first successful growth of molybdenum oxide thin films by ALD [63]. But it is interesting to set forth that this is also the first successful ALD growth using a new class of metal precursor: the carbonyl precursors. Molybdenum hexacarbonyl, $Mo(CO)_6$, was chosen as metal precursor for the growth of molybdenum oxide by ALD as it is highly volatile and thus convenient to use in gas phase. Also, $Mo(CO)_6$ diffusion ability inside a porous structure was well known as it is generally used in catalysis as molybdenum precursor in gas phase adsorption on porous supports [64]. Moreover, $Mo(CO)_6$ adsorption on numerous surfaces has been studied intensively [64-67], confirming its ability to adsorb on molybdenum and molybdenum oxides surfaces [68].
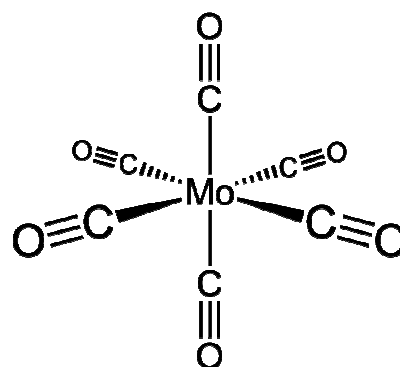

Molybdenum hexacarbonyl

3.4.2 Cobaltocene

The use of cyclopentadienyl precursors for ALD processes has been successful in many systems. Cyclopentadienyl precursors were mixed with water in order to grow oxides such as MgO, Sc_2O_3, NiO and Y_2O_3 [36]; also, $RuCp_2$ used together with oxygen has enabled the growth of metallic ruthenium [69]. However, the sensitivity of these precursors towards air makes them difficult to handle.

Various types of precursors have been investigated in the past in order to deposit cobalt oxides by ALD. For instance, cobalt oxides were obtained using the thd chemistry with $Co(thd)_2$ and $Co(thd)_3$ as metal precursors together with ozone [70, 71]. However these precursors are barely reactive towards oxygen, inhibiting the process of cobalt deposition inside a porous structure, as ozone will not be available decomposing to oxygen inside the pores.

Cobaltocene
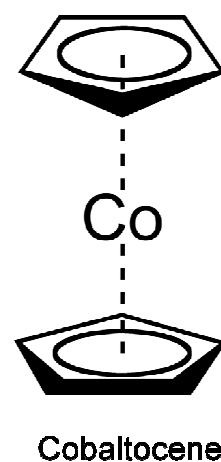
A convenient way to deposit indium oxide in alumina porous structures by ALD was proposed by using indium cyclopentadienyl together with ozone or a mix of water and oxygen [72, 73]. Moreover, M. Daub et al. were previously able to deposit nanotubes of CoO by ALD into an anodisc using $CoCp_2$ and oxygen [48]. Knowing the possibility to deposit cobalt into an alumina porous structure and that a cyclopentadienyl precursor could react with ozone, we chose to study the growth of cobalt oxide using $CoCp_2$ together with ozone and to investigate cobalt coverage of alumina membranes.

4 Experimental methods

The standard characterization techniques have been used in order to investigate our thin films obtained by ALD as deposited and after annealing. The equipment used in this work is listed in Table 4.1. These techniques are well known and already described intensively in the literature; they are therefore not set forth in this chapter. We will, however, describe some more non-conventional methods: *in situ* quartz crystal micro balance (QCM), argon sputtering and angle resolved XPS, combined AFM/Raman, *in situ* TEM imaging, and we will present the experimental set up used for the catalytic testing for the ammonia decomposition process and the hydrodesulfurization process.

Technique	Instrument used
Ellipsometry	α-SE^{TM} ellipsometer from J.A. Woollman Co., Inc.
X-ray reflectometry (XRR)	Siemens D5000 x-ray diffractometer equipped with a Göbel-mirror providing parallel Cu Kα$_1$ radiation
X-ray diffraction (XRD)	Siemens D5000 x-ray diffractometer equipped with single crystal Ge monochromator providing high purity Cu Kα$_1$ radiation
X-ray fluorescence (XRF)	Philips PW2400
X-ray photoelectron spectroscopy (XPS)	Kratos Axis Ultra Instrument using monochromatic AlKα-radiation produced by an anode operated at 15 kV and 10 mA
Atomic force microscopy (AFM)	XE-70 Park System
Scanning electron microscopy (SEM)	Environmental SEM Quanta 200F equipped with a field emission gun
Raman spectroscopy	Jobin Yvon LabRam confocal microscope, equipped with a HeNe-laser (632.8 nm, Melles Griot, 17 mW)

Table 4.1 List of standard characterization techniques and equipment used in this work.

4.1   *In situ* Quartz Crystal Micro Balance

When a new type of precursor is to be developed for atomic layer deposition, it is essential to study *in situ* the growth dynamics of the new deposition process. Quartz crystal microbalance (QCM) is an efficient mass sensor which can be used *in situ* to investigate the gas sorption during the ALD process. The growth dynamics were examined using a Matex TM400 QCN unit; a schematic representation of the QCM setup is presented Figure 4.1. The sensor is made of quartz for its strong piezoelectric response, essential in order to measure the mass variations of the adsorbing molecules during the deposition process. The changes in frequency of the crystal is linearly dependent on the mass of the deposited material according to the Sauerbrey equation [74]. Therefore it is possible to calculate the fluctuations in the deposited film mass as function of the deposition parameters variations, such as pulse time and oxidant nature. The processing of the data is the following. The obtained QCM data exhibits the changes in frequency as function of the time as shown Figure 4.1. One measures the change in frequency for one ALD cycle which is linearly proportional to the deposited mass for one cycle. By multiplying the obtained volume for one ALD cycle and the density of the deposited materials, we obtain the deposited mass on a selected area per ALD cycle. Finally, we relate this increase of mass to the change in frequency obtained by *in situ* QCM for one cycle. In our work we have been using the alumina growth in order to normalize the obtained data and calculate the increase of mass per cycle for our Co-Mo oxides.
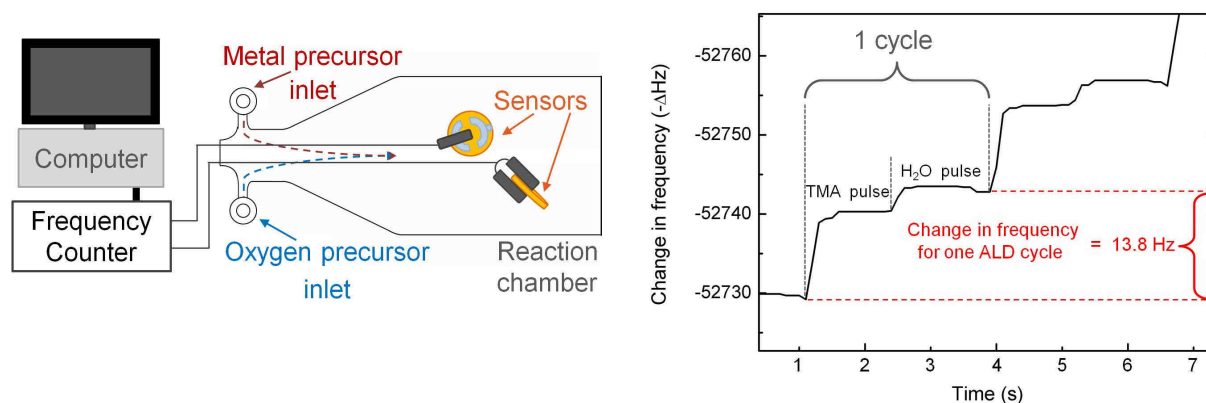

Figure 4.1 Schematic representation of the QCM setup on top and a typical example of QCM data for the alumina deposition in the bottom.

4.2 Ar⁺ sputtering and angle resolved XPS

The molybdenum oxide thin films obtained by ALD are amorphous as deposited ; moreover, they dissolve in water and basic solvents which cumberomes the preparation of the samples for TEM investigations of interfaces. Therefore it was challenging to characterize the composition and interface of such as deposited films. In order to overcome these limitations, a combination of argon sputtering and angle resolved XPS study of MoO_3 films has been performed and the principles of the techniques are described here.

4.2.1 Ar⁺ sputtering XPS

The X-ray photoelectron spectroscopy is among the most frequently used techniques in order to characterize catalysts. XPS investigations allow the determination of the elemental composition and oxidation state of a sample. Soft x-rays radiations excite the atom which absorbs a photon of energy hv and ejects an electron called photoelectron. The intensity of the photoelectron is measured as function of the kinetic energy which is converted into binding energy. The binding energy of photoelectron is fully characteristic of the element from which it originates. The electrons are travelling only a few nanometers through the solid, which makes the technique a surface characterization technique for bulk materials. In order to characterize the bulk of the sample, it is possible to combine the XPS technique with argon sputtering. This technique is called XPS depth profiling. The acquired survey spectra are recorded at different times during etching and exhibit the elemental composition of the sample at each step. It is therefore possible to characterize the bulk of the sample and its interface. However, in some cases, as seen later in this work, the argon etching can create oxygen deficiency in an oxide sample due to overall reduction of the etched oxide [75, 76]. A schematic representation of the process is described Figure 4.2.
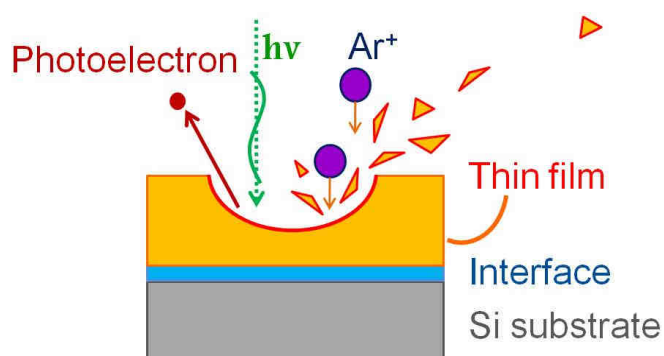

Figure 4.2 Schematic representation of the XPS argon sputtering principle.

4.2.2 Angle resolved XPS

It is possible to record photoelectron spectra as function of the angle of incidence of the soft x-rays emission by tilting the sample during an XPS acquisition. The regular 0° emission angle corresponds to the emission perpendicular to the surface of the sample. For an ultra thin film (about a couple of nanometers thick), at 0° emission angle, the electrons are excited through the whole layer above the substrate. The increase of emission angle reduces the depth from which the photoelectron arise. Thus, the analysis is more surface sensitive for grazing take-off angles than for angles close to the surface normal [77, 78]. The most important application of angle resolved XPS is the estimation of the thickness and uniformity of the thin films [79]. For instance, the absence of collected photoelectrons from the substrate at grazing angles is characteristic of a homogeneous layer. On the other hand, if all the recorded spectra at the different angles of emission exhibit the presence of photoelectrons from the substrate, the film roughness is higher and the coating is inhomogeneous. The angle resolved XPS principle is represented Figure 4.3.
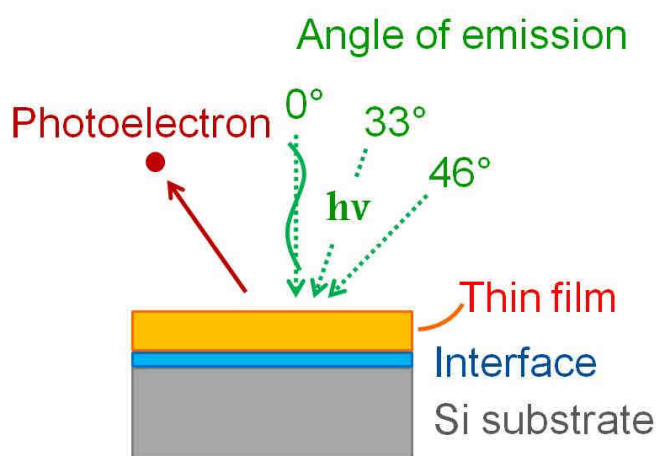

Figure 4.3 Schematic representation of the angle resolved XPS principle.

4.3 Combined AFM/Raman

The recent combination of atomic force microscopy (AFM) with Raman spectroscopy offers a new possibility to investigate the composition and structure of a sample. Combined AFM-Raman systems can provide information about the topography of a sample down to the nanoscale and relate it to chemical information obtained from the local Raman spectra [80]. As represented Figure 4.4, the excitation laser is focused on the zone under AFM investigation; the local Raman spectra is collected and directly related to the investigated topographic features. The combined AFM/Raman investigation was performed at the University of Utrecht, in the Inorganic Chemistry and Catalysis group. A combined AFM/Raman setup was used, with an NT-MDT NTEGRA Spectra upright AFM unit integrated with a Renishaw InVia Raman microscope.
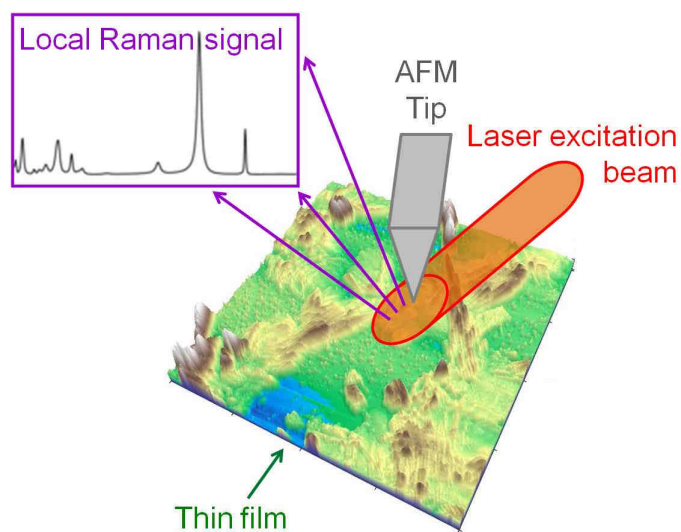

Figure 4.4 Schematic representation of the combined AFM/Raman principle.

4.4 *In situ* TEM imaging

Transmission electron microscopy (TEM) is one of the best tools with sufficiently high resolution and magnification to image nanostructured materials. In general, TEM investigations are performed under vacuum. However, environmental transmission electron microscopes (ETEM) allow investigations under higher pressures. It is therefore possible to characterize *in situ* the dynamic behavior of nanostructured materials under the influence of variable temperatures and gas pressures, as well as study chemical reactions at the atomic level. In this work, TEM imaging investigations were performed at the research center of the company Haldor Topsøe, Denmark, using a Philips CM300 ST FEG-TEM instrument and a Titan 80–300 transmission electron microscope (FEI Company) equipped with a gas mixing unit and a mass spectrometer to control and determine the gas composition at the specimen (represented Figure 4.5). The instruments were either operated at standard high vacuum conditions of approx. 10^{-6} mbar (used for standard *ex situ* TEM investigations) or at *in situ* conditions (with gas flow and variations in temperature).

Figure 4.5 Illustration of the Titan 80–300 ETEM microscope and its in situ units (adapted from [81]).

4.5   Catalytic testing

This paragraph describes the experimental set up used for the catalytic testing performed in this work.

The ammonia decomposition process

The testing of our catalysts in the ammonia decomposition process was performed at the University of Oslo. The ammonia decomposition reaction was carried out on irregular pieces of quartz (about 2 mm) coated with CoMo-oxides thin films by ALD, varying the molybdenum and cobalt content. Prior to catalytic testing, the catalyst was reduced under a hydrogen flow of 10 ml/min at 600 $^\circ$C for 2 h. The temperature was raised from room temperature to 600 $^\circ$C at a heating rate of 5 $^\circ$C/min. After reduction, the reactor was cooled down to room temperature (5 $^\circ$C/min) under an argon flow about 25 ml/min. Temperature programmed ammonia decomposition over the thin film catalyst, was performed by flowing NH_3 (25 ml/min) and Ar (25 ml/min) from room temperature to 900 $^\circ$C at a heating rate of 5 $^\circ$C/min. The effluent gas was analyzed using a micro gas chromatograph (Model: Agilent 3000 Micro GC) equipped with Molecular sieve column/PLOTU pre-column (Ar carrier gas) for detecting N_2 and H_2 and PLOTU column/PLOTQ pre-column (He carrier gas) for detecting NH_3. The columns were equipped with thermal conductivity detectors (TCD).

The hydrodesulfurization process

The activity of our catalysts in the hydrodesulfurization process was studied at Haldor Topsøe, Denmark. Catalytic tests were performed by the means of a tubular high-pressure reactor with n-heptane solutions of the reactants as feed. Catalysts were loaded as 600–850 µm granulates diluted with glass microbeads. In order to ensure that samples were fully sulfided before the catalytic test, *in situ* sulfidation was made for 4 h at 350 °C by means of a 2.5 % solution of dimethyldisulfide (DMDS) in n-heptane and with $p(H_2) = 42$ atm. Under these conditions DMDS decomposes readily to generate H_2S. This partial pressure of H_2S ensures that catalysts remain fully sulfidized during the catalytic tests. During the 24 hours catalytic test of a catalyst sample, the composition of the exit gas from the reactor was

continuously determined and quantified by GC–FID. The retention times of the various reactant and product species were known from previous GC–MS analyses using the same column (non-polar WCOT, Hewlett-Packard Ultra 2) as the GC–FID. The conversions determined were expressed as pseudo first-order rate constants for hydrodesulfurization (HDS), hydrodenitrogenation (HDN), and hydrogenation (HYD) [26]. In this work, we will treat HDS conversion results only.

5 Synopsis of the results

The aim of this Ph D work was to design thin film model materials by ALD for catalysis. The evolution of this work from the growth of the films by ALD to the catalytic testing of the model materials will be described in this chapter. The outline concerning the work on cobalt molybdenum oxides can be divided in five thematics. First, a novel process was elaborated to grow molybdenum oxide by ALD. Then model materials of the different polymorphs of MoO_3 were obtained. A third part consisted in the investigation of the coating of porous alumina membranes with cobalt and molybdenum by ALD. A next thematic was to grow cobalt molybdenum oxides thin films by ALD. Finally, the catalytic activity of the films was tested in the ammonia decomposition and the hydrodesulfurization processes. A last piece of work was to design multilayered thin films of $CuO/ZnO/Al_2O_3$ by ALD as model materials for the methanol synthesis catalyst investigation.

It is important to set forth the different aspects which have driven this work. In a first time, new ALD processes have been proposed, therefore it was of high interest to study the growth dynamics of the molybdenum oxide and the cobalt-molybdenum oxide processes. As molybdenum and cobalt-molybdenum oxides were new grown materials in the ALD history, the films had to be characterized carefully. It was of main concern to verify the feasibility to coat porous materials by ALD with our equipment. Finally, a last purpose was to confirm the value of our model materials in industrial research projects.

5.1 MoO_3 synthesis by ALD and characterization of the films

The first challenge in this work was to synthesize molybdenum containing thin films by ALD. Thin films of MoO_3 have been obtained by the atomic layer deposition (ALD) technique using molybdenum hexacarbonyl ($Mo(CO)_6$), ozone and water as precursors. A temperature window for ALD growth was found to be from 152 to 172 ℃. Self limiting growth was verified at a deposition temperature of 163 ℃. The upper temperature range was determined

by the thermal stability of the $Mo(CO)_6$ precursor and the lower range by the precursor reactivity.

The growth dynamics were investigated by QCM in order to elaborate whether or not carbonyls are suitable metal precursors to be used for the ALD technique. Furthermore, QCM investigations enabled to determine the effect of ozone and water on the deposition process (Figure 5.1). Growth using only water as oxygen source was hardly detectable. When ozone was used as oxidant, the overall growth rate was strongly increased and further improved to 0.75 Å/cycle when water and ozone were pulsed at the same time. We assume the ozone to be the main oxidant. As pulsed without water, $Mo(CO)_6$ adsorbs directly on MoO_3. When water is added, hydroxyl groups are deposited on the surface of the film; they present a better efficiency towards $Mo(CO)_6$ adsorption than oxygen sites and therefore enhance the MoO_3 growth rate. By looking at the relative increase of mass for the $Mo(CO)_6$ and following oxidant pulses, we were able to suggest a growth mechanism following the schema represented Figure 5.2. As about 70 % of the overall increase of mass for one ALD cycle is gained at the $Mo(CO)_6$ adsorption, one can suppose the carbonyls to adsorb on several rather than one site at the time. This investigation has clearly proven the capability of carbonyls as useful precursors for ALD growth of oxides.
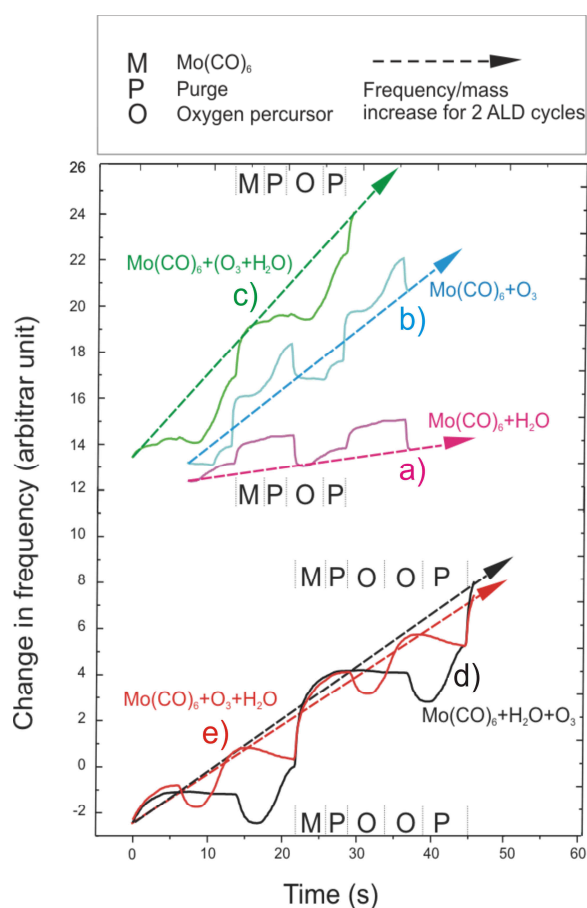

Figure 5.1 Growth dynamics for growth of molybdenum oxide at 167 °C, as measured by QCM, using $Mo(CO)_6$ and different combinations of water and ozone as precursors.
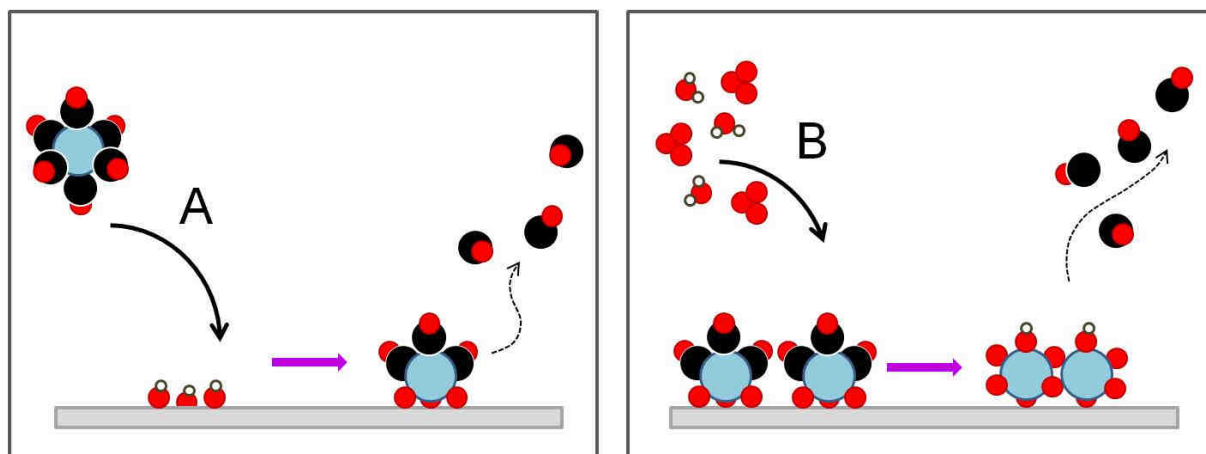
Figure 5.2 Principle of the molybdenum oxide ALD growth according to our QCM measurements. The Mo(CO)$_6$ adsorb on several sites at the time before to react with ozone.

The investigation of the MoO$_3$ ALD growth and *in situ* QCM studies are described in the paper I.

The MoO$_3$ thin films are amorphous as deposited as indicated by x-ray diffraction analysis. Analysis by x-ray photoelectron spectroscopy showed the surface of the films to contain Mo(VI).

The chemical composition, including probing of the Mo-oxidation state throughout the film structures was investigated by two XPS approaches; depth profile studies using Ar$^+$ sputtering on a 40 nm thick film and angle resolved measurements on a 10 nm thick film. Unfortunately, the sputtering influenced strongly the analysis results and induced reduction of the Mo-O film (down to metallic molybdenum at the interface) prior to XPS data collection (Figure 5.3). On the other hand, angle resolved XPS proved the molybdenum to be in oxidation state VI throughout the entire film.
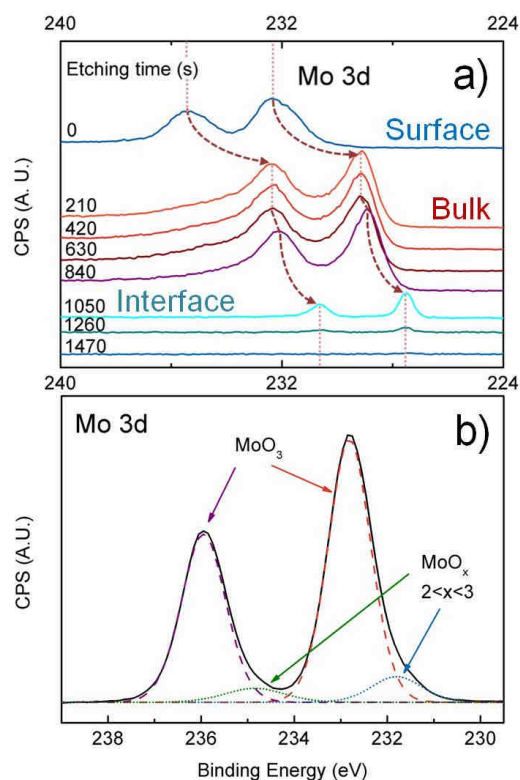

Figure 5.3 XPS spectra showing a) the reduction of MoO$_3$ induced by Ar$^+$ sputtering and b) the lower oxidation state present at the interface.

However molybdenum in a lower oxidation state was still observed at the substrate interface, representing the initial stage of film formation (Figure 5.3).

The combined XPS study of the MoO_3 thin films as deposited is reported in the paper II.

MoO_3 thin films obtained by ALD and the films characterized carefully, the next challenge was to crystallize the films in order to obtain the different polymorphs of MoO_3.

5.2 Obtaining the different MoO_3 polymorphs from ALD films

Upon annealing under air, the as-deposited amorphous thin films of MoO_3 crystallize. The main interest here was to visualize and describe the full crystallization pathway from amorphous to the orthorhombic α-MoO_3 pure phase.

Thin films of each polymorph of MoO_3 and their subsequent characterization were obtained. We demonstrated that upon annealing under air, molybdenum oxide crystallizes first into metastable β-MoO_3 at 400 °C, followed by further crystallization towards polycrystalline α-MoO_3 at higher temperature, to finally complete the crystallization to the orthorhombic α-MoO_3 phase at 600 °C. By analysing the topography of the films for different polymorphs with AFM, we were able to show the morphology evolution of the films during the crystallization process.
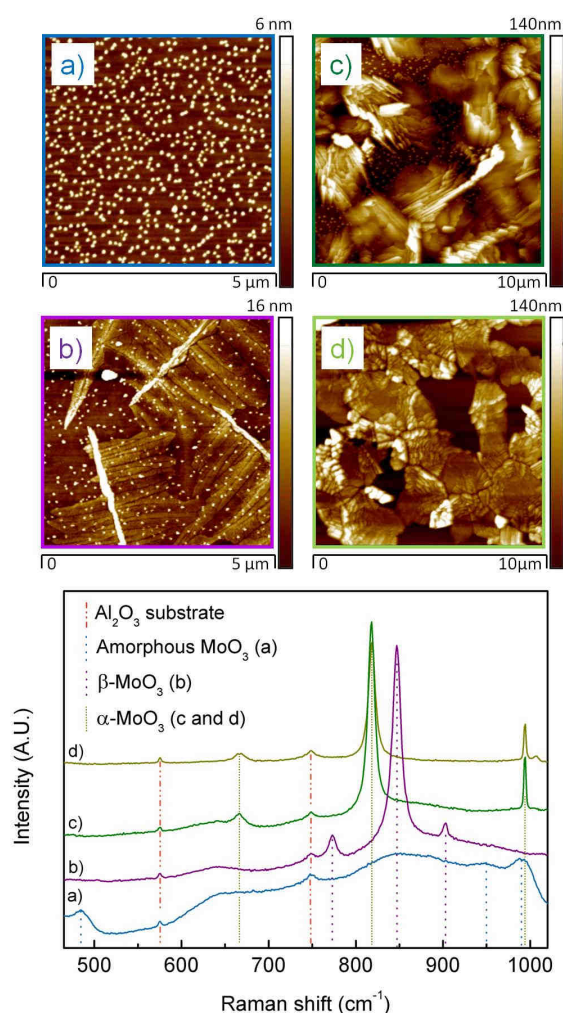

Figure 5.4 AFM topography and related Raman spectra for the MoO_3 polymorphs: a) amorphous MoO_3, b) β-MoO_3, c) polycrystalline α-MoO_3 and d) orthorhombic α-MoO_3.

The amorphous MoO_3 is very uniform and has a smooth base layer. During crystallization into β-MoO_3, a crystalline structure of axial flakes appears in the layer. The flakes then protrude from the surface when the films transform into α-MoO_3, to finally pack into a floral morphology for the final orthorombic α-MoO_3 phase (Figure 5.4). By analysing the Raman spectra of each polymorph (Figure 5.4) we were wondering what influenced the intensity of the vibration modes and appearance of a shoulder for the peak at 995 cm^{-1} for the orthorombic phase. We thus performed combined AFM/Raman on a polycrystalline α-MoO_3 film recording the Raman spectra for each feature, proving the size, shape and orientation of crystallites to have a strong impact on vibration modes and Raman shift intensities (Figure 5.5).
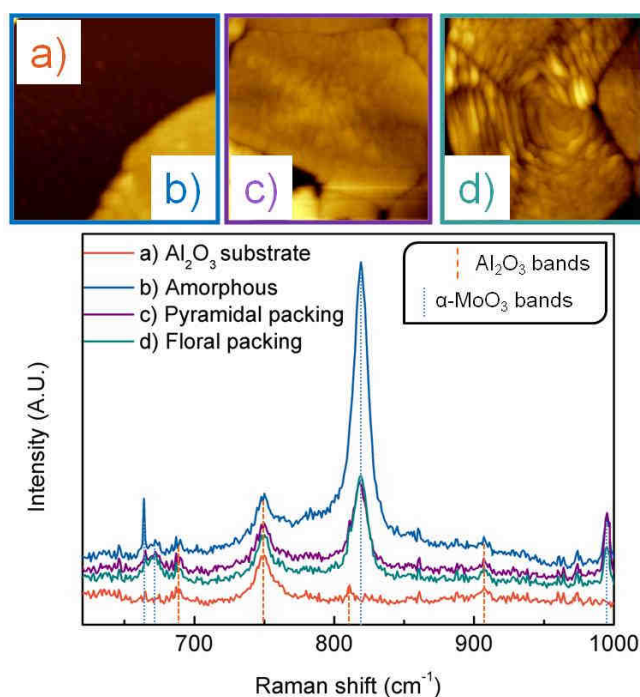
Figure 5.5 AFM topographies (top) and Raman spectra (bottom) of the different features of a polycrystalline α-MoO_3.

The recipe to acquire β- and α-MoO_3 crystalline states from amorphous thin film of MoO_3 obtained by ALD and their subsequent investigations are treated in the paper II.

The different polymorphs of MoO_3 being obtained and characterized, the next step was to investigate the ability to coat porous substrates with cobalt and molybdenum by ALD. Previously, at the University of Oslo, cobalt oxide was grown by ALD using $Co(thd)_2$ and ozone as precursors; this combination of precursors was therefore examined to coat AAO membranes.

5.3 Investigation of the coverage of porous AAO membranes

A main objective in this project was to control and study the depth profile of the coating inside nanopores. In the first step, the ability to coat anodiscs with molybdenum deposited by ALD was tested and confirmed by SEM imaging. As expected, the pores remained uncoated when the ALD process pulsing $Co(thd)_2$ and ozone was evaluated to deposit cobalt into the porous structure, due to ozone decomposition into the pores. Therefore a new process to deposit cobalt oxide by ALD had to be investigated in order to allow the cobalt coating of a porous structure. Thin films of polycrystalline Co_3O_4 were obtained by ALD using cobaltocene ($CoCp_2$) and ozone as precursors. SEM imaging of coated anodiscs showed a homogeneous distribution of cobalt oxide on the 5 µm upper part of the pores extremities. A comparison of the three different ALD coatings of the AAO membranes is represented Figure 5.
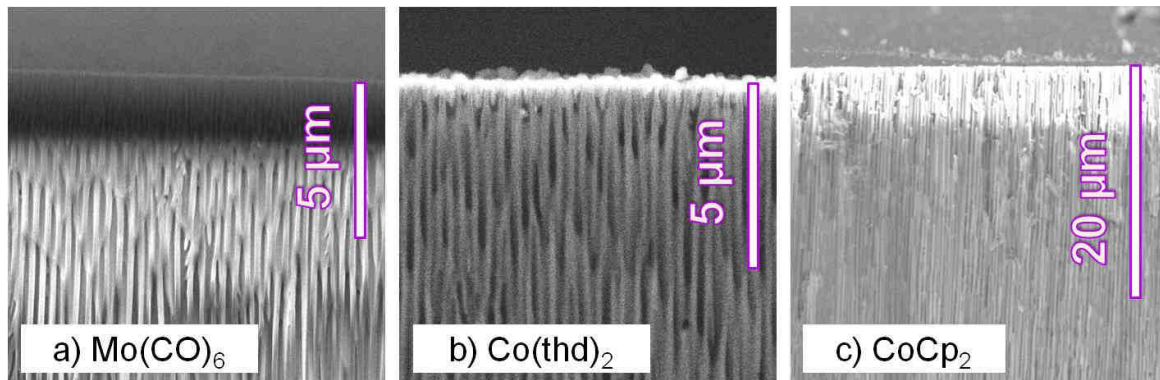
Figure 5.6 SEM images of anodiscs coated by ALD pulsing a) $Mo(CO)_6$ and (H_2O+O_3), b) $Co(thd)_2$ and O_3 and c) $CoCp_2$ and O_3 as precursors. The films were 40 nm thick in order to visualize a difference in the contrast between Al_2O_3 and the deposited oxides.

By studying different configurations of the anodiscs in the reaction chamber of our flow type reactor, we could point out the influence of the fluid dynamics on the cobalt coating profile of the pores. In one configuration, the disc was placed perpendicular the precursors gas flow, on the other hand the disc was positioned parallel to the flow. A second study consisted in an EDS mapping investigation of the AAO pores coverage profile in the two tested configurations.

It clearly proved the presence of cobalt inside the discs with a cobalt content higher at the extremities of the discs and decreasing inwards the pores (Figure 5.7). This particular profile and the slope of decreasing thickness in the coverage profile was well in line with the observations made by Elam et al. [52] and Perez et al. [51]. Longer pulse and purge times were tested in order to improve the conformality of the cobalt coating in the porous structure but without success.
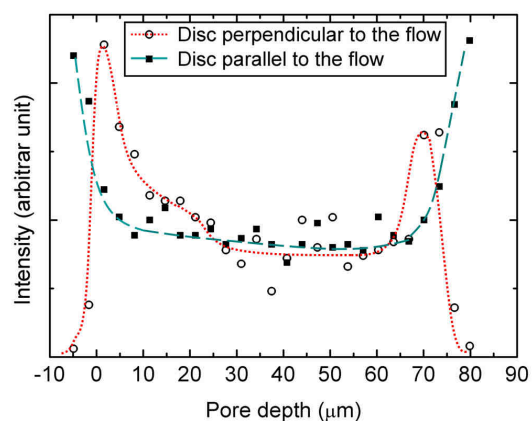

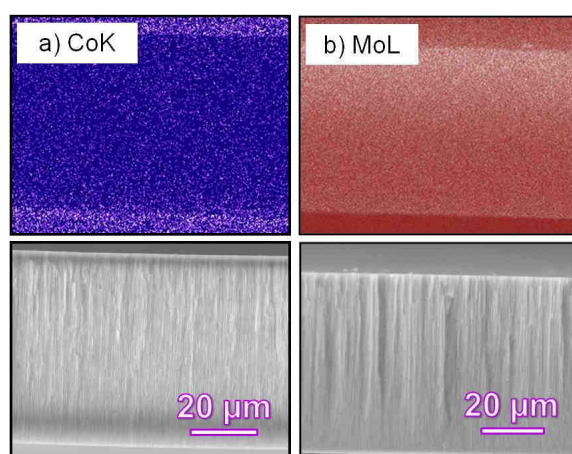**Figure 5.7** Relative cobalt content in anodiscs measured by EDS as function of pore depth.

Figure 5.8 Cross sectional EDS mapping of an anodisc coated with Co (a) and Mo (b) thin films deposited by ALD. The films were about 10 nm thick.

The molybdenum content in the anodiscs structure coated with a 10 nm thin film was investigated by EDS mapping, showing a very high content of molybdenum in the whole pores for long purges times (about 10 seconds). The coating was homogeneous on a length scale of almost 30 μm before to gradually decrease inside the pores. The overall content of molybdenum inside the pores was considerably high. A comparison between the cobalt and molybdenum coating profiles is represented Figure 5.8. The molybdenum hexacarbonyl had proven here to be successful in the coating of high aspect ratio pores when used as precursor in the ALD process.

The investigations of the cobalt oxide growth by ALD using $CoCp_2$ as metal precursor and the porous AAO membrane cobalt coating profiling are described in the paper III.

The next step was to combine the cobalt oxide and molybdenum oxide processes in order to grow cobalt molybdate by ALD.

5.4 Cobalt-molybdenum oxide thin films grown by ALD

First, Co-Mo oxides thin films were obtained by ALD using the precursors combination $Mo(CO)_6$ + (H_2O+O_3) and $Co(thd)_2$ +O_3. The films were amorphous and their compositions varied quite linearly as function of the number of subcycles of $Mo(CO)_6$. But a preferential growth was seen for the $CoMoO_4$ phase at the surrounding compositions (Figure 5.9 **C**). The ALD growth of oxides obtained pulsing $Co(thd)_2$ as cobalt precursor was not investigated further considering the thd precursor unable to react in a porous structure.

The next step was to grow Co-Mo oxide thin films replacing the thd cobalt precursor by $CoCp_2$. The composition of the films obtained remained constant around $CoMoO_4$ quite independently on the number of $Mo(CO)_6$ subcycles up to 50 % (Figure 5.9 **B**). In order to understand what induced this highly surface sensitive growth, it was decided to drop the water precursor in the Mo-O subcycle to verify any effect of water on the overall growth process. Co-Mo oxide films were therefore synthesized with the precursors set $Mo(CO)_6$ + O_3 and $Co(thd)_2$ +O_3. The molybdenum concentration in the films obtained by this second approach increased drastically with the number of $Mo(CO)_6$ subcycles, to reach a plateau of 80 % of molybdenum in the metal ratio of the oxide (Figure 5.9 **A**). The effect of water on the overall growth and composition of the films was confirmed here. The $CoMoO_4$ films crystallized to the β-$CoMoO_4$ phase under annealing, while the excess of molybdenum in the films of higher Mo content crystallized into α-MoO_3.
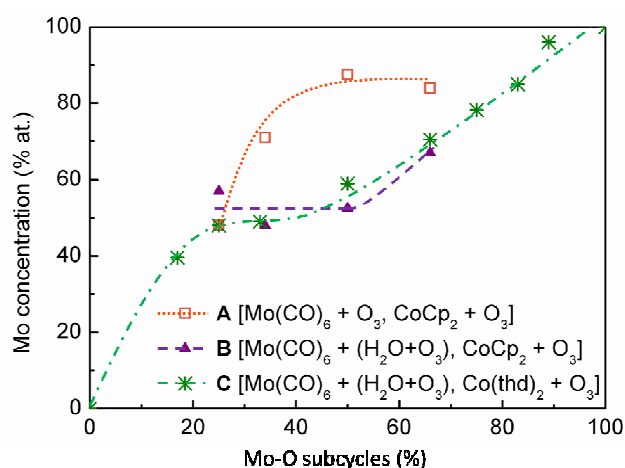

Figure 5.9 Mo content in the Co/Mo ratio of Co-Mo oxides films obtained by ALD, as function of the Mo-O subcycles (%).

The growth dynamics investigation of the Co-O and the Co-Mo-O systems by *in situ* QCM proved the water to affect the growth of Co-O and Mo-O in the different subsequences. (Figure 5.10). This is most evident for the most Co rich pulsing (2Co+1Mo and 3Co+1Mo) in combination **B**, where a gradual increase in mass is observed for each consecutive Co pulse until another Mo-pulse is introduced. This may be correlated with the reduced growth of Co when water is used. However the effect of water on the Co-Mo oxide growth is still not fully understood.
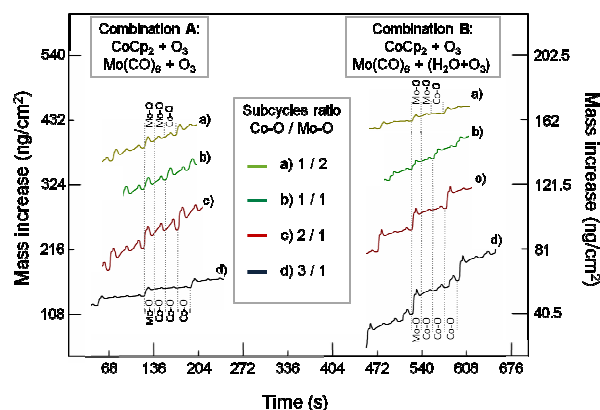
Figure 5.10 Growth dynamics for growth of Co-Mo oxides with and without water, as measured by quartz crystal microbalance.

It is interesting to point out the fact that water added to ozone enhances the growth rate in the MoO_3 growth, while on the other hand water added to the Co-O process inhibits the growth of cobalt oxide both on its own and in the Co-Mo-O process.

As cobalt molybdenum thin films were eventually obtained by ALD, it was time to test their catalytic activity as deposited on quartz in the ammonia decomposition process. The reduced compounds evidenced a decrease of the ammonia decomposition temperature and their catalytic activity was increased with the molybdenum content (Figure 5.11).

Figure 5.11 Ammonia decomposition temperature over Co-Mo oxide thin films, obtained using $Mo(CO)_6$ and $CoCp_2$ as metal precursors.

The investigation of the Co-Mo oxides synthesis by ALD, the study of the growth dynamics and the results of the catalytic testing in the ammonia decomposition process are presented in the paper IV.

At this time we were able to coat porous supports with molybdenum and cobalt and further grow the ternary CoMo-oxide by ALD. After demonstrating the activity of cobalt-molybdenum oxide ALD films in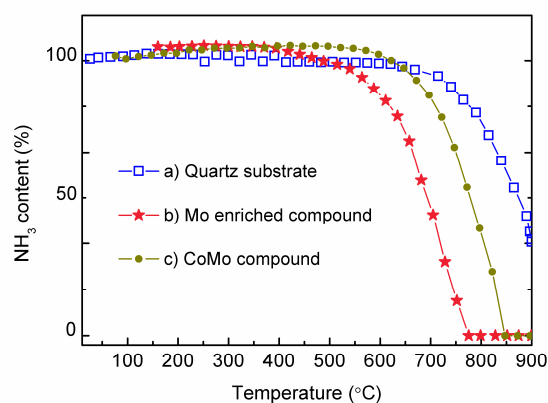 the ammonia decomposition process, our main aspiration was to investigate the deposition of cobalt and molybdenum oxides films on industrial catalysts carriers and investigate their activity in the hydrodesulfurization process (HDS conversion) at the industrial research scale.

5.5 Investigation of the catalytic activity of the Co-Mo oxide thin films in the hydrodesulfurization process

The main goal in this sub project was to study the catalytic properties of cobalt-molybdenum oxides thin films deposited by atomic layer deposition on industrial alumina carriers (grained into 600-850 μm granulates), as function of the thickness of the films. Another aspect of the work was to compare the catalytic activity of $Co_3O_4/MoO_3/Co_3O_4$ multilayered compounds with $CoMoO_4$ thin films obtained by ALD. Such study was empowered by the excellent control which ALD provides towards the composition and thickness of the grown materials. The various compounds designed for this study are listed in Table 5.1.

The pore of the alumina substrates were too narrow (about 40 Å) to enable the ALD coating of the porous structure. Molybdenum exhibited a better penetration into the pores than cobalt, probably due to a higher reactivity of the carbonyls than of cyclopentadienyl when adsorbing on the alumina surface. However, the pores were coated with molybdenum only for the outer 2 µm at their open extremities. Consequently, our materials displayed a low activity towards HDS conversion. Nevertheless, some trends were evident and are represented Figure 5.12.
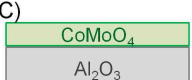
Table 5.1 Building of the multilayered films and the $CoMoO_4$ films deposited by ALD on the Al_2O_3 granulates for the HDS catalytic activity testing.

The catalysts made of cobalt and molybdenum oxides multilayer exposed higher activity than the catalysts made of a $CoMoO_4$ single phase coating. The $CoMoO_4$ films indicated a constant activity independently on the thickness of the coating. The HDS conversion study as function of the thickness of the cobalt oxide and molybdenum oxide films showed an increase of activity with the thickness of the films, followed by a drop in the conversion for the thickest MoO_3 layer. This decline in the activity was assumed to be caused by the leveling of the active surface area.
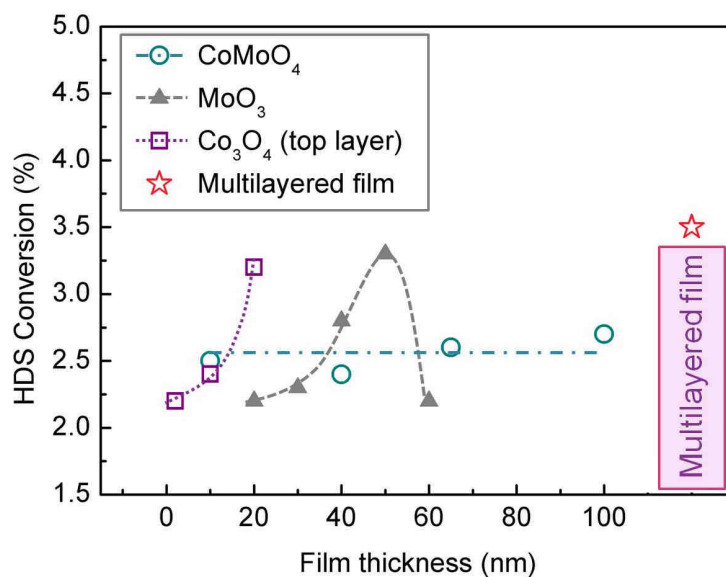
Figure 5.12 HDS conversion over the different catalysts as function of the thickness of the films.

The higher activity of the multilayered films as compared with the films made of $CoMoO_4$ can be explained by additional interactions between the metallic atoms and the sulfur at the interfaces. This hypothesis would be well in line with the Co-Mo-S model, however a rigorous characterization of the ALD nanostructures before and after sulfidation is required to confirm any theory.

The study of the catalytic properties of our ALD model materials in the hydrodesulfurization process is described in the unpublished results I.

5.6 *In situ* TEM imaging of the CuO reduction to metallic Cu from a CuO/ZnO/Al$_2$O$_3$ multilayered film obtained by ALD

This last part of the PhD work could be considered as an external project since the involved materials differ from the conceived Co-Mo compounds. Nevertheless, this study corroborates the valuable potential of model materials made by ALD for catalysis purposes; it is therefore considered as integrated part of this work.

ALD was adopted to build up multilayered thin films of copper oxide, zinc oxide and alumina; *in situ* TEM imaging was performed on the samples in order to investigate the changes in morphology of the films during the reduction of CuO to metallic Cu. Initially, CuO/ZnO thin films were obtained by ALD at 175 °C and investigated by TEM imaging. The high roughness of zinc oxide and the low content of copper cumbersomed the discrimination between the copper oxide and the zinc oxide films. An under layer of alumina was there from deposited prior to zinc oxide coating and the depositions were performed at lower temperatures in the mean of confining the ZnO crystallinity.

In situ TEM imaging of the CuO/ZnO/Al$_2$O$_3$ multilayered compound was performed under hydrogen at 250 °C. The morphology of the multilayered film showed an evolution of the grains morphology towards larger grain size and higher crystallinity during the ramp of temperature and the stabilization at 250 °C (Figure 5.13). Images of the Cu/ZnO/Al$_2$O$_3$ multilayered film were acquired at 250 °C; selected images are represented Figure 5.14. Dark particles about 10 to 15 nm large appeared on the surface of the multilayered film, some of them being particularly edgy.
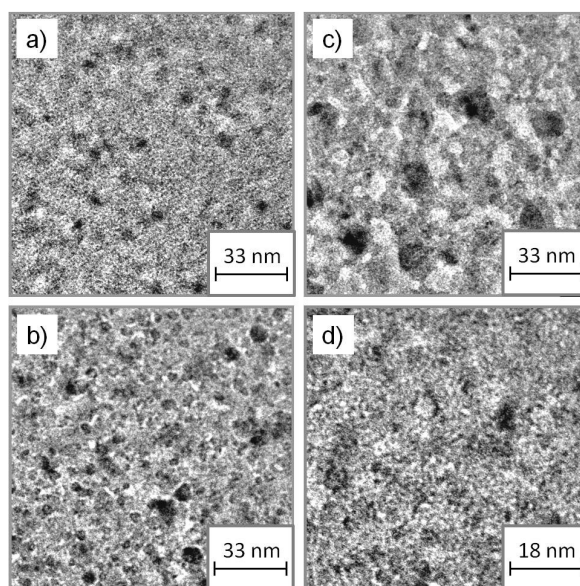
Figure 5.13 *In situ* TEM imaging of the CuO/ZnO/Al$_2$O$_3$ multilayered film: a) H$_2$ introduced at room T°, b) under H$_2$ during the ramp of temperature, c) under H$_2$ stabilized at 250 °C, d) under H$_2$ back to room T° and stabilized.
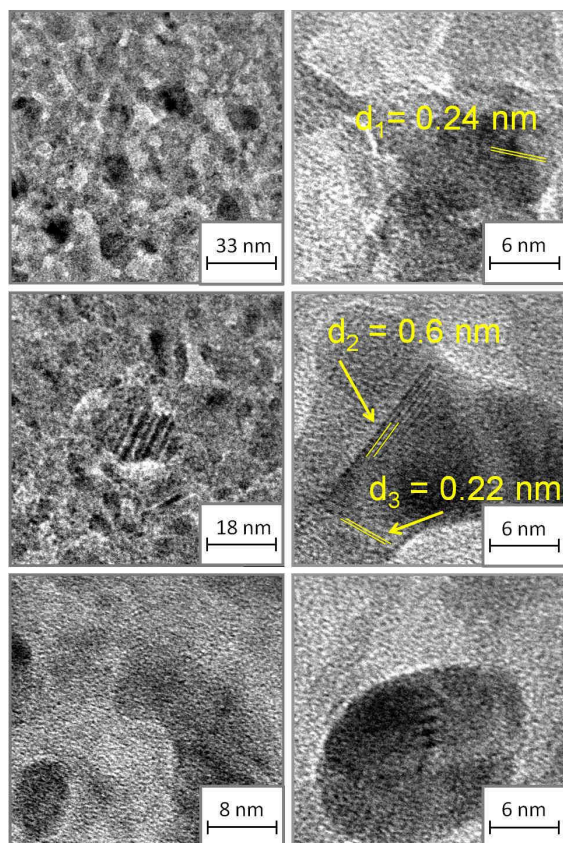
Figure 5.14 TEM imaging of the Cu/ZnO/Al$_2$O$_3$ multilayered film under H$_2$ stabilized at 250 °C, at different magnitudes (left column) and of different particles seen at high magnitude (right column).

These particles were most likely reduced Cu phase, i.e Cu(s). Fringes were seen all over the film, overlapping the light surface and the particles. Most of the fringes spacing were interpreted as of crystalline plans from crystalline ZnO. Overlapping of diverse fringes, indicated the superposition of Cu crystalline particles on top of the ZnO film (Figure 5.14). The particles disappeared after cooling down to room temperature supposedly due to reoxidation into copper oxide in the microscope.

The uniform ALD films gave well dispersed copper nanoparticles upon reduction. As a result, the imaging of the particles was effortless in comparison with *in situ* TEM investigation of a real catalyst. The ALD grown thin films have proven here to be promising model materials for further investigations of Cu/ZnO catalysts.

The *in situ* TEM investigation of the copper oxide reduction in the ALD CuO/ZnO/Al$_2$O$_3$ multilayered compound is treated in the unpublished results II.

6   Summarizing conclusion

The aim of this work was to investigate the potential of model materials designed by atomic layer deposition toward applications in catalysis research. Molybdenum based catalysts promoted with cobalt were selected as target materials, considering their important roles in various industrial processes. Particular attention was paid to understand the growth dynamics of the ALD processes involved and further to characterize the obtained materials carefully. It was of main concern to verify the feasibility to coat porous materials by ALD with our equipment. Another ambition was to confirm the advantages of the atomic layer technique to create model materials for industrial research projects in catalysis.

Thin film growth of molybdenum trioxide has been demonstrated by the atomic layer deposition technique using molybdenum-hexacarbonyl, water and ozone as precursors. A narrow ALD-window is observed at relatively low temperatures, leading to amorphous films as deposited. The effect of different oxygen precursors on the growth mechanism of the molybdenum oxide has been assessed by QCM investigations.

The chemical composition and Mo-oxidation state in MoO_3 thin films grown by ALD have been investigated by two XPS approaches. The sputtering based studies affects strongly the analysis results by inducing reduction of the Mo-O film prior to XPS data collection. The ARXPS proves that molybdenum is in oxidation state VI throughout the bulk of the film. Molybdenum in a lower oxidation state is observed at the substrate interface, representing the initial stage of film formation.

A convenient process to achieve thin film model materials of MoO_3 polymorphs has been proposed, describing the crystallization behavior of the thin films from the as-deposited amorphous state via metastable β-MoO_3 to the orthorhombic α-MoO_3 phase. A significant mass transport, in particular during recrystallization into α-MoO_3 is demonstrated. By means of combined AFM/Raman studies we have been able to relate morphology and vibration mode of α-MoO_3 features.

The ability to coat porous materials with our ALD equipment has been confirmed by means of coating anodiscs with the current molybdenum process and a cobalt process. ALD thin film growth of cobalt oxide has been obtained using cobaltocene and ozone as precursors. SEM

and EDS investigations of coated porous anodiscs show the specific coverage profile to be dependent on the fluid dynamics in the reactor.

Cobalt molybdate has been grown by atomic layer deposition, varying the cobalt oxide precursor between $Co(thd)_2$ and $CoCp_2$. The growth dynamics of the films, their composition and crystallization have been examined as function of the subcycles ratio, proving $CoMoO_4$ to be the preferential composition and the excess of molybdenum to crystallize into α-MoO_3. The films catalytic activity in the ammonia decomposition process is assessed at the laboratory scale. The growth dynamics have been investigated using quartz crystal microbalance (QCM) where it is evident that the different precursor chemistries affect each other's growth. When water is combined in the reactions, a surface controlled mechanism takes place which guides the deposited stoichiometry towards the $CoMoO_4$ phase over a range of different cobalt rich pulsed compositions. This is a rare example of how surface chemistry can control stoichiometry of depositions in ALD.

The catalytic properties of cobalt-molybdenum oxide thin films deposited by ALD on industrial alumina carriers have been studied as function of the thickness of the films. Cobalt molybdenum multilayered thin films activity has proven to increase with the thickness of the films up to a certain extend. Multilayered films show a better activity in the HDS conversion as compared with cobalt molybdate single phase films.

Finally, TEM imaging characterization of copper particles on top of a zinc oxide film has been achieved by first depositing an underlayer of Al_2O_3, thereafter coated with zinc oxide and copper oxide thin films by ALD at low temperatures. *In situ* TEM imaging of the multilayered film at 250 °C under H_2 shows crystallization of the ZnO grains and reduction of the copper oxide film leading to Cu particles formation.

Suggestions for future work

It would be interesting to study *in situ* sulfidation of the MoO_3 polymorphs model materials obtained by ALD using Raman and environmental TEM. Multilayered thin films of cobalt-molybdenum oxides and cobalt molybdate thin films have been deposited by ALD on TEM chips and it would be of high interest to explore the structural changes of the materials under sulfidation. The main goal would be to understand what governs the catalytic activity of the cobalt molybdenum based catalysts in the hydrodesulfurization process.

In order to learn more about the copper/zinc/alumina materials obtained by ALD, it would be interesting to perform *in situ* TEM investigations on the existing samples under different atmospheres in order to study the structural changes of the copper particles.

A possible way to pursue the study about HDS conversion over Co-Mo oxide materials could be to employ a mesoporous support comprising larger pores in order to facilitate the diffusion of the ALD precursors inside the structure. Such a structure could also be coated with alumina prior to cobalt and molybdenum compounds in order to tune the diameter of the pores. Using the benefits from an ALD close type reactor could be explored to enhance the conformality of the coating and offer a good control over the thickness of the deposited films deep into the frame.

Since the ALD deposited CoMo oxide films are quite active in the decomposition of ammonia, extended studies could lead to even higher activity. It would be interesting to investigate further the ammonia decomposition process over multilayered and cobalt molybdate thin films as function of the thickness of the films, first on quartz and then on porous supports.

In the end, the study of the precursors chemistries and the effect of water on the processes growth is a hot topic and it would be possible to understand more about it by coupling the QCM study with other *in situ* techniques such as quadrupole mass spectrometer (QMS). Concerning precursors chemistry investigation, an exploratory work has been performed where molybdenum hexacarbonyl was reacting directly with cobaltocene by ALD without pulsing an oxidant. Thin films containing cobalt and molybdenum in a complex matrix were obtained and could represent a new class of deposited films by ALD; it would be therefore exciting to learn more about these materials.

References

1. Henrik Topsøe, B.S.C., Franklin E. Massoth, *Hydrotreating* Catalysis science and technology, 1996. **11**.
2. Ivanova ,T., et al., *Electrochromic properties of atmospheric CVD MoO_3 and MoO_3-WO_3 films and their application in electrochromic devices.* Materials Science and Engineering B, 2005. **119**(3): p. 232-239.
3. Diaz-Droguett, D.E. and V.M. Fuenzalida, *Gas effects on the chemical and structural characeristics of porous MoO_3 and MoO_{3-x} grown by vapor condensation in helium and hydrogen.* Materials Chemistry and Physics, 2011. **126**(1-2): p. 82-90.
4. Ressler, T., et al., *Bulk Structural Investigation of the Reduction of MoO_3 with Propene and the Oxidation of MoO_2 with Oxygen.* Journal of Catalysis, 2002. **210**(1): p. 67-83.
5. Ressler, T., et al., *In Situ XAS and XRD Studies on the Formation of Mo Suboxides during Reduction of MoO_3.* The Journal of Physical Chemistry B, 2000. **104**(27): p. 6360-6370.
6. Carcia, P.F. and E.M. McCarron Iii, *Synthesis and properties of thin film polymorphs of molybdenum trioxide.* Thin Solid Films, 1987. **155**(1): p. 53-63.
7. Fournier, M., A. Aouissi, and C. Rocchiccioli-Deltcheff, *Evidence of beta-MoO_3 formation during thermal treatment of silica-supported 12-molybdophosphoric acid catalysts.* Journal of the Chemical Society, Chemical Communications, 1994(3): p. 307-308.
8. Juárez Ramírez, I. and A. Martínez-de la Cruz, *Synthesis of beta-MoO_3 by vacuum drying and its structural and electrochemical characterisation.* Materials Letters, 2003. **57**(5-6): p. 1034-1039.
9. Juárez, R. and C. Martínez-de la, *Electrochemical lithium insertion in beta-MoO_3: novel Li MoO_3 bronzes.* Journal of Solid State Electrochemistry, 2003. **7**(5): p. 259-263.
10. Jacobs, G. et al., *Fischer-Tropsch synthesis: Temperature programmed EXAFS/XANES investigation of the influence of support type, cobalt loading, and noble metal promoter addition to the reduction behavior of cobalt oxide particles.* Applied Catalysis A: General, 2007. **333**(2): p. 177-191.
11. Breejen, J.P.d., *Cobalt Particles Size Effects in Catalysis*, 2010, Universiteit Utrecht: Utrecht.
12. Bahlawane, N., *Kinetics of methane combustion over CVD-made cobalt oxide catalysts.* Applied Catalysis B: Environmental, 2006. **67**(3-4): p. 168-176.
13. Lojewska, J. et al., *Structured cobalt oxide catalyst for VOC combustion. Part I: Catalytic and engineering correlations.* Applied Catalysis A: General, 2009. **366**(1): p. 206-211.
14. Lojewska, J., et al., *Engineering and chemical aspects of the preparation of microstructured cobalt catalyst for VOC combustion.* Catalysis Today, 2005. **101**(2): p. 81-91.
15. Zhang, W., et al., *Supported cobalt oxide on MgO: Highly efficient catalysts for degradation of organic dyes in dilute solutions.* Applied Catalysis B: Environmental, 2010. **95**(1-2): p. 93-99.
16. Rossetti, G.A., J.L. Burger, and R.D. Sisson, *Characterization of Mixed Cobalt-Molybdenum Oxides Prepared by Evaporative Decomposition of Solutions.* Journal of the American Ceramic Society, 1989. **72**(10): p. 1811-1815.
17. Chojnacki, J., and R. Kozlowski, *Disordered modifications of cobalt molybdate.* Journal of Solid State Chemistry, 1975. **14**(2): p. 117-121.
18. Brito, J.L., and A.L. Barbosa, *Effect of Phase Composition of the Oxidic Precursor on the HDS Activity of the Sulfided Molybdates of Fe(II), Co(II), and Ni(II).* Journal of Catalysis, 1997. **171**(2): p. 467-475.
19. Joaquín, L. Brito, A.L.B., *Effect of Phase Composition of the Oxidic Precursor on the HDS Activity*

of the Sulfided Molybdates of Fe(II), Co(II), and Ni(II). Journal of Catalysis, 1997. **171**: p. 467-475.

20. G. W. Smith, J.A.I., *The crystal structure of Cobalt Molybdate, CoMoO₄.* Acta Cryst., 1965. **19**: p. 269-275.

21. I. Chorkendorff, J.W.N., *Concepts of Modern Catalysis and Kinetics*2007: 2007 WILEY-VCH Verlag GmbH & Co. KGaA.

22. Kojima, R., and K.-i. Aika, *Cobalt molybdenum bimetallic nitride catalysts for ammonia synthesis: Part 1.* Applied Catalysis A: General, 2001. **215**(1-2): p. 149-160.

23. Ni, M., D.Y.C. Leung and M.K.H. Leung, *Electrochemical modeling of ammonia-fed solid oxide fuel cells based on proton conducting electrolyte.* Journal of Power Sources, 2008. **183**(2): p. 687-692.

24. Sørensen, R.Z., et al., *Catalytic ammonia decomposition: miniaturized production of COx-free hydrogen for fuel cells.* Catalysis Communications, 2005. **6**(3): p. 229-232.

25. Okamura, (J.H.-s., JP), Kirishiki, Masaru (Suita-shi, JP), Yoshimune, Masanori (Suita-shi, JP), Tsuneki, Hideaki (Suita-shi, JP), *Ammonia decomposition catalysts and their production processes, as well as ammonia treatment method.* 2011.

26. Hermann, N., M. Brorson, and H. Topsøe, *Activities of unsupported second transition series metal sulfides for hydrodesulfurization of sterically hindered 4,6-dimethyldibenzothiophene and of unsubstituted dibenzothiophene.* Catalysis Letters, 2000. **65**(4): p. 169-174.

27. Brorson, M., A. Carlsson, and H. Topsøe, *The morphology of MoS₂, WS₂, Co-Mo-S, Ni-Mo-S and Ni-W-S nanoclusters in hydrodesulfurization catalysts revealed by HAADF-STEM.* Catalysis Today, 2007. **123**(1-4): p. 31-36.

28. Kibsgaard, J., et al., *Comparative atomic-scale analysis of promotional effects by late 3d-transition metals in MoS₂ hydrotreating catalysts.* Journal of Catalysis, 2010. **272**(2): p. 195-203.

29. Vesborg, P.C.K., et al., *Transient behavior of Cu/ZnO-based methanol synthesis catalysts.* Journal of Catalysis, 2009. **262**(1): p. 65-72.

30. Long, N.J., and A.K. Petford-Long, *In-situ electron-beam-induced reduction of CuO: A study of phase transformations in cupric oxide.* Ultramicroscopy, 1986. **20**(1-2): p. 151-159.

31. Behrens, M., *Meso- and nano-structuring of industrial Cu/ZnO/(Al₂O₃) catalysts.* Journal of Catalysis, 2009. **267**(1): p. 24-29.

32. Meille, V., *Review on methods to deposit catalysts on structured surfaces.* Applied Catalysis A: General, 2006. **315**: p. 1-17.

33. Kim, H., H.-B.-R. Lee, and W.J. Maeng, *Applications of atomic layer deposition to nanofabrication and emerging nanodevices.* Thin Solid Films, 2009. **517**(8): p. 2563-2580.

34. Leskelä, M., and M. Ritala, *Atomic layer deposition (ALD): from precursors to thin film structures.* Thin Solid Films, 2002. **409**(1): p. 138-146.

35. Ritala, M., and M. Leskelä, *Atomic layer deposition*, in *Handbook of Thin Films*, N. Hari Singh, M.Sc, and Ph.D, Editors. 2002, Academic Press: Burlington. p. 103-159.

36. Puurunen, R.L., *Surface chemistry of atomic layer deposition: A case study for the trimethylaluminum/water process.* Journal of Applied Physics, 2005. **97**(12): p. 121301-52.

37. Hurst, K.E., et al. *Study of the nucleation and growth of platinum-ruthenium catalyst on ion-implanted highly oriented pyrolitic graphite by atomic layer deposition*. 2011. American Chemical Society.

38. Keränen, J., et al., *Preparation by atomic layer deposition and characterization of active sites in nanodispersed vanadia/titania/silica catalysts.* Catalysis Today, 2004. **91-92**: p. 67-71.

39. Enterkin, J.A., et al., *Propane Oxidation over Pt/SrTiO₃ Nanocuboids.* ACS Catal., 2011. **1**: p. 629-635.

40. Feng, H., et al., *Subnanometer Palladium Particles Synthesized by Atomic Layer Deposition.* ACS Catal., 2011. **1**: p. 665-673.

41. E. Rauwel, O.N., A. Galeckas, J. C. Walmsley, E. Rytter H. Fjellvåg *ALD Applied to Conformal Coating of Nanoporous γ-Alumina: Spinel Formation and Luminescence Induced by Europium Doping.* ECS Transaction, 2011.

42. Setthapun, W., et al., *Genesis and Evolution of Surface Species during Pt Atomic Layer Deposition on Oxide Supports Characterized by in Situ XAFS Analysis and Water–Gas Shift Reaction.* The Journal of Physical Chemistry C, 2010. **114**(21): p. 9758-9771.

43. Mikko Ritala, M.L., *Atomic layer epitaxy - a valuable tool for nanotechnology?* Nanotechnology, 1999. **10**: p. 19-24.

44. Ying-Bing Jiang, N.L., Henry Gerung, Joseph L. Cecchi, C. Jeffrey Brinker, *Nanometer-Thick conformal pore sealing of self-assembled mesoporous silica by plasma-assisted atomic layer deposition.* JACS communications, 2006. **128**: p. 11018-11019.

45. Booyong S. Lim, A.R., Roy G. Gordon, *Atomic layer deposition of transition metals.* Nature materials, 2003. **2**: p. 749-754.

46. Mackus A. J. M., J.J.L.M., M. C. M. van de Sanden, W. M. M. Kessels, *Local deposition of high-purity Pt nanostructures by combining electron beam induced deposition and atomic layer deposition.* J. Appl. Phys., 2010. **107**(116102).

47. Hakim, L.F., J.H. Blackson, and A.W. Weimer, *Modification of interparticle forces for nanoparticles using atomic layer deposition.* Chemical Engineering Science, 2007. **62**(22): p. 6199-6211.

48. Nielsch, K., et al., *Ferromagnetic Nanostructures by Atomic Layer Deposition: From Thin Films Towards Core-Shell Nanotubes.* ECS Transactions, 2007. **11**(7): p. 139-148.

49. Li, X.L., C.W. Cheng, and H.J. Fan, *Atomic layer deposition ZnO film as seed layer for hydrothermal growth of ZnO nanorods.* Mater. Res. Soc. Symp. Proc., 2010. **1258**: p. No pp. given, Paper #: 1258-Q11-10.

50. Chang, Y.-H., et al., *Fabrication and characteristics of self-aligned ZnO nanotube and nanorod arrays on Si substrates by atomic layer deposition.* J. Electrochem. Soc., 2010. **157**: p. K236-K241.

51. Perez, I., et al., *TEM-Based Metrology for HfO$_2$ Layers and Nanotubes Formed in Anodic Aluminum Oxide Nanopore Structures.* Small, 2008. **4**(8): p. 1223-1232.

52. Elam, J.W., et al., *Conformal Coating on Ultrahigh-Aspect-Ratio Nanopores of Anodic Alumina by Atomic Layer Deposition.* Chemistry of Materials, 2003. **15**(18): p. 3507-3517.

53. Dendooven, J., et al., *Modeling the Conformality of Atomic Layer Deposition: The Effect of Sticking Probability.* Journal of The Electrochemical Society, 2009. **156**(4): p. P63-P67.

54. Chen, W., J.-H. Yuan, and X.-H. Xia, *Characterization and Manipulation of the Electroosmotic Flow in Porous Anodic Alumina Membranes.* Analytical Chemistry, 2005. **77**(24): p. 8102-8108.

55. Dendooven, J., et al., *Conformality of Al$_2$O$_3$ and AlN Deposited by Plasma-Enhanced Atomic Layer Deposition.* Journal of The Electrochemical Society, 2010. **157**(4): p. G111-G116.

56. Maarit Kariniemi, J.N., Matti Putkonen, Marko Vehkamäki, Marianna Kemell, Mikko Ritala, Markku Leskelä, *Conformality of remote plasma enhanced ALD processes: an experimental study.* ALD-AVS, 2011.

57. Maarit Kariniemi, J.N., Timo Hatanpää, Marko Vehkamäki, Marianna Kemell, Timo Sajavaara, Mikko Ritala, Markku Leskelä, *PEALD of Silver Thin Films.* ALD-AVS, 2011.

58. Knoops, H.C.M., et al., *Conformality of Plasma-Assisted ALD: Physical Processes and Modeling.* Journal of The Electrochemical Society, 2010. **157**(12): p. G241-G249.

59. Dendooven, J., et al., *In Situ X-ray Fluorescence Measurements During Atomic Layer Deposition: Nucleation and Growth of TiO$_2$ on Planar Substrates and in Nanoporous Films.* The Journal of Physical Chemistry C, 2011. **115**(14): p. 6605-6610.

60. Hiltunen, L., et al., *Nitrides of titanium, niobium, tantalum and molybdenum grown as thin films by the atomic layer epitaxy method.* Thin Solid Films, 1988. **166**: p. 149-154.

61.   Juppo, M., M. Ritala, and M. Leskela, *Use of 1,1-Dimethylhydrazine in the Atomic Layer Deposition of Transition Metal Nitride Thin Films.* Journal of The Electrochemical Society, 2000. **147**(9): p. 3377-3381.

62.   Miikkulainen, V., M. Suvanto, and T.A. Pakkanen, *Atomic Layer Deposition of Molybdenum Nitride from Bis(tert-butylimido)-bis(dimethylamido)molybdenum and Ammonia onto Several Types of Substrate Materials with Equal Growth per Cycle.* Chemistry of Materials, 2006. **19**(2): p. 263-269.

63.   Madeleine Diskus, O.N., Helmer Fjellvåg, *Thin films containing molybdenum oxide*, E.P. Office, Editor 2010, Universitetet i Oslo, Madeleine Diskus, Ola Nilsen, Helmer Fjellvåg. p. WO 2010114386 (A1).

64.   Kurhinen, M. and T.A. Pakkanen, *CoMo/alumina prepared from carbonyl precursors: DRIFT, TPR and HDS studies.* Applied Catalysis A: General, 2000. **192**(1): p. 97-103.

65.   Huang, H.H., et al., *Thermal and photoinduced chemistry of $Mo(CO)_6$ on clean and chemically modified Ru(001).* Surface Science, 1996. **365**(3): p. 769-778.

66.   Jiang, Z., et al., *Thermal decomposition of $Mo(CO)_6$ on thin Al_2O_3 film: A combinatorial investigation by XPS and UPS.* Surface Science, 2007. **601**(3): p. 844-851.

67.   Myllyoja, S., et al., *Interactions of $M(CO)_6$ (M=Cr, Mo, W) with surface sites of Al_2O_3: a theoretical study.* Surface Science, 1999. **441**(2-3): p. 454-460.

68.   Jiang, Z., L. Xu, and W. Huang, *Adsorption and reaction of $Mo(CO)_6$ on chemically modified Pt(1 1 0) model surfaces.* Journal of Molecular Catalysis A: Chemical, 2009. **304**(1-2): p. 16-21.

69.   Aaltonen, T., et al., *Ruthenium Thin Films Grown by Atomic Layer Deposition.* Chemical Vapor Deposition, 2003. **9**(1): p. 45-49.

70.   Klepper, K.B., O. Nilsen, and H. Fjellvåg, *Growth of thin films of Co_3O_4 by atomic layer deposition.* Thin Solid Films, 2007. **515**(20-21): p. 7772-7781.

71.   Gandrud, K.B., *Thin films of multiferroic $BiCoO_3$ by ALD*, in *Department of Chemistry,* 2009, University of Oslo: Oslo.

72.   Elam, J.W., et al., *Atomic Layer Deposition of In_2O_3 Using Cyclopentadienyl Indium: A New Synthetic Route to Transparent Conducting Oxide Films.* Chemistry of Materials, 2006. **18**(15): p. 3571-3578.

73.   Libera, J.A., J.N. Hryn, and J.W. Elam, *Indium Oxide Atomic Layer Deposition Facilitated by the Synergy between Oxygen and Water.* Chemistry of Materials, 2011. **23**(8): p. 2150-2158.

74.   Sauerbrey, G., *Verwendung von Schwingquarzen zur Wägung dünner Schichten und zur Mikrowägung.* Zeitschrift für Physik A Hadrons and Nuclei, 1959. **155**(2): p. 206-222.

75.   Sullivan, J.L., W. Yu, and S.O. Saied, *A study of the compositional changes in chemically etched, Ar ion bombarded and reactive ion etched GaAs(100) surfaces by means of ARXPS and LEISS.* Applied Surface Science, 1995. **90**(3): p. 309-319.

76.   Anwar, M., et al., *X-ray photoelectron spectroscopic (XPS) investigations of etching and annealing effects on thin films of MoO_3.* Spectrochimica Acta Part B: Atomic Spectroscopy, 1989. **44**(8): p. 789-793.

77.   Champaneria, R., et al., *Non-destructive analysis of ultrathin dielectric films.* Surface and Interface Analysis, 2003. **35**(13): p. 1028-1033.

78.   Jeurgens, L.P.H., M.S. Vinodh, and E.J. Mittemeijer, *Quantitative analysis of multi-element oxide thin films by angle-resolved XPS: Application to ultra-thin oxide films on MgAl substrates.* Applied Surface Science, 2006. **253**(2): p. 627-638.

79.   Oswald, S., et al., *Angle-resolved XPS: a critical evaluation for various applications.* Surface and Interface Analysis, 2006. **38**(4): p. 590-594.

80.   *Raman combined with AFM.* Nano Today, 2006. **1**(2): p. 55-55.

81.   FEI. *Transmission electron microscopes* Available from: http://www.fei.com/products/transmission-electron-microscopes/titan/etem.aspx.

Paper I

"Growth of thin films of molybdenum oxide by atomic layer deposition"

Madeleine Diskus, Ola Nilsen and Helmer Fjellvåg,
Journal of Materials Chemistry **2011**, 21, 705-710.

Growth of thin films of molybdenum oxide by atomic layer deposition

Madeleine Diskus,* Ola Nilsen and Helmer Fjellvåg

Thin films of MoO_3 have been obtained by the atomic layer deposition (ALD) technique using molybdenum hexacarbonyl ($Mo(CO)_6$), ozone, and water as precursors. A window for ALD growth was found in the temperature range 152 to 172 ºC. Self limiting growth was verified at a deposition temperature of 163 ºC. The upper temperature range is determined by the thermal stability of the $Mo(CO)_6$ precursor. The growth dynamics was further investigated by quartz crystal microbalance to
10 determine the effect of ozone and water on the deposition process. Growth using only water as oxygen source is hardly detectable. The growth rate increases to 0.75 Å/cycle when ozone is introduced. X-ray diffraction analysis indicates that the films are amorphous as deposited, but crystallise into the α- and β-MoO_3 phases during annealing in air at 500 ºC and to phase-pure, highly oriented α-MoO_3 at 600 ºC. Analysis by x-ray photoelectron spectroscopy show that both as-deposited and annealed films contain Mo(VI). Atomic force microscopy proves a very low surface roughness for as deposited films, which
15 becomes rather rough for annealed films. This investigation has clearly proven the capability of carbonyls as useful precursors for ALD growth of oxides.

Introduction

20 Molybdenum trioxide (MoO_3) has received interest for its electrochromic[1-3] and good catalytic properties[4-7]. Furthermore, thin films of MoO_3 are used in nanostructured gas sensors[8], and in solid-state lithium ion batteries[9]. Thin films of MoO_3 have previously been deposited by techniques such
25 as thermal vapour deposition[10] and metal organic chemical vapour deposition[11, 12]. This is currently extended to include the atomic layer deposition (ALD) technique. The main advantages of the ALD technique are uniform and conformal growth on complex surfaces together with control of film
30 thickness at the atomic level[13-16]. There are previously no reports on deposition of molybdenum oxides by ALD, however, molybdenum nitrides and elemental molybdenum are frequently reported grown by ALD. Molybdenum nitrides are mostly made using a combination of precursors like
35 molybdenum pentachloride ($MoCl_5$) and ammonia, but also reactants like bis(tert-butylimido),bis(dimethylamido)molyb-denum and ammonia[16-19]. Elemental molybdenum is commonly grown using $MoCl_5$ and Zn as reactants[20]. A possible reason for lack of prior reports on growth of
40 molybdenum oxides may be that the most common molybdenum precursor, $MoCl_5$[16], is unable to form oxides due to an etching process connected with formation of stable oxychlorides, analogous to what observed for attempted growth of Nb_2O_5 using $NbCl_5$[21]. As mentioned, molybdenum
45 oxides take part in numerous catalytic processes. Most of these utilise molybdenum oxide as a thin layer on a high surface area support. The ALD technique should be most suitable for conformal deposition on such complex supports. It is therefore important do develop a suitable process for
50 deposition of such molybdenum oxides by ALD in order to be able to explore its interesting catalytic properties. This work presents the first successful attempt to deposit molybdenum oxide by ALD.

The present study utilizes molybdenum hexacarbonyl, 55 $Mo(CO)_6$, as precursor in combination with ozone and water to grow molybdenum oxides by ALD. There are previously limited reports of successful application of carbonyls as metal precursor in ALD-growth. We will therefore also elaborate on whether carbonyls could represent a useful novel type of
60 precursor for atomic layer deposition of oxides.

Experimental details

Thin films of MoO_3 were deposited in a commercial F-120 Sat reactor (ASM Microchemistry Ltd.) using ozone, water and $Mo(CO)_6$ (molybdenum hexacarbonyl 98% from Aldrich)
65 as precursors. $Mo(CO)_6$ was used as solid at room temperature in a bubbler, using nitrogen as carrier gas. The ozone was generated by feeding O_2 (99.999% AGA) into an OT-020 ozone generator (Ozone Technology), providing an ozone concentration of ap. 15 vol.% according to specifications. An
70 ozone flow of ap. 500 cm^3 min^{-1} was used during the ozone pulses. During all depositions, a background pressure of ap. 3.5 mbar was obtained by applying a N_2 carrier gas flow of 300 cm^3 min^{-1}. The carrier gas was produced in a Schmidlin UHPN3001 N_2 purifier with a claimed purity of 99.999% with
75 regard to N_2+Ar content. The process was evaluated for CVD-type of growth by performing experiments at the specified conditions for $Mo(CO)_6$ sublimation and a mix of ozone and water flow, with one of the reactants not being pulsed. The films were deposited on substrates of single crystalline
80 Si(111) and on soda lime glass. The onset of thermal decomposition of the $Mo(CO)_6$ precursor was a priori determined under vacuum conditions by investigating the thermal stability using a method as described in Ref. 24. Most films were deposited within a temperature window of 152 -
85 172 ºC using a total of 1000 cycles, resulting in films thickness between 35 and 75 nm. A selection of as-deposited films grown at 167 ºC were annealed at 200, 300, 400, 500 and 600 °C, respectively, all for 15 minutes in air.

The films were examined with a Siemens D5000 x-ray
90 diffractometer equipped with a Göbel-mirror providing

parallel Cu Kα radiation. The setup was used to measure x-ray reflectivity (XRR), x-ray diffraction (XRD) in reflection mode, as well as rocking curve analysis (ω-scans). *In situ* measurements of the growth dynamics of the Mo-oxide were achieved by a quartz crystal microbalance technique using AT cut crystals and a Maxtec TM400 unit[22,23]. X-ray photoelectron spectroscopy (XPS) was recorded on a Kratos Axis Ultra Instrument. A conventional Al Kα anode was used at 15 kV and 10 mA as the source of x-ray radiation. The pressure in the analysis chamber during measurements was approximately $6.7 \cdot 10^{-9}$ mbar.

Results and discussion

The thermal stability of the $Mo(CO)_6$ precursor was determined by decomposing its vapour under vacuum conditions in an oven with a controlled thermal gradient[24]. The results from this experiment provide an upper limit for a possible ALD-window. The experiment was conducted for 24 h and provided evidence for onset of decomposition at 163 ºC. Since the duration is much longer than a normal ALD-cycle one may anticipate that the precursor would be suitable even at somewhat higher temperatures during ALD-growth.

The thin film growth dynamics was investigated *in situ* using QCM analysis, mainly in order to assess the effect of the different oxygen precursors. The resonance frequency of the QCM sensor is linearly dependent on the mass of the sensor, according to the Sauerbrey equation[25], and as such a sensitive tool for detection of product deposition on the sensor. However, the sensor is affected by variations in temperature, which was taken into account qualitatively when interpreting the measurements.

The effect of type of oxygen precursor on the Mo-oxide growth was studied at 167 ºC using water, ozone, and different combinations of water and ozone as reactants, see Figure 1. The observed change in QCM frequency when water is used as precursor alone is very small, and effectively there is no formation of film. The film growth is quite notable when ozone is used as oxygen source, either alone or in combination with water. Five different variations in oxygen precursors were tested (Figure 1): water (curve a), ozone (curve b), water and ozone simultaneously (curve c) and successive intro-ductions of water and ozone (curve d) or ozone and water (curve e). The highest growth rate is obtained when ozone and water are pulsed simultaneously. This was therefore chosen as the preferred procedure for growth in the remaining part of this study.

The growth dynamics for $Mo(CO)_6$ and H_2O reveals a very low overall growth rate. It was nevertheless feasible to detect a minor increase in mass or, equivalently, a small decrease in temperature during $Mo(CO)_6$ pulsing, and the opposite variation during H_2O pulsing, however, these being too small to allow quantitative considerations. When ozone is used as oxygen source (curve b), the overall growth rate of molybdenum oxide is dramatically increased, though the growth dynamics follows a similar pattern as with water (curve a). Significant variations in QCM frequency is observed also during purging. This is most probably due to thermal variations connected with ozone, both as an unstable
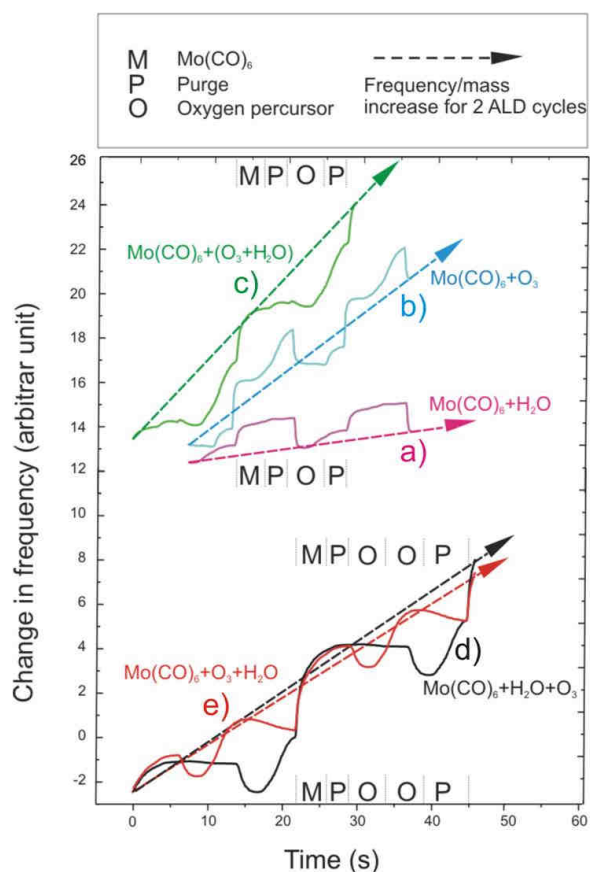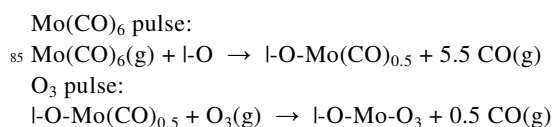

Figure 1. Growth dynamics for growth of molybdenum oxide at 167 °C, as measured by quartz crystal microbalance, using $Mo(CO)_6$ and different combinations of water and ozone as precursors. The different pulsing regions and their durations are given in the figure. The slope of the dashed lines indicates relative growth rates in terms of growth per cycle. The curves are represented by the pulsing sequences: a) $Mo(CO)_6$ + purge + H_2O + purge, b) $Mo(CO)_6$ + purge + O_3 + purge, c) $Mo(CO)_6$ + purge + (H_2O + O_3) + purge, d) $Mo(CO)_6$ + purge + H_2O + O_3 + purge, e) $Mo(CO)_6$ + purge + O_3 + H_2O + purge.

gas providing heat through its exothermic decomposition or acting as cooling agent introduced at ambient temperature. The relative role of the oxygen precursors was investigated by pulsing them sequentially in different orders. The order appears to have only a modest effect on the overall growth rate, however, from the studies it is evident that introduction of ozone affects the frequency of the sensor, probably due to variations in temperature as outlined above.

If one disregards this effect of temperature and consider the relative increase in mass for the $Mo(CO)_6$ and the following oxidant pulses, one observes that ap. 77% of the mass gain occurs during the $Mo(CO)_6$ pulse. This can be explained by the growth mechanism (l- denotes surface species; the final composition is MoO_3):
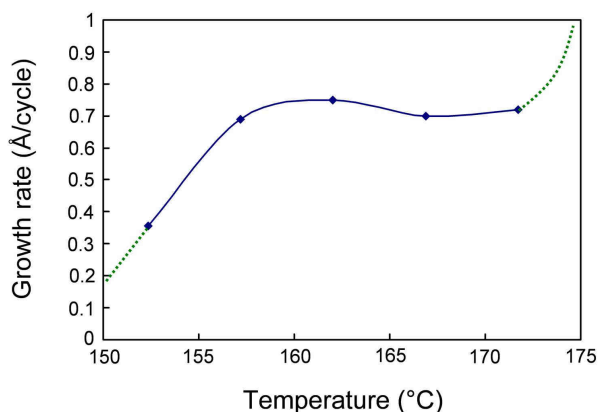
$Mo(CO)_6$ pulse:
$Mo(CO)_6(g)$ + l-O $\rightarrow$ l-O-$Mo(CO)_{0.5}$ + 5.5 CO(g)
O_3 pulse:
l-O-$Mo(CO)_{0.5}$ + $O_3(g)$ $\rightarrow$ l-O-Mo-O_3 + 0.5 CO(g)

Figure 2. Growth rates of MoO_3 as function of the substrate temperature for depositions using $Mo(CO)_6$ and $(O_3 + H_2O)$ as precursors in a pulsing scheme of 1.4 s $Mo(CO)_6$ − 1 s purge − 5 s $(O_3 + H_2O)$ pulse - 3 s purge.
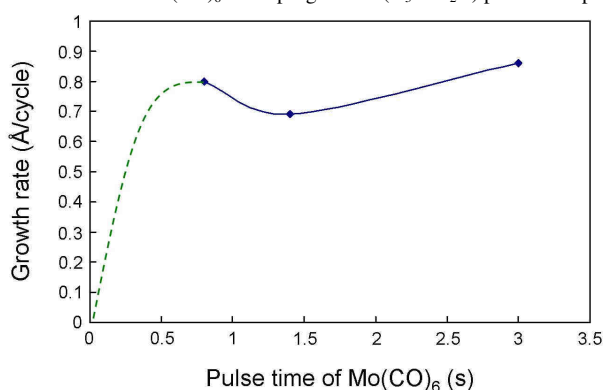

5 **Figure 3.** The effect of pulse time of $Mo(CO)_6$ on the growth rate of thin films of MoO_3 as measured by x-ray reflectivity of films made at 167 °C using 1000 cycles of $Mo(CO)_6$ − 1 s purge − 5 s $(H_2O + O_3)$ − 3 s purge.
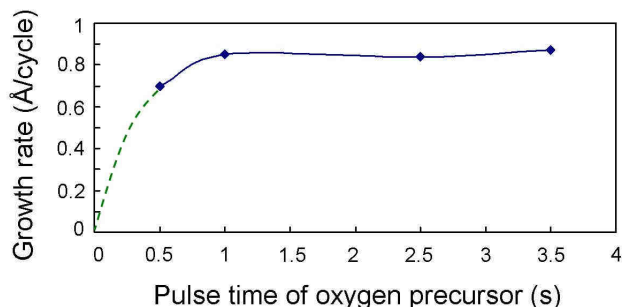

10

Figure 4. The effect of pulse time of the oxygen precursor on the growth rate of thin films of MoO_3 as measured by x-ray reflectivity of films made at 167 °C using 500 cycles of 3.1 s $Mo(CO)_6$ − 2 s purge − $(H_2O + O_3)$ −
15 6 s purge.

It is plausible that a larger number of CO ligands should remain on the adsorbed complex in order to maintain a self hindered growth. The suggested mechanism should rather be
20 treated as indicative. It is difficult to assess the implications of temperature effects, however, they ought to average out and have no overall impact. The data considered were recorded within a longer pulsing campaign and chosen for a region where thermal effects was interpreted to have reached a steady
25 state offset and the growth rate was linear with respect to number of cycles over the chosen region. It is therefore

reasonable to assume that the overall variation in frequency is due to mass effects, although frequency changes within a cycle may be affected by thermal reactions.

30   The effect of deposition temperature on the growth rate was investigated by depositing thin films during 1000 cycles in the temperature range 152 - 172°C (Figure 2). Thin films with good uniformity were obtained in the temperature range 157 - 172 °C with a rather constant growth rate of approximately
35 0.70 Å/cycle. The growth is probably limited by reduced reactivity of the $Mo(CO)_6$ at the lower temperatures, whereas the upper range is limited by thermal decomposition of the precursor. CVD tests were performed for both the $Mo(CO)_6$ and oxygen precursors at temperatures of 157, 167 and 172 °C
40 without any evidence of uncontrolled growth. Considering the crystal structure of MoO_3[26], a growth rate of 0.70 Å/cycle indicates a surface utilisation of about 18% for each cycle, inducing ap. 5.6 cycles for achieving one crystalline layer of MoO_3 material. This indicates that the number of remaining
45 CO ligands on the adsorbed complex is larger than what suggested by the mechanism from the QCM data, alternatively that the reactivity towards the substrate is limited
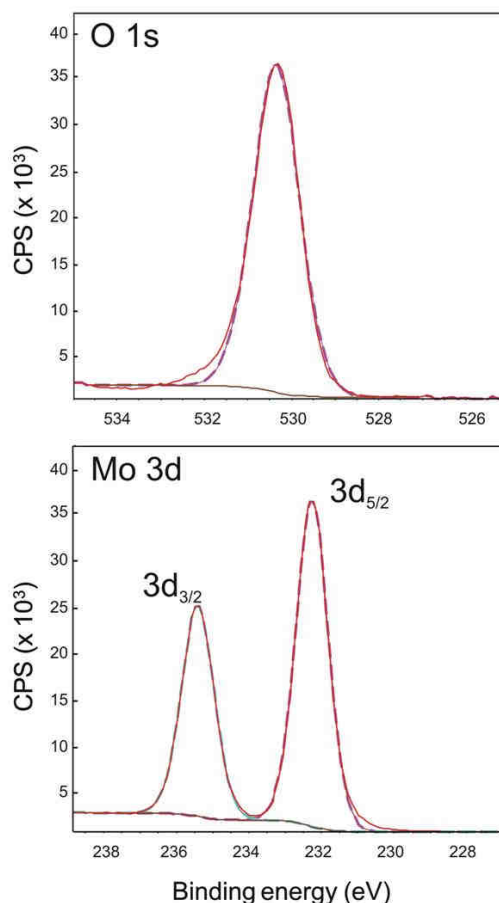by a low number of active sites.

50

Figure 5. Bonding energies, as measured by XPS for thin films deposited using $Mo(CO)_6$ pulses for 1.4 s, ozone and water 3 s, 152 °C and 1000 cycles.
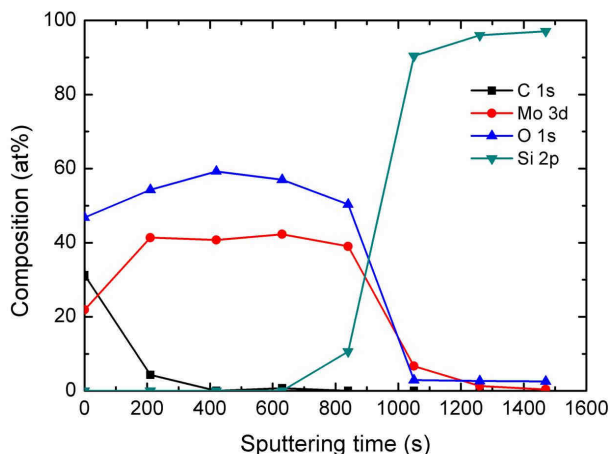
Figure 6. Elemental composition as function of Ar sputtering time, as measured by XPS for a thin film deposited using $Mo(CO)_6$ pulses for 3.1 s, purge 2s, ozone and water 3 s, purge 6s, at 167 °C and 500 cycles.

The effect of the precursors pulse durations on the growth rate was investigated at a temperature of 167 °C in order to verify self-limiting growth. The effect of pulse time of $Mo(CO)_6$ proved no visible gradients for pulse times of 1.4 s and above (Figure 3). For the investigation of the effect of the duration of the oxygen precursor (mixed water and ozone at the same time), gradient free films and a constant growth rate of 0.85 Å/cycle was obtained for pulse times of 1 s and above (Figure 4). This verifies a self-limiting nature of the film growth for both precursors.

The bonding states in the surface layers of the thin films of MoO_3 deposited at 152 and 167 °C and the film annealed at 600 °C were probed by means of XPS. There were no significant differences in the collected XPS data for any of the temperatures, and Figure 5 shows the obtained spectra for the film deposited at 152 °C. The energy scale was defined by adjusting the C(1s) binding energy for the omnipresent air-borne hydrocarbons to 284.6 eV. The obtained data are well modelled by the Mo3d5/2,3/2 (at 232.396 and 235.552 eV) and O1s (at 530.317 eV) peaks (dashed lines on the Figure) for the oxide MoO_3[27]. This shows that for the as deposited amorphous films and the annealed films at 600 °C, the top layer of the films are of MoO_3. In order to characterise the bulk of the film, Ar sputtering has been applied during the XPS analysis on a film deposited at 167 °C. The elemental composition as function of the time of sputtering of this sample is shown in Figure 6. The quantitative XPS depth profiling shows that the carbon level in the bulk of the film is below the detection limit (about 0.1 at %), which indicates that the carbon on the surface of the film is post deposited. Angle resolved XPS measurements on a 10 nm thin film was perfomed to investigate a possible variation in oxidation state of Mo between bulk and surface. This proved that Mo was hexavalent all from the surface to the substrate and that any indications of variations in oxygen level in Figure 6 are due to the Ar sputtering.
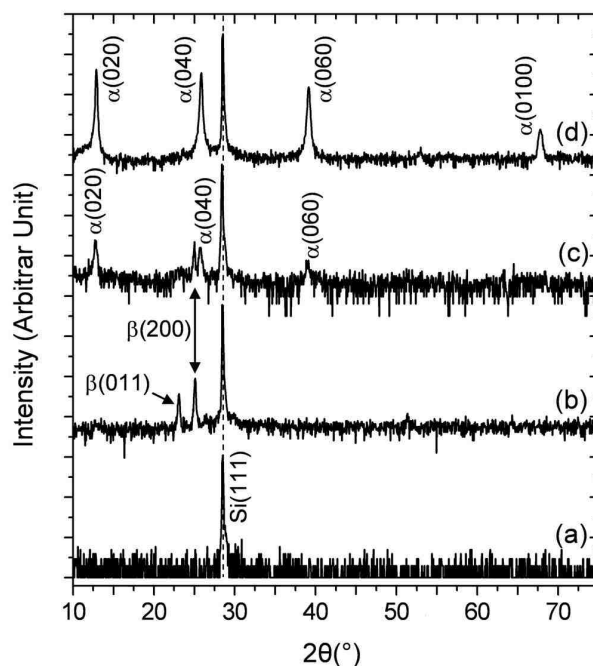

Figure 7. X-ray diffraction pattern obtained for thin film grown at 167 °C on Si (111) substrate; a) as grown, b) annealed for 12 minutes at 500 °C in air, c) annealed for 15 minutes at 500 °C in air and d) annealed for 15 min in air at 600 °C.
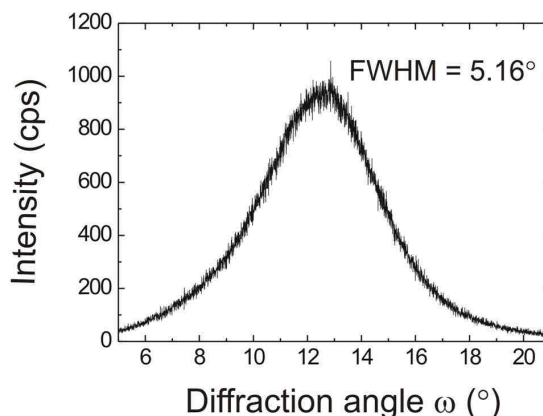

Figure 8. Rocking curve profile of the α-MoO_3 (040) reflection on Si(111) substrate for film annealed for 15 min in air at 600 °C.

Selected thin films deposited in the temperature range 152 – 172 °C using 1000 cycles were analysed by x-ray diffraction in order to assess crystallinity and phase content. However, the x-ray data proved all as-deposited films to be amorphous (Figure 7 a). Selected samples were annealed for 15 minutes in air at 200, 300, 400, 500, and 600 °C, respectively (Figure 7). There were no indications of crystallisation in any of the samples annealed at temperatures below 500 °C. For annealing at 500 °C for 12 minutes a pure β-MoO_3 was obtained, but when annealed at 15 minutes a second phase appeared and a two-phase mixture of α- and β-MoO_3 was observed[28]. When annealed at 600 °C only the orthorombic α-MoO_3 phase was observed[29, 30], and the peak intensities were highly improved. All observed reflections for the α-MoO_3 phase are of the (0k0) type, indicating an orientation of the *b*-
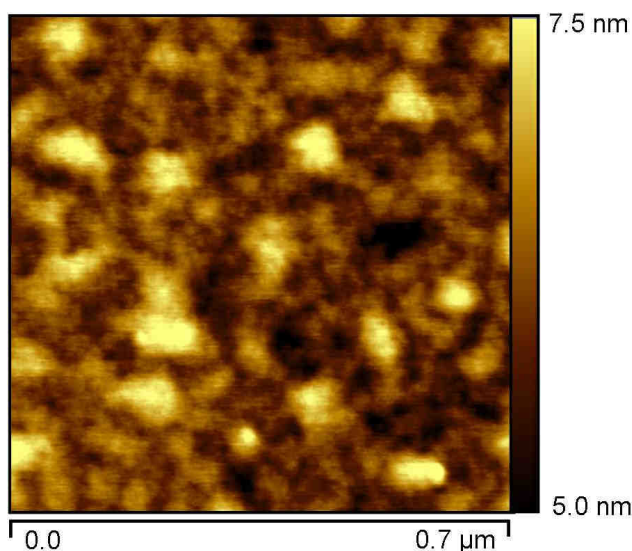
Figure 9. Topography as measured by AFM for a MoO₃ film deposited on Si(111) at 167 ºC. Total film thickness is about 75 nm.
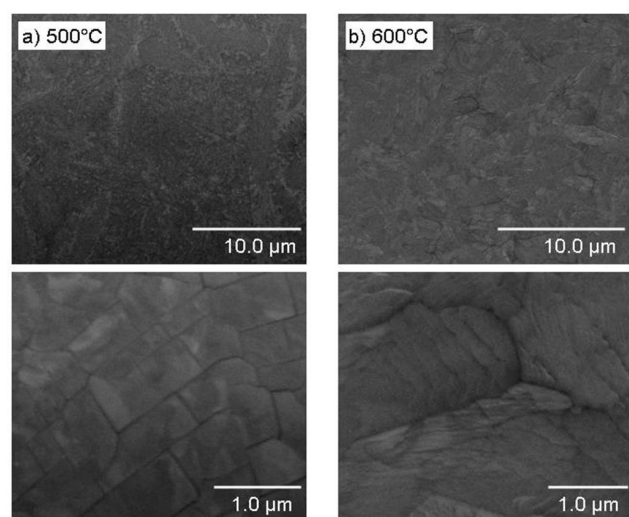

Figure 10. SEM pictures of thin films of MoO₃ annealed for 15 min at a) 500 °C and b) at 600 °C.

axis normal to the substrate surface. The calculated *b*-axis of the orthorhombic structure is 13.82 Å ±0.02. Rocking curve analysis of the (020), (040) and (060) reflections showed for each reflections one single peak which could be fitted by a Gaussian shaped curve. See Figure 8 for the rocking curve of the α-MoO₃ (040) reflection which is representative for all the obtained rocking curves. This resulted in peak full widths at half maximum (FWHM) for the (020), (040), and (060) reflections of 4.46, 5.16 and 5.05°, respectively. The fact that the FWHM is almost the same for the different reflections indicates that the broad rocking curves are due to tilt in a fibrous or columnar texture of the sample rather than limited crystallite size.

The topographies of selected films were investigated by AFM and SEM and reveal a very low roughness for as deposited films (root mean square (RMS) = ap. 0.5 nm Figure 9), which is typical of amorphous materials. It was not possible to measure the topographies for annealed films by AFM since their large roughness repeatedly damaged the AFM probe tips, but SEM analysis of the films annealed at 500 and 600 ºC during 15 minutes in air, confirm rather rough surfaces (Figure 10). The SEM images obtained for the film annealed at 600 ºC show a surface terminated by crystallites of a lamellar structure, whereas the topography for the film annealed at 500 ºC show indications of cracking during the annealing procedure.

The present study has shown that metal carbonyls can be used as precursor for deposition of oxides by ALD. The ALD window is relatively small, but clearly present. It is limited at high temperature by its thermal stability, and probably at low temperatures by its limited reactivity. It may therefore seem that applications of metal carbonyls are limited to application near its thermal decomposition region, which is relatively low. The low reaction temperature is one of the main asset of the ALD growth, but also the uniformity and low roughness of the films. Indeed, these are the main characteristics of the films provided by using a metal carbonyl as precursor in this study.

Conclusions

Thin film growth of MoO₃ has been demonstrated by the ALD technique using molybdenum-hexacarbonyl, water and ozone as precursors at relatively low temperatures. A narrow ALD-window is observed between 157 and 172 ºC. QCM investigations have assessed the effect of different oxygen precursors on the growth mechanism of the molybdenum oxide. The films are amorphous as deposited, and crystallize to the α-MoO₃ phase upon annealing in air at 600ºC.

Acknowledgements

Notes and references

University of Oslo, Department of Chemistry, Innovative Natural Gas Processes and Products, Centre for Material Science and Nanotechnology, Oslo, Norway. Fax: +47 228 55 441 ;
Tel: +47 228 55 535;
E-mail: madeleine.diskus@kjemi.uio.no

1   S. S. Mahajan, S. H. Mujawar, P. S. Shinde, A. I. Inamdar, P. S. Patil, *Applied Surface Science,* 2008, **254**, 5895.
2   T. Ivanova, K. A. Gesheva, G. Popkirov, M. Ganchev, E. Tzvetkova, *Materials Science and Engineering B,* 2005, **119**, 232.
3   J. Scarminio, A. Lourenço, A. Gorenstein, *Thin Solid Films* 1997, **302**, 66.
4   Z. Song, N. Mimura, J. J. Bravo-Suárez, T. Akita, S. Tsubota, S. T. Oyama, *Applied Catalysis A: General,* 2007, **316**, 142.
5   E. A. El-Sharkawy, A. S. Khder, A. I. Ahmed, *Microporous and Mesoporous Materials,* 2007, **102**, 128.
6   K. V. R. Chary, K. R. Reddy, G. Kishan, J. W. Niemantsverdriet, G. Mestl, *Journal of Catalysis,* 2004, **226**, 283.

7   J. B. Wagner, N. D. Othman, D. S. Su, S. B. A. Hamid, R. Schlögl, *Journal of Microscopy,* 2006, **223**, 216.

8   O. M. Hussain, K. S. Rao, *Materials Chemistry and Physics,* 2003, **80**, 638; DOI: 10.1016/s0254-0584(03)00101-9.

9   H. Ohtsuka, Y. Sakurai, *Solid State Ionics,* 2001, **144**, 59.

10   T. S. Sian, G. B. Reddy, A. Babu, *Physica E: Low-dimensional Systems and Nanostructures,* 2009, **41**, 408.

11   R. M. Guerrero, J. R. V. Garcia, V. Santes, E. Gomez, *Journal of Alloys and Compounds,* 2007, **434-435**, 701.

12   T. Itoh, I. Matsubara, W. Shin, N. Izu, *Thin Solid Films,* 2006, **515**, 2709.

13   H. Kim, H.-B.-R. Lee, W. J. Maeng, *Thin Solid Films,* 2009, **517**, 2563.

14   M. Leskelä, M. Ritala, *Thin Solid Films,* 2002, **409**, 138.

15   M. Ritala, M. Leskelä, in *Handbook of Thin Films*, 2002, 103.

16   R. L. Puurunen, *Journal of Applied Physics,* 2005, **97**, 52.

17   L. Hiltunen, M. Leskelä, M. Mäkelä, L. Niinistö, E. Nykänen, P. Soininen, *Thin Solid Films,* 1988, **166**, 149.

18   M. Juppo, M. Ritala, M. Leskela, *Journal of The Electrochemical Society,* 2000, **147**, 3377.

19   V. Miikkulainen, M. Suvanto, T. A. Pakkanen, *Chemistry of Materials,* 2006, **19**, 263.

20   M. Juppo, M. Vehkamaki, M. Ritala, M. Leskela, *Journal of Vacuum Science & Technology A: Vacuum, Surfaces, and Films,* 1998, **16**, 2845.

21   K.-E. Elers, M. Ritala, M. Leskelä, E. Rauhala, *Applied Surface Science,* 1994, **82-83**, 468-474.

22   V. M. Mecea, J. O. Carlsson, R. V. Bucur, *Sensors and Actuators A: Physical,* 1996, **53**, 371.

23   A. L. Smith, H. M. Shirazi, S. R. Mulligan, *Biochimica et Biophysica Acta (BBA) - Protein Structure and Molecular Enzymology,* 2002, **1594**, 150.

24   O. Nilsen, H. Fjellvåg, A. Kjekshus, *Thermochimica Acta* 2003, **404**, 187.

25   G. Sauerbrey, *Zeitschrift für Physik A Hadrons and Nuclei,* 1959, **155**, 206.

26   G. L. O. Glemser, *Z. Anorg. Allg. Chem.,* 1950, **263**, 2.

27   Z. Li, L. Gao, S. Zheng, *Applied Catalysis A: General,* 2002, **236**, 163.

28   S. H. Mohamed, S. Venkataraj, *Vacuum,* 2007, **81**, 636.

29   A. Bouzidi, N. Benramdane, H. Tabet-Derraz, C. Mathieu, B. Khelifa, R. Desfeux, *Materials Science and Engineering B,* 2003, **97**, 5.

30   C.-S. Hsu, C.-C. Chan, H.-T. Huang, C.-H. Peng, W.-C. Hsu, *Thin Solid Films,* 2008, **516**, 4839.

Paper II

"Combination of characterization techniques for ALD MoO$_3$ coatings: from the amorphous to the orthorhombic alpha-MoO$_3$ crystalline phase"

M. Diskus, O. Nilsen, S. Diplas, P. Beato, C. Harvey, E. van Schrojenstein Lantman, B. M. Weckhuysen and H. Fjellvåg,

Combination of characterization techniques for ALD MoO_3 coatings: from the amorphous to the orthorhombic α–MoO_3 crystalline phase

Madeleine Diskus*[a], Ola Nilsen [a], Spyros Diplas [a-b], Pablo Beato [c], Clare Harvey [d], Evelien van Schrojenstein Lantman [d], Bert M. Weckhuysen [d] and Helmer Fjellvåg [a]

[a] University of Oslo, Department of Chemistry, Innovative Natural Gas Processes and Products, Centre for Material Science and Nanotechnology, N-0315 Oslo, Norway
[b] Sintef Materials and Chemistry, N-0314 Oslo, Norway
[c] Haldor Topsøe, Nymøllevej 55, DK-2800 Kgs, Lyngby, Denmark
[d] Inorganic Chemistry and Catalysis, Debye Institute for NanoMaterials Science, Utrecht University, 3584 CA Utrecht, The Netherlands

madeleine.diskus@kjemi.uio.no

Abstract

Thin films of MoO_3 deposited on Si(111) and Al_2O_3(001) substrates by atomic layer deposition (ALD) have been investigated by x-ray photoelectron spectroscopy (XPS), atomic force microscopy (AFM) and Raman spectroscopy for detailed characterisation of composition and morphology. Comparison of Angle Resolved XPS (ARXPS) and XPS depth profiles based on Ar^+ sputtering are reported. Sputtering induces a reduction of molybdenum in MoO_3 from +IV to metallic Mo as the interface towards Si is approached, whereas ARXPS on a 10 nm thin film show that Mo(VI) remains outside the interface towards Si where lower valent molybdenum compounds are formed. Upon annealing, the as-deposited amorphous thin films of MoO_3 crystallize into β- or α-MoO_3 as identified by x-ray diffraction (XRD). The current study provides a convenient route towards formation of metastable β-MoO_3 and a full crystallization pathway from amorphous to crystalline α-MoO_3. Combined AFM and Raman analysis have been performed on thin films of α-MoO_3 deposited on Al_2O_3(001) and prove that the crystallization proceeds via island growth at 600 ℃. The Raman intensity ratios between different bands depend strongly on morphology and size of crystalites.

Introduction

Progress in materials science and technology requires frequently model systems where characteristic parameters are well controlled and detailed studies facilitated. Thin films are increasingly used as such model materials, especially in catalysis, due to the possibility of controlling bulk and surface properties. A very suitable method for growth of such thin film model systems is atomic layer deposition (ALD) which exploits self-limiting processes between gaseous precursors and surfaces. The technique offers good control over

composition and thickness of the films([1-4]) as well of texture and topography in certain cases ([5]). Furthermore, a wide range of characterization techniques are available to investigate films and coatings deposited on flat surfaces. This includes in situ methods, such as Raman and Fourier transform infrared spectroscopy(FTIR)([6, 7]), quartz crystal microbalance (QCM) ([8]), and mass spectrometry (MS)([9, 10]).

Molybdenum trioxide MoO_3 is of interest for wide applications in electrochromic devices([11]), gas sensors([12]) and catalysis([13, 14]). Despite intense studies, the difference in catalytic activity between the α- and β-MoO_3 polymorphs is still not fully understood([15]). For instance, metastable β-MoO_3 has higher catalytic activity in the synthesis of formaldehyde than the stable α-MoO_3 phase ([15]). Moreover, molybdenum oxides are used as catalysts in the oxidation of alkenes where the catalytic mechanism proceeds via a redox mechanism of the molybdenum oxide. Therefore reduction of MoO_3 and oxidation of MoO_2 has attracted considerable attention([16, 17]). The Mo-O chemistry is very complex, ranging from Mo_3O to MoO_3 and includes a number of mixed valence compounds, particularly in the MoO_3 - MoO_2 range. Furthermore, in lithium batteries β-MoO_3 forms lithium molybdenum bronzes as active electrode materials while α-MoO_3 may prevail as impurity([18, 19]). To be able to establish improved structure - property relationships it is of fundamental interest to have access to well defined model materials of MoO_3 polymorphs in pure form, including thin films.

Amorphous thin films of MoO_3 have previously been grown by ALD using molybdenum hexacarbonyl and a mixture of water and ozone as precursors ([20]). A simple and convenient way to achieve crystalline films of both the α- and β-polymorphs was found by annealing in air. In this way model materials can be made for further studies of effects of processing, polymorph development, and crystallization, as well as physical performance. This calls for careful characterization of MoO_3 thin films made by ALD and subsequent calcinations.

The present study focuses on a simple and convenient process to design and grow thin film model materials of polymorphs of MoO_3 and subsequent characterisation. This includes studies of the amorphous as-deposited films, studies of crystallization pathways, and characterization of annealed MoO_3 thin films.

TEM analysis of cross sections and interfaces of MoO_3 films is cumbersome due to difficulties in sample preparation since the material dissolves easily in water. Alternative characterization tools have been combined in the current work where chemical information have been collected by means of Ar^+ sputtering for depth profiled XPS([21]) as well as Angle Resolved XPS([22, 23]). Attention has been paid to the possibility of reducing the initial

oxidation state of molybdenum during sputtering(*24, 25*) by comparing spectral information derived by the two types of XPS experiments. The second part of this work focuses on structural conversions of as-deposited amorphous films of MoO_3 into metastable β-MoO_3 and orthorombic α-MoO_3 upon annealing. Combined AFM and Raman investigations have been performed in order to associate distinctive morphology changes upon calcination to the crystalline polymorphs and to investigate direct correlations between size and shape of particles on vibration modes and Raman shift intensities.

Experimental details

Thin films of MoO_3 were deposited in a commercial F-120 Sat reactor (ASM Microchemistry Ltd.) using ozone, water and $Mo(CO)_6$ (molybdenum hexacarbonyl 98%, Aldrich) as precursors. Solid $Mo(CO)_6$ was introduced at room temperature into a bubbler, using nitrogen as carrier gas. Ozone was generated by feeding O_2 (99.999% AGA) into an OT-020 ozone generator (Ozone Technology), providing O_3 concentrations of about 15 vol.% according to specifications. An ozone flow of approx. 500 cm^3 min^{-1} was used during the ozone pulses. During all depositions, a background pressure of approx. 3.5 mbar was obtained by applying a N_2 carrier gas flow of 300 cm^3 min^{-1}. The gas was produced in a Schmidlin UHPN3001 N_2 purifier with a claimed purity of 99.999% with respect to N_2+Ar content. The films were deposited on substrates of single crystalline Si(111) and on alumina wafers. The depositions were done at 167 ºC using a total of 500 cycles, giving films thicknesses of about 40 nm (*20*). Selected as-deposited films were post-annealed in air at 400 and 600 ℃, for 4 to 8 minutes.

The films were examined with a Siemens D5000 X-ray diffractometer equipped with a Göbel-mirror providing parallel CuKα-radiation. The setup was used to measure X-ray reflectivity (XRR) and X-ray diffraction (XRD) in reflection mode. X-ray photoelectron spectroscopy (XPS) was performed on a Kratos Axis Ultra Instrument using monochromatic AlKα-radiation produced by an anode operated at 15 kV and 10 mA. The pressure in the analysis chamber during measurements was 6 - 7·10^{-9} mbar. Depth profiles were obtained both destructively by Ar+ etching (2 keV) and non-destructively by angle resolved ARXPS studies on a 10 nm thick MoO_3 film deposited on Si(111). For the latter, the spectra were acquired at emission angles of 0º, 33º, 46º, 54º, 59º(*26*). For zero angle the emitted electrons were normal to the sample surface. At this angle the photoelectrons are emitted from the bulk of the film whilst at 59° the analysis is rather surface sensitive. C 1s spectra were used for calibration of recorded binding energies for as-deposited films.

Selected films were studied with atomic force microscopy (AFM; XE-70 Park System) to characterize topography and roughness. Raman spectra were recorded on a Jobin Yvon LabRam confocal microscope, equipped with a He-Ne-laser (632.8 nm, Melles Griot, 17 mW) used for excitation. The laser light was focused onto the sample using a 50x long distance objective lens (Olympus). The confocal hole was set to 200 μm and the entrance slit to 100 μm resulting in a spectral width of 2 cm^{-1}. Each recorded spectrum is the average of 3 data accumulations, each with an integration time of 60 seconds. Optical filters were used to adjust the laser power at the sample to ~ 1 mW. A combined AFM/Raman setup was used, with an NT-MDT NTEGRA Spectra upright AFM unit integrated with a Renishaw InVia Raman microscope. For all Raman measurements a 100x 0.6 NA Mitutoyo objective, and a 300 mW 785 nm diode laser were used. Olympus AC 160TS 'elephant trunk' tips were used for all AFM and AFM-Raman measurements.

Results and discussion

The homogeneity of the deposited films was studied by XPS depth profiling using Ar$^+$ sputtering. A 40 nm thick film of MoO_3 deposited on Si(111) was selected. A montage of acquired survey spectra is shown Figure 1. The XPS spectra recorded at etching time 0 s corresponds to the initial surface. The interface between the molybdenum oxide and the Si(111) substrate is identified at etching times between 840 and 1050 s by vanishing intensity of the Mo 3d peak and appearance of Si 2s and Si 2p signals. In Figure 2, the Mo 3d spectrum recorded from the outermost surface of the film shows the characteristic 3d$_{3/2}$ and 3d$_{5/2}$ doublet due to spin orbit coupling at binding energies 235.41 and 232.34 eV in good agreement with literature values for Mo(VI) in MoO_3[27]. After etching by Ar$^+$ ions for 210 s, a shift of the doublet position occurs towards lower energies, 232.35 and 229.15 eV for Mo 3d$_{3/2}$ and Mo 3d$_{5/2}$, respectively. Ar$^+$ induced reduction is frequently encountered for transition metal oxides, and it is well known that Ar$^+$ ion etching causes oxygen deficiency in the MoO_3 structure yielding Mo-species of lower valence [21, 24, 25]. Due to the complexity of the Mo-O system, it is not possibly to make any phase assignments during this stage of the XPS measurements. Between 210 and 630 s of sputtering most Mo(VI) has been reduced to Mo(IV), i.e. MoO_2[25]. After 840 s a further shift of 0.25 eV towards lower binding energies is observed, indicating further reduction. A larger shift is seen after 1050 s of sputtering. The values of the Mo 3d$_{3/2}$ and 3d$_{5/2}$ signals at the final stage are 230.65 and 227.5 eV respectively, close to values for metallic Mo[25]. We conclude that Ar$^+$ ion etching reduces Mo(VI) to Mo(IV) until a thin layer of MoO_x remains at the interface between the film and the substrate, which finally is reduced to metallic Mo. There is no change in the O 1s spectra for

sputtering times between 0 and 840 s, Figure 2. This is in accordance with literature(*24*) showing that O 1s values for Mo oxides remains around 530.70 eV. The fact that O 1s is not shifted provides confidence that the shifts in Mo(3d) positions are not energy referencing related. The C 1s spectra in Figure 3 show that carbon is present only at the surface of the film as post deposition contaminations whilst the Si(2p) spectra exhibit no change in binding energy between the interface and the Si(111) substrate proving that molybdenum silicides have not formed. The element composition profile upon Ar^+ etching as function of depth show reduced oxygen amounts consistent with the Mo 3d shifts rationalized in terms of reduction of MoO_3 to MoO_2 and absence of carbon in the bulk of the film.
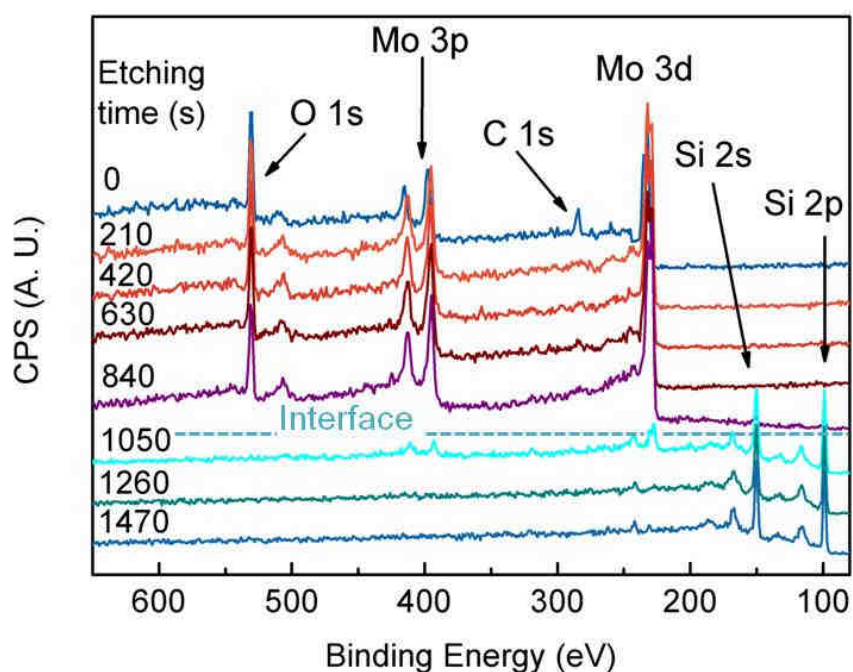

Figure 1: XPS survey spectra of a MoO_3 thin film deposited on Si(111) by ALD as function of exposure time to Ar^+ etching.
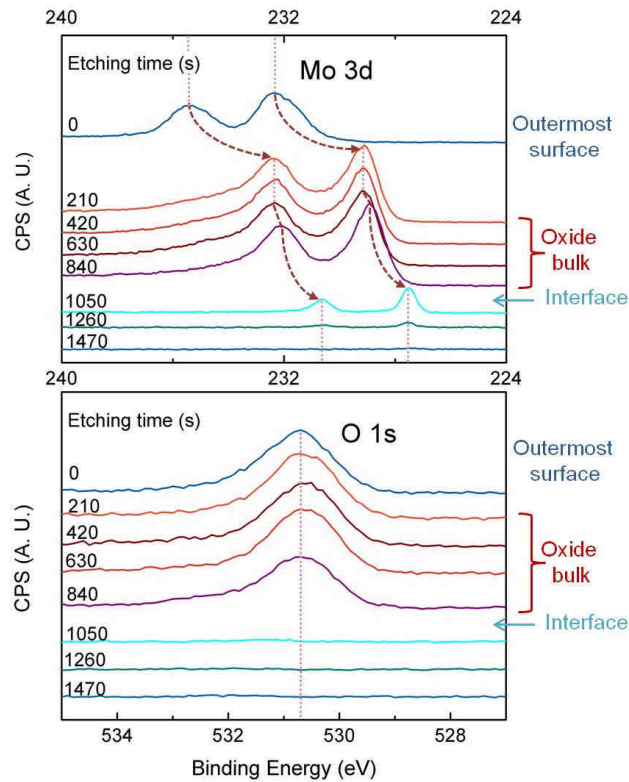
Figure 2: High resolution XPS core level Mo 3d and O 1s spectra of a MoO$_3$ thin film deposited on Si(111) by ALD as function of exposure time to Ar$^+$ sputtering.
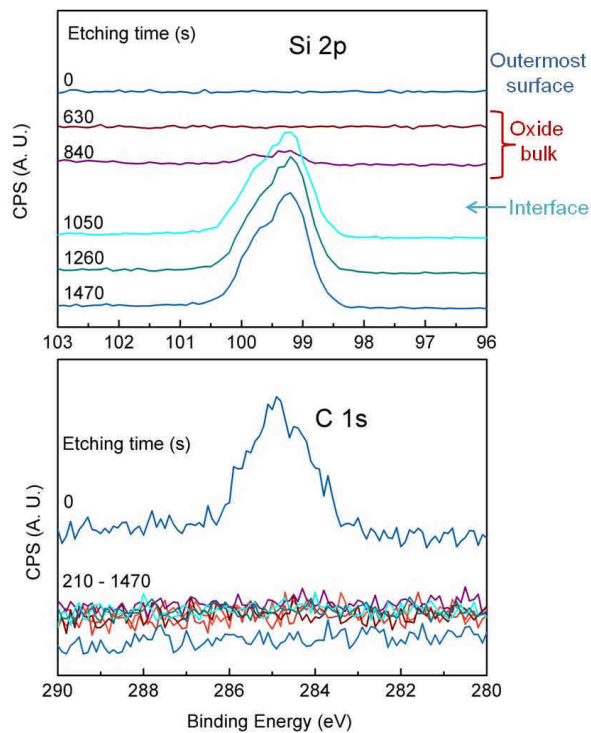

Figure 3: High resolution XPS core level peaks Si 2p and C 1s measured for a MoO$_3$ thin film deposited on Si(111) by ALD and etched by Ar$^+$.

In order to avoid the undesired effect of oxide reduction upon sputtering the MoO_3 thin film structure was investigated by angle resolved XPS. A 10 nm thick film was selected. High resolution XPS spectra for Mo 3d, O 1s and C 1s were acquired with ARXPS. All peaks exhibited a 0.05 eV shift towards higher binding energies with increasing angle of emission [i.e. increasing surface sensitivity], however, since being similar for both Mo 3d, O 1s and C 1s it was concluded that the shift is due to systematic changes connected with the energy reference and not indicative of changes in material chemistry (Figure 4). The constant energy of the Mo 3d peak with varying angle of emission proves that the chemical state of Mo is unperturbed troughout the film with constant composition MoO_3. Figure 5 shows the high resolution spectra for the core level Mo 3d at $0°$ emission angle, corresponding well to Mo(VI) (235.96 and 232.82 eV for Mo $3d_{3/2}$ and Mo $3d_{5/2}$, respectively). Note that a tiny contribution of Mo in lower oxidation states (between VI and IV) is indicated by the small shoulder at energies of 234.82 and 231.76 eV, see Figure 5. This contribution indicates that the interface is also visible in the spectra collected for the 10 nm thick film that basically are dominated by bulk nucleated MoO_3. The lower oxidation state is suggested caused by nucleation and interface effects. When subjecting this film to Ar^+ sputtering for 10 s the Mo 3d signal was again shifted towards lower binding energy, as discussed above. The Si 2p high resolution spectra from ARXPS loose intensity on turning the emission angle from $0°$ to of $59°$, see Figure 6. This shows that the Si(111) substrate was covered by a continuous 10 nm film of MoO_{3-x} and notably not of MoO_{3-x} islands. In summary, these two sets of XPS data prove successful deposition of uniform and homogeneous films of molybdenum trioxide.
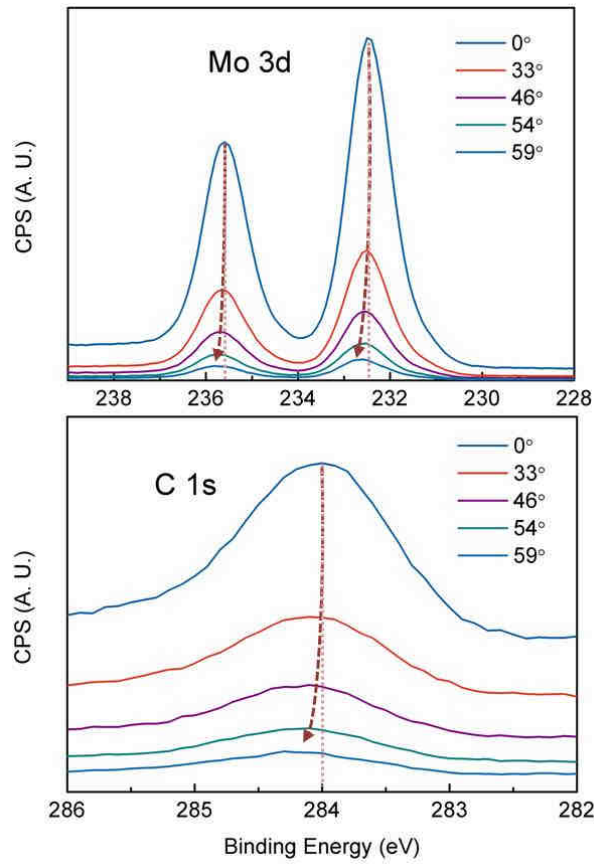
Figure 4: Angle dependent XPS data for core level Mo 3d and C 1s peaks from a 10 nm MoO$_3$ thin film deposited by ALD on Si(111).
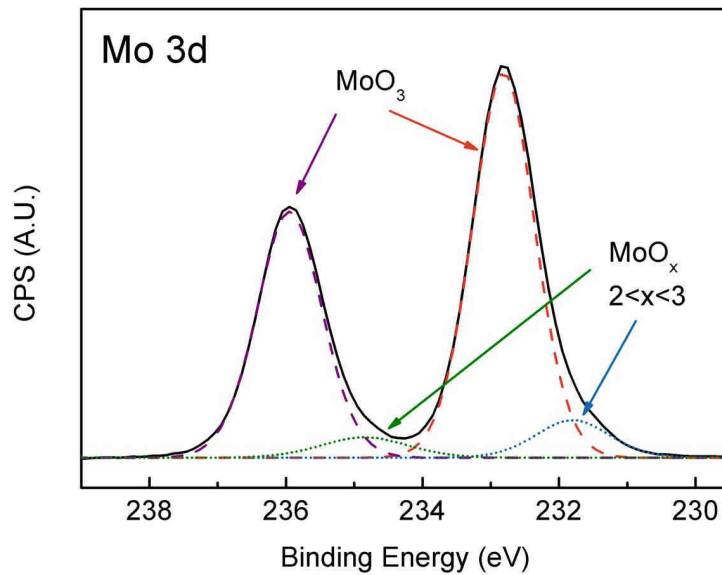

Figure 5: High resolution XPS core level peaks for Mo 3d at 0° emission angle from a 10 nm MoO$_3$ film deposited on Si(111) by ALD.
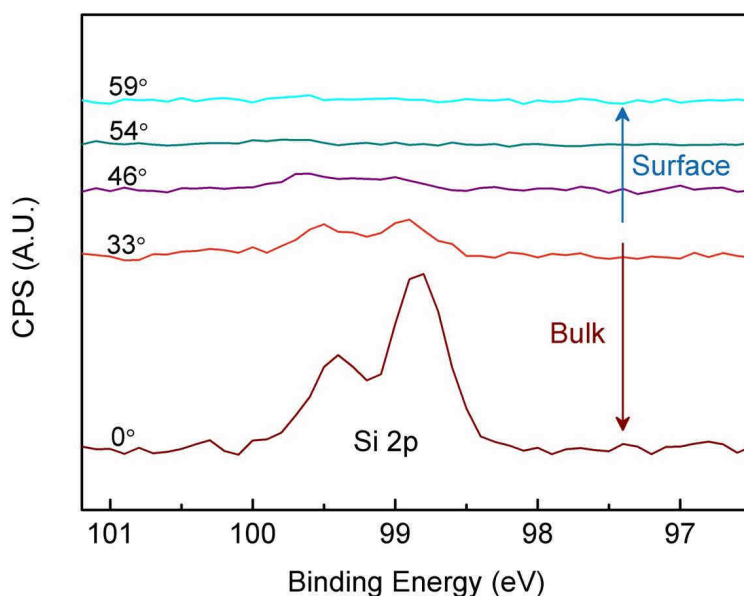
Figure 6: Angle dependent XPS data for Si(2p) core level of a 10 nm MoO_3 film deposited on Si(111) by ALD.

The crystallisation behaviour of the 40 nm amorphous films of MoO_3 on Al_2O_3 was studied ex situ for samples subjected to annealing in air (8 minutes at 400°C, 4 minutes, 6 minutes and 7.5 minutes at 600°C). These treatments resulted in conversion of amorphous MoO_3 via β-MoO_3 to orthorhombic α-MoO_3 (Figure 7) as evidenced by XRD, AFM and Raman. The X-Ray data show that the film annealed for 8 minutes at 400°C consists of crystalline β-MoO_3 (28) with small impurities of α-MoO_3 (Figure 7). However, when annealed at 600°C for 4 minutes or more, the films consists of polycrystalline α-MoO_3, Figure 7(28). The conversion of β- to α-MoO_3 is reconstructive. For bulk samples the conversion is reported to take place between 250 and 450°C in good agreement with present observations(15). Topography analysis of these films by AFM (Figure 8) show that the amorphous MoO_3 is very uniform and has a smooth base layer with small grains of approx. 6 nm in diameter protruding from the surface. During crystallization into β-MoO_3, the smooth base layer transforms into a crystalline structure of main axial flakes with spikes growing perpendicular to the central axis (Figure 8b). The height of these features is about 10 nm, however, with the 6 nm grains still residing on the surface. For the films annealed at 600°C pronounced crystalline features evidenced by flakes protruding from the surface appear. The large height of these features, 140 nm, implies that MoO_3 now forms islands and exposes parts of the Al_2O_3 substrate, however, still small 6 nm grains are present on the base layer (Figure 8c). At this stage the film transforms from β-MoO_3 into fully crystalline α-MoO_3. After annealing for 7.5 minutes at 600°C, the small grains and the base layer have disappeared while the crystalline floral

morphology remains. Similar features were observed by AFM for α-MoO₃ films deposited on Si(111) and annealed at 600 °C. This indicates that crystallization and morphology is independent of the substrate.

Raman spectra were recorded for the MoO₃ films described above, see Figure 9. The crystal structure of α-MoO₃ contains three non-equivalent oxygen atoms in the MoO₆ octahedral building units: terminal Mo=O (O1), two-fold bridged Mo-O-Mo (O2) and three-fold bridged O-Mo₃ (O3). The associated stretching vibrations correspond to the observed Raman shifts at 995 (O1), 820 (O2) and 666 cm⁻¹ (O3), see Figure 9 c, d, for samples annealed at 600 °C. For polycrystalline α-MoO₃ the relative intensity ratio is approximately $0.5(I_{995}):(I_{820}):0.2(I_{666})$. The amorphous film exhibits very broad Raman features at about 640, 850, 950 and 989 cm⁻¹, which are explained by a wide distribution of different Mo-O bond length and connectivities. The Raman spectrum for the sample heated at 400 °C corresponds to β-MoO₃ and is characterized by sharp bands at 773, 845 and 904 cm⁻¹(*12, 28*). The absence of a band around 1000 cm⁻¹ is a result of the three dimensional crystal structure of the β-phase and lack of terminal Mo=O bonds. After annealing the film for 4 minutes at 600 °C, the spectrum of β-MoO₃ disappears while evidence of α-MoO₃ appears. A background contribution from amorphous MoO₃ is still visible. This background disappears completely after annealing for 7.5 minutes at 600 °C. At this stage a weak new band at 1006 cm⁻¹ appears, Figure 9(d). This band is occasionally reported for crystalline α-MoO₃, usually only for high quality spectra. The origin of this band is still under debate. Py and Maschke assigned a very weak Raman band at 1002 cm⁻¹ observed for α-MoO₃ single crystals to an IR active crystal mode due to longitudinal-transversal splitting of the (Mo=O) Bᵤ mode of α-MoO₃ layer(*29*). Mestl *et al.* assigned a similar band in ball-milled α-MoO₃ to Mo=O bonds connected to oxygen vacancies generated during the mechanical treatment(*30*).

By combining AFM and Raman it is feasible to associate the MoO₃ polymorphs with respect to morphologies, vibration modes and Raman shift intensities. Such combined studies were performed on a 40 nm thin film of MoO₃ deposited on Al₂O₃ and annealed for 6 min at 600 °C in air. The Raman laser is now positioned at the extremity of the AFM probe. This allows collection of spectra from selected areas of the film. The topography of the α-MoO₃ film obtained by AFM and corresponding Raman spectra are shown in Figure 10. Three different types of morphologies are recognized: a random packing, here termed amorphous packing (Figure 10 b), a pyramidal packing of grains (Figure 10 c) and a floral packing of orthorombic α-MoO₃ crystals (Figure 10 d). As already discussed, the crystals form islands on the substrate and leave areas of uncoated alumina (Figure 10 a). The differences in observed

AFM features are likely due to the use of two different AFM instruments, the topographies in Fig. 10 with a combined AFM/Raman instrument. The three vibration modes of α-MoO$_3$ are observed at 672, 819 and 995 cm^{-1} in the Raman spectrum (Figure 10). The weak peak at 664 cm^{-1} for all spectra in Figure 10 is probably due to distortions of Mo-O coordinations. The collected spectra of the amorphous packing exhibit a broad background. Further the intensity of the peak at 819 cm^{-1} is very high compared to the peaks at 672 and 995 cm^{-1}. Their intensity ratio is reduced in the spectra from pyramidal and floral packings. This significant difference in relative intensities shows that the size and shape of crystallites have impact on vibration modes and Raman shift intensities. The different band intensity ratio can probably be explained by a crystal orientation effect, and would be well in line with the AFM images in Figure 8 that show highly oriented sheet-like crystals for the film annealed for 4 minutes at 600 ℃.
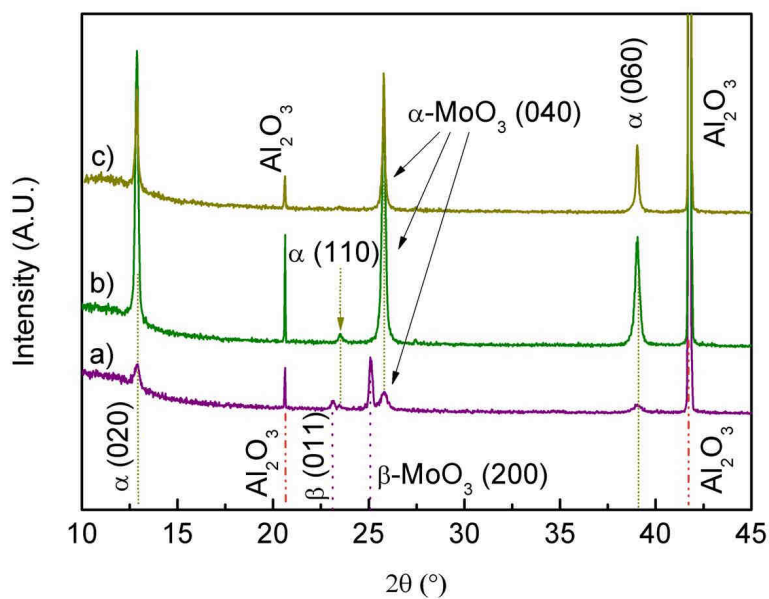

Figure 7: X-Ray diffraction pattern of 40 nm thin films of MoO$_3$ deposited on Al$_2$O$_3$ by ALD, annealed in air a) 8 min at 400 ℃, b) 4 min at 600 ℃ and c) 7.5 min at 600 ℃.
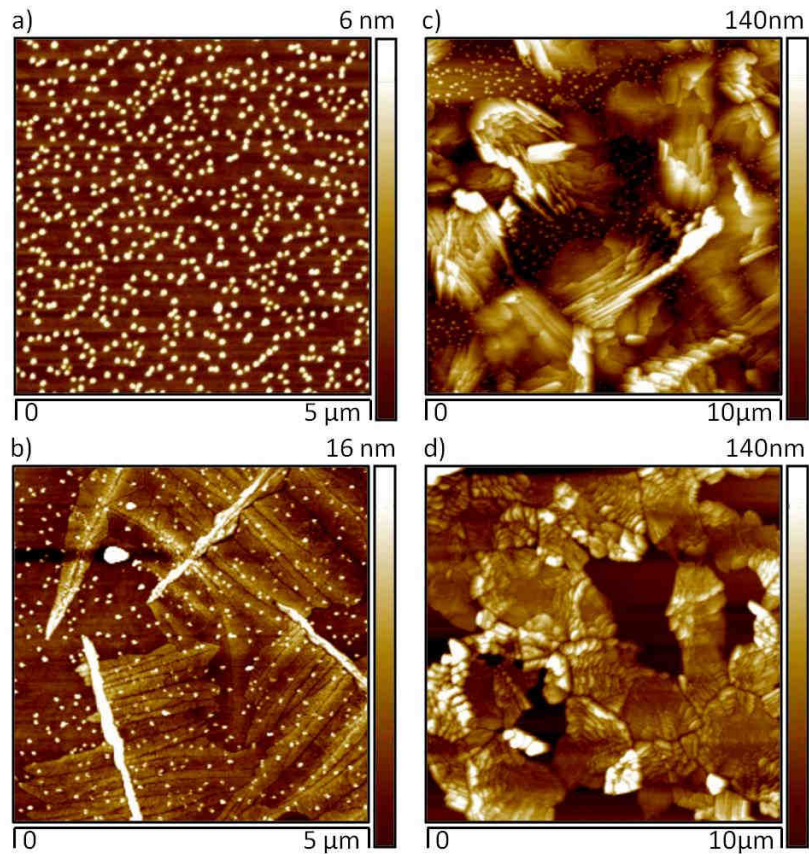
Figure 8: AFM topographies of 40 nm thin films of MoO_3 deposited on Al_2O_3 by ALD, a) as deposited, and annealed in air b) 8 min at 400 °C, c) 4 min at 600 °C and d) 7.5 min at 600 °C.
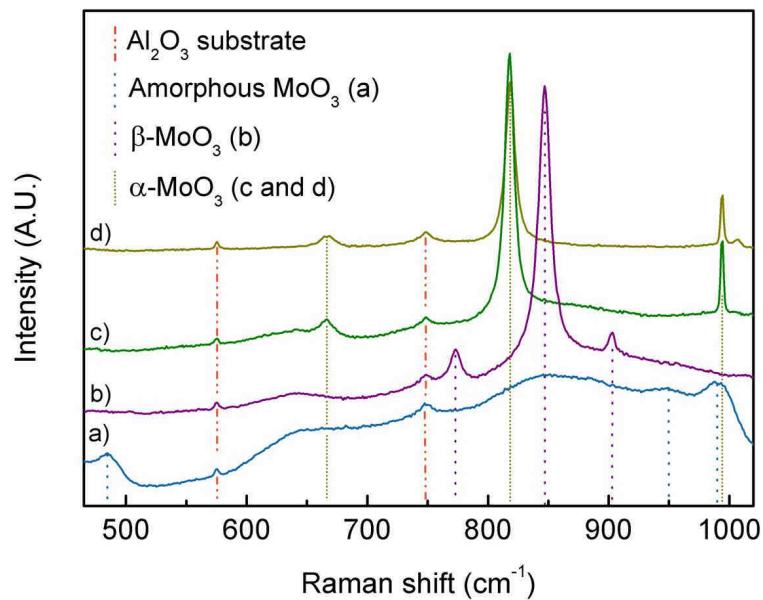

Figure 9: Raman spectra of 40 nm thin films of MoO_3 deposited on Al_2O_3 by ALD, a) as deposited, and annealed in air b) 8 min at 400 °C, c) 4 min at 600 °C and d) 7.5 min at 600 °C.
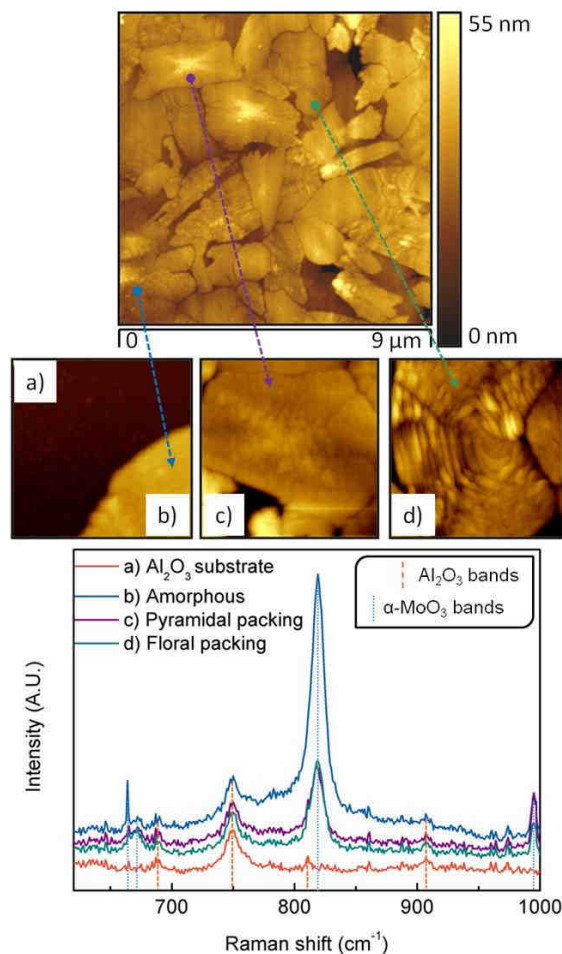
Figure 10: AFM topographies (top) and Raman spectra (bottom) of a) alumina substrate, b) amorphous packing, c) pyramidal packing and d) floral packing features of a 40 nm thin film of MoO_3 deposited on Al_2O_3 by ALD and annealed 6 min at 600 °C.

Conclusion

A convenient process to achieve thin film model materials of MoO_3 in amorphous, α- or β-MoO_3 crystalline states has been described. The chemical composition, including probing of the Mo-oxidation state througout the film structures have been investigated by two XPS approaches; depth profile studies using Ar^+ sputtering and angle resolved measurements. The sputtering based studies influences strongly the analysis results and induces reduction of the Mo-O film prior to XPS data collection. The ARXPS proves that molybdenum is in oxidation state VI throughout the entire film. Molybdenum in a lower oxidation state is still observed at the substrate interface, representing the initial stage of film formation.

The crystallization behavior of the thin films from the as-deposited amorphous state via metastable β–MoO_3 to the orthorhombic α–MoO_3 phase involves significant mass transport,

in particular during recrystallization into α-MoO₃, thereby creating areas of uncoated substrate. By means of combined AFM/Raman studies we have been able to collect specific Raman spectra for individual morpological features of the coatings and thereby relate morphology and crystallographic state (i.e. α–MoO₃ polymorphs).

Acknowledgements

References:

1. Kim, H., Lee, H.-B.-R., and Maeng, W. J. (2009) Applications of atomic layer deposition to nanofabrication and emerging nanodevices, *Thin Solid Films 517*, 2563-2580.
2. Leskelä, M., and Ritala, M. (2002) Atomic layer deposition (ALD): from precursors to thin film structures, *Thin Solid Films 409*, 138-146.
3. Ritala, M., and Leskelä, M. (2002) Atomic layer deposition, In *Handbook of Thin Films* (Hari Singh, N., M.Sc, and Ph.D, Eds.), pp 103-159, Academic Press, Burlington.
4. Puurunen, R. L. (2005) Surface chemistry of atomic layer deposition: A case study for the trimethylaluminum/water process, *Journal of Applied Physics 97*, 121301-121352.
5. Nilsen, O., Fjellvåg, H., and Kjekshus, A. (2004) Growth of calcium carbonate by the atomic layer chemical vapour deposition technique, *Thin Solid Films 450*, 240-247.
6. O'Mahony, A., Pemble, M. E., and Povey, I. M. (2010) Infrared and near-infrared spectroscopic probing of atomic layer deposition processes, *Journal of Molecular Structure 976*, 324-327.
7. Goldstein, D. N., McCormick, J. A., and George, S. M. (2008) Al2O3 Atomic Layer Deposition with Trimethylaluminum and Ozone Studied by in Situ Transmission FTIR Spectroscopy and Quadrupole Mass Spectrometry, *The Journal of Physical Chemistry C 112*, 19530-19539.
8. Du, X. D., Y.; George, S. M. (2005) In situ examination of tin oxide atomic layer deposition using quartz crystal microbalance and Fourier transform infrared techniques *Journal of Vacuum Science & Technology, A: Vacuum, Surfaces, and Films 23*, 581-588.
9. Rose, M., Niinistö, J., Endler, I., Bartha, J. W., Kücher, P., and Ritala, M. (2010) In Situ Reaction Mechanism Studies on Ozone-Based Atomic Layer Deposition of Al2O3 and HfO2, *ACS Applied Materials & Interfaces 2*, 347-350.
10. Knapas, K. H., Timo; Ritala, Mikko; Leskela, Markku (2010) In Situ Reaction Mechanism Studies on Atomic Layer Deposition of Sb2Te3 and GeTe from (Et3Si)2Te and Chlorides *Chemistry of Materials 22*, 1386-1391.
11. Ivanova, T., Gesheva, K. A., Popkirov, G., Ganchev, M., and Tzvetkova, E. (2005) Electrochromic properties of atmospheric CVD MoO3 and MoO3-WO3 films and

their application in electrochromic devices, *Materials Science and Engineering B 119*, 232-239.

12. Diaz-Droguett, D. E., and Fuenzalida, V. M. (2011) Gas effects on the chemical and structural characeristics of porous MoO3 and MoO3-x grown by vapor condensation in helium and hydrogen, *Materials Chemistry and Physics 126*, 82-90.

13. Chary, K. V. R., Reddy, K. R., Kishan, G., Niemantsverdriet, J. W., and Mestl, G. (2004) Structure and catalytic properties of molybdenum oxide catalysts supported on zirconia, *Journal of Catalysis 226*, 283-291.

14. El-Sharkawy, E. A., Khder, A. S., and Ahmed, A. I. (2007) Structural characterization and catalytic activity of molybdenum oxide supported zirconia catalysts, *Microporous and Mesoporous Materials 102*, 128-137.

15. Fournier, M., Aouissi, A., and Rocchiccioli-Deltcheff, C. (1994) Evidence of [small beta]-MoO3 formation during thermal treatment of silica-supported 12-molybdophosphoric acid catalysts, *Journal of the Chemical Society, Chemical Communications*, 307-308.

16. Ressler, T., Wienold, J., Jentoft, R. E., and Neisius, T. (2002) Bulk Structural Investigation of the Reduction of MoO3 with Propene and the Oxidation of MoO2 with Oxygen, *Journal of Catalysis 210*, 67-83.

17. Ressler, T., Jentoft, R. E., Wienold, J., Gunter, M. M., and Timpe, O. (2000) In Situ XAS and XRD Studies on the Formation of Mo Suboxides during Reduction of MoO3†, *The Journal of Physical Chemistry B 104*, 6360-6370.

18. Juárez, R., and Martínez-de la, C. (2003) Electrochemical lithium insertion in β-MoO<sub>3</sub>: novel Li<sub> <i>x</i> </sub>MoO<sub>3</sub> bronzes, *Journal of Solid State Electrochemistry 7*, 259-263.

19. Juárez Ramírez, I., and Martínez-de la Cruz, A. (2003) Synthesis of [beta]-MoO3 by vacuum drying and its structural and electrochemical characterisation, *Materials Letters 57*, 1034-1039.

20. Diskus, M., Nilsen, O., and Fjellvaag, H. (2011) Growth of thin films of molybdenum oxide by atomic layer deposition, *J. Mater. Chem. 21*, 705-710.

21. Sullivan, J. L., Yu, W., and Saied, S. O. (1995) A study of the compositional changes in chemically etched, Ar ion bombarded and reactive ion etched GaAs(100) surfaces by means of ARXPS and LEISS, *Applied Surface Science 90*, 309-319.

22. Oswald, S., Zier, M., Reiche, R., and Wetzig, K. (2006) Angle-resolved XPS: a critical evaluation for various applications, *Surface and Interface Analysis 38*, 590-594.

23. Champaneria, R., Mack, P., White, R., and Wolstenholme, J. (2003) Non-destructive analysis of ultrathin dielectric films, *Surface and Interface Analysis 35*, 1028-1033.

24. Anwar, M., Hogarth, C. A., Khan, G. A., and Bulpett, R. (1989) X-ray photoelectron spectroscopic (XPS) investigations of etching and annealing effects on thin films of MoO3, *Spectrochimica Acta Part B: Atomic Spectroscopy 44*, 789-793.

25. Schroeder, T., Zegenhagen, J., Magg, N., Immaraporn, B., and Freund, H. J. (2004) Formation of a faceted MoO2 epilayer on Mo(1 1 2) studied by XPS, UPS and STM, *Surface Science 552*, 85-97.

26. Cumpson, P. J. (1995) Angle-resolved XPS and AES: depth-resolution limits and a general comparison of properties of depth-profile reconstruction methods, *Journal of Electron Spectroscopy and Related Phenomena 73*.

27. Plyuto, Y. V., Babich, I. V., Plyuto, I. V., Van Langeveld, A. D., and Moulijn, J. A. (1997) XPS studies of MoO3/Al2O3 and MoO3/SiO2 systems, *Applied Surface Science 119*, 11-18.

28. McCarron, E. M. (1986) [small beta]-MoO3: a metastable analogue of WO3, *Journal of the Chemical Society, Chemical Communications*, 336-338.
29. Py, M. A., and Maschke, K. (1981) Intra- and interlayer contributions to the lattice vibrations in MoO3, *Physica B+C 105*, 370-374.
30. Dieterle, M., Weinberg, G., and Mestl, G. (2002) Raman spectroscopy of molybdenum oxides Part I. Structural characterization of oxygen defects in MoO3- by DR UV/VIS, Raman spectroscopy and X-ray diffraction, *Physical Chemistry Chemical Physics 4*, 812-821.

Paper III

"Thin films of cobalt oxide deposited on high aspect ratio supports by atomic layer deposition"

Madeleine Diskus, Ola Nilsen and Helmer Fjellvåg,
Journal of Chemical Vapor Deposition **2011**, 17, 135-140.

Paper IV

"Influence of the precursors chemistry on the ALD growth of cobalt-molybdenum oxide films"

Madeleine Diskus, Ola Nilsen and Helmer Fjellvåg,
Dalton Transactions, accepted.

ARTICLE TYPE

Influence of precursors chemistry on ALD growth of cobalt-molybdenum oxide films

Madeleine Diskus,[a] **Ola Nilsen***[a] **and Helmer Fjellvåg**[a]

Cobalt molybdenum compounds are important catalytic materials in many processes, e.g. in splitting of ammonia to form CO free hydrogen fuel. We here report on deposition of such cobalt molybdenum oxides by atomic layer deposition (ALD) using different types of metal precursors $CoCp_2$ (Cp = cyclopentadienyl), $Co(thd)_2$ (Hthd = 2,2,6,6-tetramethylheptan-3,5-dione), $Mo(CO)_6$ and oxygen precursors O_3, H_2O, and ($O_3 + H_2O$). The growth dynamics have been investigated using quartz crystal microbalance (QCM) methods. It

10 is evident that mixing of the different precursor chemistries affect the growth patterns. When water is introduced to the reactions, a surface controlled mechanism takes place which guides the deposited stoichiometry towards the $CoMoO_4$ phase over a wide range of cobalt rich pulsed compositions. This is a rare example of how surface chemistry can control stoichiometry of depositions in ALD. The deposited films have been investigated by X-ray diffraction, Raman spectroscopy and atomic force microscopy. The catalytic activity of selected films have been characterized by temperature programmed ammonia decomposition, proving the films to be catalytically active

15 and lowering the decomposition temperature by some 200 °C.

Introduction

Conventional processes for production of hydrogen are typically

20 associated with formation of carbon monoxide, CO. Additional purification is thus required before hydrogen can be used as fuel for proton-exchange membrane fuel cells, since carbonyls will poison the actual platinum catalysts. An alternative route to hydrogen is by decomposition of ammonia, which leads to high

25 purity hydrogen fuel [1]. Liquid ammonia represents a good storage medium for hydrogen, and is easy to handle and store compared to many current hydrogen storage media. However, practical solutions would greatly benefit from catalytic processes that reduce the decomposition temperature of ammonia as much as

30 possible. Numerous types of catalysts have been explored for decomposition of ammonia, for instance nickel and iron based catalysts are capable to decrease the temperature for complete NH_3 decomposition from 900 °C to 500 – 700 °C [2-4]. Ruthenium and cobalt-molybdenum based catalysts show the highest activity

35 with a lowering of the decomposition temperature to 400 °C. The most promising catalyst is a CoMo-based catalyst due to lower costs [5-7]. Improved catalysts are still sought today in order to decrease the NH_3 decomposition temperature further and to comply with the functional range of solid oxide fuel cells. CoMo-

40 based catalysts are furthermore used industrially in the hydrotreating processes with R&D still ongoing [8-12]. Hydrotreating processing refers to saturation, unsaturation of hydrocarbons and removal of S, N, O and metals from petroleum streams in a refinery [13].

45

Thin film deposition techniques have become important tools in catalysis research, providing model materials with surfaces and geometries well suited for detailed investigations. Atomic layer

50 deposition (ALD) is one such technique. It exploits sequential self-limiting processes between gaseous precursors and surfaces to build materials by atomic layer control [14, 15]. We have earlier used this technique to grow oxides of the elements of interest here: i.e. molybdenum oxide MoO_3 and cobalt oxide Co_3O_4. The

55 molybdenum trioxide was grown by ALD using molybdenum hexacarbonyl as metal precursor and a combination of water and ozone to enhance the growth rate [16]. Cobalt oxides have been deposited using either $Co(thd)_2$ (Hthd = 2,2,6,6-tetramethylheptan-3,5-dione) or $CoCp_2$ (Cp = cyclopentadienyl)

60 as metal precursors coupled with ozone as oxygen source [17, 18].

The present study aims at characterising the effect of precursor combinations and oxidants on ALD growth of Co-Mo oxide films, varying the type of cobalt precursor between $Co(thd)_2$ and

65 $CoCp_2$. The $CoCp_2$ precursor is expected to have a higher reactivity than $Co(thd)_2$ as it is proven to coat porous materials in a more complete manner [17]. The effect of water pulsed during deposition of $Mo(CO)_6$ was investigated previously for the Mo-O system [16] and is currently extended to the Co-Mo-O system

70 during pulsing of $CoCp_2$ and $Mo(CO)_6$ as metal precursors.

The ALD technique is best recognized for deposition of binary compounds, however, the method is highly applicable for deposition of complex compositions due to complete control in

75 precursor delivery. Prior work on deposition of complex compositions by ALD has shown that the deposition rates of complex oxides are determined by surface chemistry of the

preceding reactions leading to self-hindering mechanisms [19]. There is therefore not a direct connection between deposited and pulsed compositions. Typically, a complex surface composition leads to deposition rates deviating noticeably from a linear combination of the deposition rates of the binary components. A self-controlling mechanism towards a particular composition over a range of different pulsing ratios has not previously been demonstrated, until now where we will show that the $CoMoO_4$ composition is particularly stable under certain conditions. In the current work we further report on the morphology of Co-Mo oxide films obtained with $CoCp_2$, as deposited and after annealing, proving a preferred growth of $CoMoO_4$. Finally, the catalytic activity of the obtained Co-Mo oxides are investigated for the ammonia decomposition process.

Experimental details

Thin films were deposited in a commercial F-120 Sat reactor (ASM Microchemistry Ltd.) using ozone, water and $Mo(CO)_6$ (molybdenum hexacarbonyl 98%, Aldrich) as molybdenum precursor [16] and either $Co(thd)_2$ (home made according to reference [20]) and ozone [18] or $CoCp_2$ (cobaltocene, Aldrich) and ozone [17] as cobalt precursors. $CoCp_2$ and $Mo(CO)_6$ were used as solids at room temperature in a bubbler, using nitrogen as carrier gas. $Co(thd)_2$ was sublimed at 110 ºC. The ozone was generated by feeding O_2 (99.999% AGA) into an OT-020 ozone generator (Ozone Technology), providing an ozone concentration of about 15 vol.% according to specifications. An ozone flow of 500 cm^3 min^{-1} was used during the ozone pulses. During all depositions, a background pressure of approx. 2.5 mbar was obtained by applying a N_2 carrier gas flow of 300 cm^3 min^{-1}. The carrier gas was produced in a Schmidlin UHPN3001 N_2 purifier with a claimed purity of 99.999 % with respect to N_2+Ar content. The films were deposited on single crystalline substrates of Si(100), α-Al_2O_3(001) and on α-SiO_2(001). All films were deposited at 167 ºC using 500 cycles.

In situ measurements of the growth dynamics were obtained using a quartz crystal microbalance (QCM) based on AT cut quartz crystals oscillating at 6 MHz and a Maxtec TM400 monitor [21, 22]. The reduction in resonance frequency of the QCM sensor is according to the Sauerbrey equation [23] linearly dependent on the increase in mass of the sensor. The QCM data were post treated by averaging over typically 16 subsequent cycles and are presented with standard deviations. The alumina growth has been used in order to normalize the obtained data and calculate the increase of mass per cycle for the Co-Mo oxides. The signal was normalized to the growth rate of the TMA-H_2O process at the same temperature, providing deposition rates of 33 ng/cycle based on a density of 3.37 g/cm^3 as measured by X-ray reflectivity.

The films were examined with X-ray diffraction (XRD) in θ-2θ mode using a Siemens D5000 X-ray diffractometer equipped with a Göbel-mirror providing parallel Cu Kα radiation. The compositions of the films were determined by X-ray fluorescence (XRF) measurements performed on a Philips PW2400. Selected films were studied with atomic force microscopy (AFM; XE-70 Park System) to determine topography and roughness. Raman spectra were recorded on a Jobin Yvon LabRam confocal microscope, equipped with a HeNe-laser (632.8 nm, Melles Griot, 17 mW).

The ammonia decomposition reaction was carried out over irregular pieces of quartz (about 2 mm) coated with Co-Mo-O thin films produced by means of the precursor pairs [$Mo(CO)_6$ + (H_2O + O_3)] and [$CoCp_2$ +O_3]. Two films were studied, with compositions of about 50 % and 80 % of molybdenum with respect to metal ratio. The 50 % film was approx. 50 nm thick, whereas the 80 % film was about 100 nm thick obtained after 500 cycles of deposition. Prior to catalytic testing, the thin film catalysts were reduced under a flow of 10 ml/min of pure hydrogen at 600 ºC for 2 h. The temperature was raised from room temperature (RT) to 600 ºC at a heating rate of 5 ºC/min. After reduction, the reactor was cooled down to RT (5 ºC/min) under a flow of Ar at 25 ml/min. Temperature programmed ammonia decomposition over the thin film catalyst was conducted by flowing NH_3 (25 ml/min) and Ar (25 ml/min) from RT to 900 ºC at a heating rate of 5 ºC/min. The effluent gas was analyzed using a microgas chromatograph (Agilent 3000 Micro GC) equipped with Molecular sieve column/PLOTU pre-column (Ar carrier gas) for detecting N_2 and H_2 and PLOTU column/PLOTQ pre-column (He carrier gas) for detecting NH_3. Thermal conductivity detectors were used.

Results and discussion

1   Composition

The variations between the pulsed and deposited composition of cobalt and molybdenum were investigated for three different precursor combinations:

A: $n[Mo(CO)_6 + O_3] + m[CoCp_2 + O_3]$,

B: $n[Mo(CO)_6 + (O_3+H_2O)] + m[CoCp_2 + O_3]$,

C: $n[Mo(CO)_6 + (O_3+H_2O)] + m[Co(thd)_2 + O_3]$,

where n and m denotes the relative amount of pulses for the Mo and Co metal precursors, respectively. The pulsing sequences were constructed in order to maximize the mixing of the precursors. All depositions were performed at a reactor temperature of 167 °C using a total of 500 individual metal cycles based on pulse and purge times as given in Table 1. The pulse and purge durations were selected based on previous studies of ALD growth in the same equipment [16-18]. This gave films with thicknesses in the range of 50 – 80 nm.

Oxide subsystem [Metal precursor]	Pulse time (s)			
	Metal precursor	Purge	Oxygen precursor	Purge
Mo-O system [Mo(CO)$_6$]	3.1	2	3.5	6
Co-O system I [CoCp$_2$]	3	6	3	6
Co-O system II [Co(thd)$_2$]	2.5	3	1.5	6

Table 1. Pulse and purge times used for different combinations of precursors.

For the different precursor combinations, **B** and **C** include water together with ozone in deposition of Mo(CO)$_6$, while **A** is free of water. Furthermore, **A** and **B** use CoCp$_2$ as cobalt precursor, while **C** uses Co(thd)$_2$.

The compositions of the obtained films for the three different precursor combinations were determined by XRF, see Figure 1A. Good reproducibility of results was verified by performing several depositions of the same films. It is evident that there are large variations between the different precursor combinations, which proves that the growth is greatly affected by surface chemistry. The growth behavior of the precursor combination **C** shows a clear tendency towards stabilization of products with equiatomic compositions of Co and Mo, as seen for both 25 and 33 % pulsed subcycles of Mo. A similar stabilization is observed for the precursor combination **B** in the range 25 – 50 % pulsed subcycles of Mo. This equiatomic composition corresponds to the CoMoO$_4$ phase. An increase in the obtained molybdenum content is observed for films deposited using excess subcycles of Mo, indicating that the use of water in the process affects the growth of cobalt more than the growth of molybdenum. A quite different behavior is observed for the precursor combination **A**, which appears to stabilize at approx. 80 % Mo, Figure 1A. The observed growth behaviors deviate significantly from linear combinations of the growth rates of the individual binary oxides (Figure 1B), indicating that the growth is surface controlled with water as a key parameter.

2 QCM

Previous studies on the effect of water and ozone on the deposition of MoO$_3$ using Mo(CO)$_6$ [16], showed that ozone is necessary while water provides no growth alone. Combined use of water and ozone gave a slightly enhanced growth rate (0.75 Å/cycle vs. 0.65 Å/cycle for pure ozone) as shown by QCM investigations.
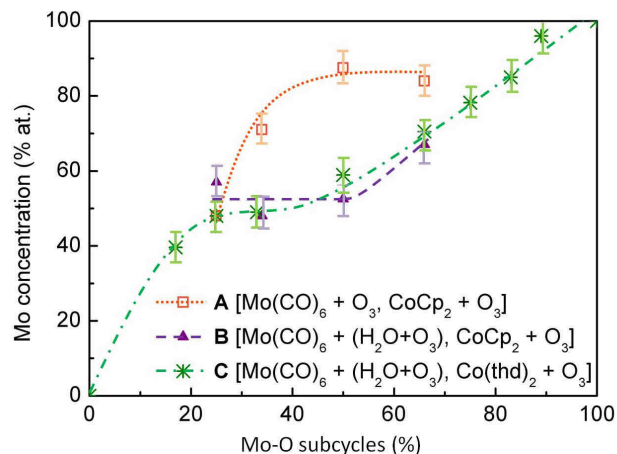

Figure 1A: Composition of deposited films at 167 °C as measured by XRF as function of pulsed composition (O content not included). Precursors combinations are defined as **A**, **B** and **C**.
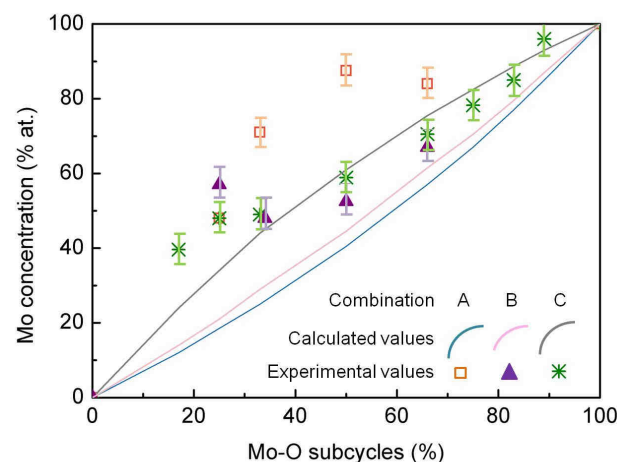

Figure 1B: Composition of deposited films at 167 °C as measured by XRF as function of the pulsed composition compared to expected composition based on a linar combination of growth rates for binary oxides under the same conditions (O content not included).

A systematic QCM investigation was performed for different combinations of pulses for the precursor combinations **A** or **B**, Figure 2. Comparative growth rates can be extracted from Figure 2 where it is evident that the Mo-O process is significantly enhanced when deposited on a Co-rich underlayer as compared to when deposited on MoO$_x$ (best seen for the 1/2 Co-O / Mo-O subcycle ratio).

It is also evident that the magnitude of the Co signal for the process **B** is increasing for each subsequent Co-O subcycle after a Mo-O subcycle, while a similar variation in signal is not observed for the process **A**. The origin behind these variations may be that the remains of water on the surface are reduced for each subsequent Co-O subcycle and that water retards the deposition of CoO$_x$, in line with the observations in Figure 3.
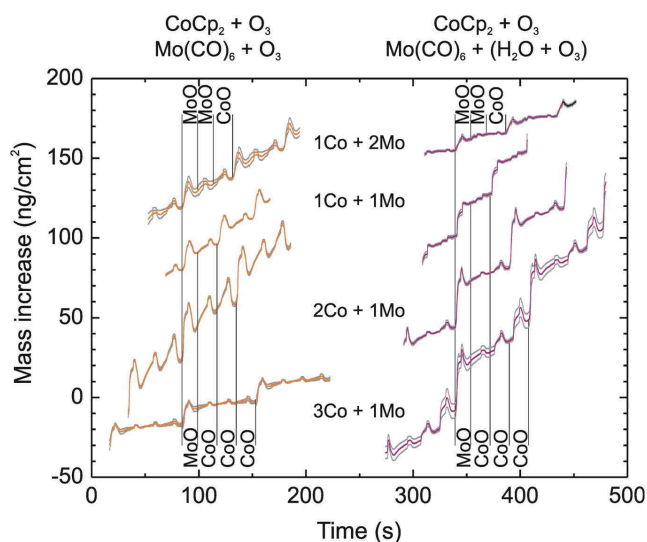
Figure 2: Growth dynamics for growth of Co-Mo oxides using the precursors combinations **A** (left) and **B** (right) at 167 °C, as measured by quartz crystal microbalance. The different pulsing regions and their durations are given in the figure. The curves have been obtained for the following Co-O / Mo-O subcycles ratio: 1 / 2, 1 / 1, 2 / 1, 3 / 1. The grey curves indicate standard deviation for the measurements.
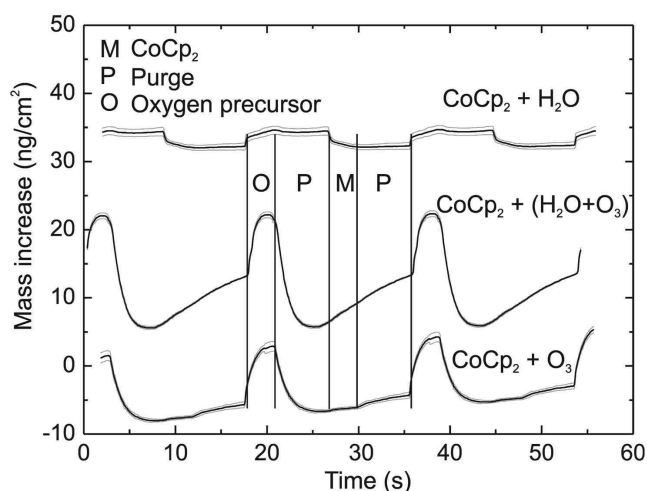

Figure 3: Growth dynamics for cobalt oxide at 167 °C as measured by quartz crystal microbalance, using $CoCp_2$ and different combinations of water and ozone as precursors. The different pulsing regions and their durations are given in the figure. The grey curves indicate standard deviation for the measurements.

This latter step has also been verified by separate attempts for deposition of CoO_x, where no film was observed for the $CoCp_2$ + H_2O combination and hardly any visible film was formed for the $CoCp_2$ + (H_2O + O_3) combination, while suitable film with a growth rate of approx. 0.40 Å/cycle was observed for the $CoCp_2$ + O_3 combination. The observed retarded growth of CoO_x when H_2O is introduced is contradictory to the effects of water on the growth of In_2O_3 from InCp as reported by A. Libera et al. in Ref. [30], where presence of water enhances the growth. The reason behind this difference is unclear, but may be connected to the strong ability of the $CoCp_2$ compound to act as reduction agent or the fact that the InCp precursor should be more steric accessible.

Based on Figure 2 it also appears that the magnitude of mass change during the Mo-O subcycle for the **B** process is dependent on the number of preceding Co-O subcycles. A similar dependency is not observed for the **A** process. The enhanced growth of MoO_x observed for the **B** process may indicate that the Mo-precursor is selectively adsorbed in connection to a Co site on the surface. This may be the mechanism for obtaining the 1:1 Co:Mo stoichiometry. The fact that the same stoichiometric relation is observed when $Co(thd)_2$ is used as cobalt source, indicates that the role of the Cp ligand is limited.

3   Physical characterization

All films where the cobalt and molybdenum oxide processes were combined are amorphous as deposited. The films obtained according to precursor combination **A** or **B** were therefore annealed in air at 600 °C for 6 or 10 minutes dependent on amount of pulsed molybdenum. The X-ray diffractograms of the annealed films are presented in Figure 4.

All films containing about 50 % of molybdenum, obtained with the schemes **A** or **B**, exhibit similar diffractograms where only (002) of β-$CoMoO_4$ is present, which is the most intense reflection of this phase, see Figure 4a [24]. Films deposited with higher molybdenum contents using precursor combination **A** reveal crystalline α-MoO_3 [25] oriented with (0k0) parallel to the substrate in addition to β-$CoMoO_4$, (Figures 4b and c). The weak additional diffraction peak at $2\theta = 27.48°$ for the diffractograms 4b and c can be interpreted as (20-2) of the β-$CoMoO_4$ phase. Lack of other reflections indicates high degree of preferred orientation in growth.

Raman spectra of the annealed films identify the same β-$CoMoO_4$ and α-MoO_3 phases (Figure 5). The double band for the vibration modes of the β-$CoMoO_4$ phase at 949 and 939.5 cm^{-1} [26] is observed for all $CoMoO_4$ films. The spectra for the samples with higher contents of molybdenum reveal additional Raman modes at 995, 820 and 666 cm^{-1}, corresponding to the stretching vibrations of crystalline α-MoO_3 [27]. Furthermore, the intensity ratio of the Raman shifts depend on the composition of the films reflecting their relative phase contents. The topographies of films obtained using pulsing precursor combination **A** or **B** were characterized by AFM, both for as-deposited films and after annealing (Figure 6). The amorphous as-deposited films show low roughnesses, with RMS roughness between 1.5 and 5 nm depending on the composition of the films (Figure 6; left column). After crystallization, the β-$CoMoO_4$ films remained uniform with little variation in the RMS roughness of about 2.5 nm (Figure 6, 1 b). However, large flakes, probably crystallites of α-MoO_3, appeared on the surface after annealing the films with higher contents of molybdenum.
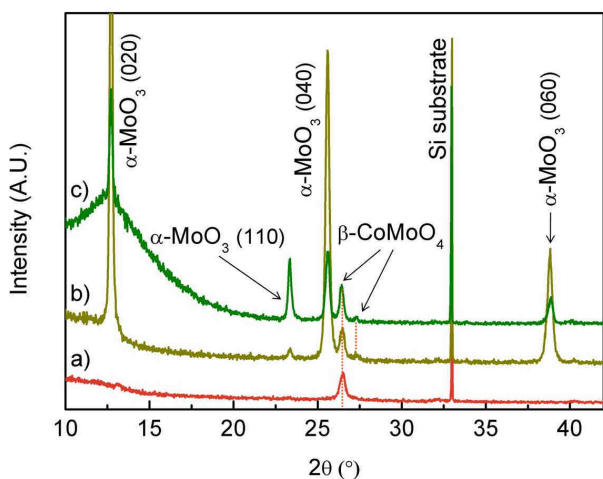
Figure 4: X-ray diffractogram of thin films deposited at 167 °C on Si(100) using precursor combination **A** [Mo(CO)$_6$,+ O$_3$, CoCp$_2$ + O$_3$]. The Mo content in the deposited films is: a) 50%, b) 70%, c) 80%. The films were annealed in air at 600 °C for a) and b) 6 min and c) 10 min.
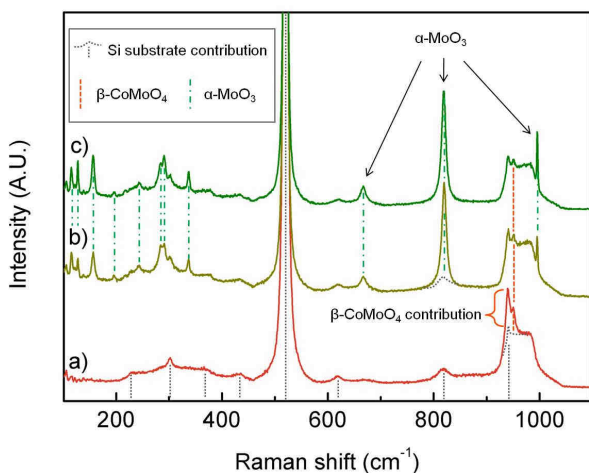

Figure 5: Raman spectra of thin films deposited at 167 °C on Si(100) using precursor combination **A** (Mo(CO)$_6$ + O$_3$ and CoCp$_2$ + O$_3$). The Mo content in the deposited films is: a) 50%, b) 70%, c) 80%. The films were annealed in air at 600 °C for a) and b) 6 min and c) 10 min.

The amount of crystallites increases with the content of molybdenum, leading to increased roughness up to RMS=12.7 nm for the film containing 85% Mo (Figure 6, 3 c). This is in good agreement with the results from the XRD and Raman investigations.

4   Catalytic testing

Selected films of CoMoO$_4$ were deposited on quartz substrates for subsequent temperature programmed ammonia decomposition and investigation of catalytic activity of films with different compositions. As deposited films of CoMoO$_4$ and molybdenum enriched films (about 80 % of molybdenum in CoMo ratio) were reduced under hydrogen flow at 600 °C for 2 h prior to catalytic testing. The catalytic activity of these samples was compared to the activity of the quartz substrate without film (Figure 7).

The activity of the samples is here evaluated in terms of the temperature at which 5 % of the ammonia is decomposed, defined as T$_{onset}$. For uncoated quartz T$_{onset}$ is about 750 °C (Figure 7) in accordance with literature [28]. T$_{onset}$ is decreased to approx. 620 °C for quartz coated with CoMoO$_4$ (Figure 7) and complete decomposition (T$_{final}$) of NH$_3$ is achieved at 847 °C, hence proving a substantial high catalytic activity of the CoMoO$_4$ film. T$_{onset}$ is reduced even further to 450 °C for the film enriched with molybdenum and complete decomposition is achieved at 775 °C (Figure 7). The catalytic films are hence able to reduce the

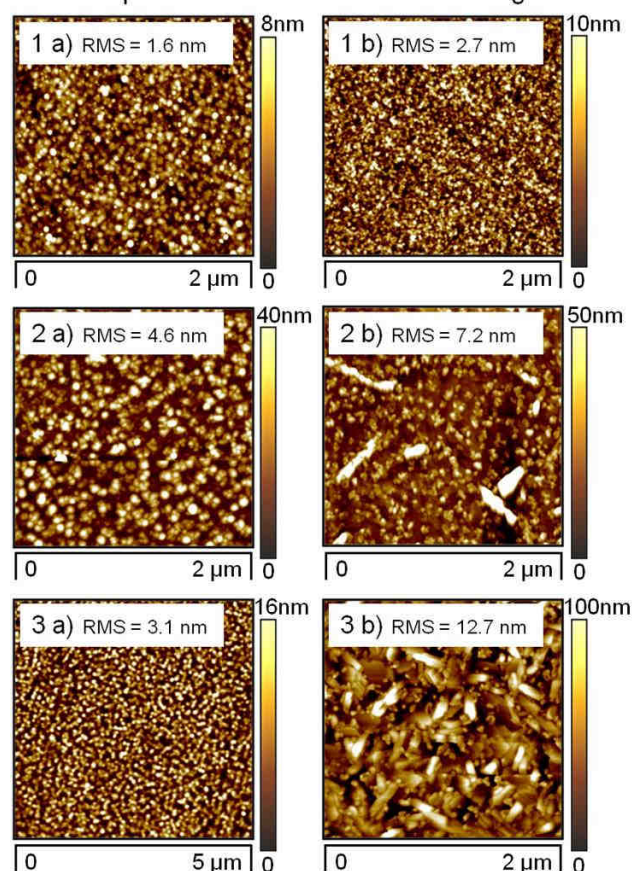
Figure 6: AFM topographies of thin films deposited at 167 °C on Si(100) using precursor combination **A** (Mo(CO)$_6$ + O$_3$ and CoCp$_2$ + O$_3$). The Mo content in the deposited films is: 1) 50%, 2) 70%, 3) 85%. Left column (a) as deposited, right column (b) annealed in air at 600 °C (1b; 2b) for 6 minutes and (3b) 10 minutes.
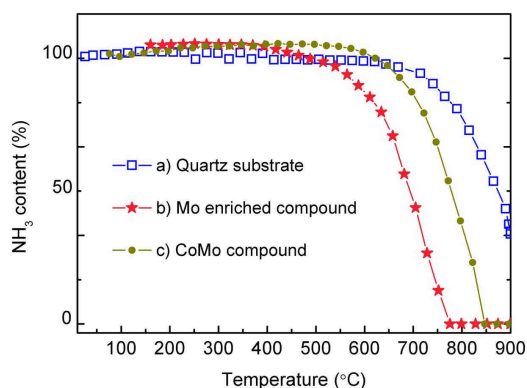
Figure 7: Ammonia content in the gas mixture after passing over catalytic film deposited at 167 °C on quartz by ALD, obtained using $Mo(CO)_6$ and $CoCp_2$ as metal precursors. The Mo content in the deposited films was b) 80 % and c) 50 %. The studies were performed in NH_3 and Ar mixtures from RT to 900 °C at a heating rate of 5 °C/min.

decomposition temperature of ammonia by approx. 200 °C. This range of catalytic activity is in good agreement with literature on similar materials [7, 29], however, being higher in temperature than for Ru catalysts which are already active in the temperature range 400 to 600 °C.

Conclusion

Cobalt molybdenum oxides were grown by atomic layer deposition (ALD) using various combinations of metal precursors; $Mo(CO)_6$, $Co(thd)_2$ and $CoCp_2$; and either O_3, H_2O, or $(O_3 + H_2O)$ as oxygen precursors. QCM investigations were used to assess the effect of different precursor chemistries on the growth of the different components. A self-controlling mechanism towards a particular composition over a range of different pulsing ratios was evidenced by combining water into the reactions, which guided the deposited stoichiometry towards the $CoMoO_4$ composition (and phase) over a wide range of cobalt rich pulsed compositions.

The films are amorphous as deposited and crystallize to β-$CoMoO_4$ under annealing, while any excess of molybdenum crystallizes into α-MoO_3. Reduced (activated) molybdenum enriched compounds were proven to reduce the decomposition temperature of ammonia by some 200 °C.

Acknowledgements

Notes and references

a University of Oslo, Department of Chemistry, Innovative Natural Gas Processes and Products, Centre for Material Science and Nanotechnology, P.O.Box 1033 Blindern, N-0315 Oslo, Norway. Fax: +47 2285 5441; Tel: +47 2285 5535; E-mail: ola.nilsen@kjemi.uio.no

† Electronic Supplementary Information (ESI) available: [details of any supplementary information available should be included here]. See DOI: 10.1039/b000000x/

‡ Footnotes should appear here. These might include comments relevant to but not central to the matter under discussion, limited experimental and spectral data, and crystallographic data.

1   M. Ni, D. Y. C. Leung and M. K. H. Leung, *Journal of Power Sources*, 2008, **185**, 233.
2   T. V. Choudhary, C. Sivadinarayana and D. W. Goodman, *Catalysis Letters*, 2001, **72**, 197.
3   M. E. E. Abashar, Y. S. Al-Sughair and I. S. Al-Mutaz, *Applied Catalysis A: General*, 2002, **236**, 35.
4   K. Kiełbasa, R. Pelka and W. Arabczyk, *The Journal of Physical Chemistry A*, 2010, **114**, 4531.
5   R. Z. Sørensen, L. J. E. Nielsen, S. Jensen, O. Hansen, T. Johannessen, U. Quaade and C. H. Christensen, *Catalysis Communications*, 2005, **6**, 229.
6   R. Kojima and K.-i. Aika, *Applied Catalysis A: General*, 2001, **215**, 149.
7   Okamura, Kirishiki, Masaru, Yoshimune, Masanori, Tsuneki, Hideaki, DOI: 20110176988, 2011.
8   N. Hermann, M. Brorson and H. Topsøe, *Catalysis Letters*, 2000, **65**, 169.
9   M. Brorson, A. Carlsson and H. Topsøe, *Catalysis Today*, 2007, **123**, 31.
10   N. Bejenaru, C. Lancelot, P. Blanchard, C. Lamonier, L. c. Rouleau, E. Payen, F. Dumeignil and S. b. Royer, *Chemistry of Materials*, 2009, **21**, 522.
11   J. M. Beuken and P. Bertrand, *Surface Science*, 1985, **162**, 329.
12   J. Kibsgaard, A. Tuxen, K. G. Knudsen, M. Brorson, H. Topsøe, E. Lægsgaard, J. V. Lauritsen and F. Besenbacher, *Journal of Catalysis*, 2010, **272**, 195.
13   B. S. C. Henrik Topsøe, Franklin E. Massoth, *Catalysis science and technology*, 1996, **11**.
14   H. Kim, H.-B.-R. Lee and W. J. Maeng, *Thin Solid Films*, 2009, **517**, 2563.
15   M. Leskelä and M. Ritala, *Thin Solid Films*, 2002, **409**, 138.
16   M. Diskus, O. Nilsen and H. Fjellvaag, *J. Mater. Chem.*, 2011, **21**, 705.
17   M. Diskus, O. Nilsen and H. Fjellvåg, *Chemical Vapor Deposition*, 2011, **17**, 135.

18   K. B. Klepper, O. Nilsen and H. Fjellvåg, *Thin Solid Films*, 2007, **515**, 7772.19   M. Lie, O. Nilsen, H. Fjellvag and A. Kjekshus, *Dalton Transactions*, 2009, 481.

20   D. C. N. G.S. Hammond, C.H.S. Wu, *Inorganic Chemistry 2*, 1963, **73**.

21   V. M. Mecea, J. O. Carlsson and R. V. Bucur, *Sensors and Actuators A: Physical*, 1996, **53**, 371.

22   A. L. Smith, H. M. Shirazi and S. R. Mulligan, *Biochimica et Biophysica Acta (BBA) - Protein Structure and Molecular Enzymology*, 2002, **1594**, 150.

23   G. Sauerbrey, *Zeitschrift für Physik A Hadrons and Nuclei*, 1959, **155**, 206.

24   A. Calafat, F. Vivas and J. L. Brito, *Applied Catalysis A: General*, 1998, **172**, 217.

25   E. M. McCarron, *Journal of the Chemical Society, Chemical Communications*, 1986, 336.

26   K.-H. Choi, Y. Korai and I. Mochida, *Applied Catalysis A: General*, 2004, **260,** 229.

27   M. Dieterle, G. Weinberg and G. Mestl, *Physical Chemistry Chemical Physics*, 2002, **4**, 812.

28   D. Dirtu, L. Odochian, A. Pui and I. Humelnicu, *Central European Journal of Chemistry*, 2006, **4**, 666.

29   A. Boisen, S. Dahl, J. K. Nørskov and C. H. Christensen, *Journal of Catalysis*, 2005, **230**, 309.

30   J. A. Libera, J. N. Hryn, et al. *Chemistry of Materials*, 2011, **23**, 2150-2158.

"Cobalt molybdenum oxides coating of alumina carriers by atomic layer deposition for the hydrodesulfurization process"

Madeleine Diskus, Michael Brorson and Helmer Fjellvåg.

Cobalt molybdenum oxides coating of alumina carriers by atomic layer deposition for the hydrodesulfurization process

Madeleine Diskus[a], Michael Brorson[b] and Helmer Fjellvåg[a]

[a] University of Oslo, Department of Chemistry, Innovative Natural Gas Processes and Products, Centre for Material Science and Nanotechnology, P.O.Box 1033 Blindern, N-0315 Oslo, Norway

[b] Haldor Topsøe, Nymøllevej 55, DK-2800 Kgs, Lyngby, Denmark

madeleine.diskus@kjemi.uio.no

INTRODUCTION

CoMo-based industrial catalysts are inter alia known as the main catalysts in the hydrodesulfurization process. Despite a large industrial use of the CoMo-based catalysts there is a considerable interest in the transition metal oxide and sulfide phases investigation in order to understand and enhance their catalytic properties[1].
The main goal in this work was to study the catalytic properties of cobalt-molybdenum oxides and multilayered thin films deposited by atomic layer deposition (ALD) on alumina carieers, as function of the thickness and order of the films.

EXPERIMENTAL DETAILS

Thin films of cobalt and molybdenum oxides were deposited by ALD (at 167 °C) in a F-120 Sat reactor (ASM Microchemistry Ltd.) using respectively ozone and $CoCp_2$ and a mix of water and ozone with $Mo(CO)_6$ as precursors[2, 3]; the metal precurors were introduced in the reactor using a bubbler with nitrogen as carrier gas. All the films were deposited on Al_2O_3 carriers designed specifically for the hydrodesulfurization process. The thicknesses of the films were investigated by ellipsometry, using an α-SE^{TM} ellipsometer from J.A. Woollman Co., Inc. An environmental SEM Quanta 200F equipped with a field emission gun was used to study the elemental distribution of the films on the extrudates.

Initially, the films were deposited on the full extrudates as films of $CoMoO_4$ and multilayered films of Co_3O_4 and MoO_3. The varying parameters were the thicknesses of the films and the

1

order of the films in the multilayers. The extrudates were then grained into 600–850 μm granulates for the catalytic testing (See Figure 1 and Table 1).

In a second time, the films where deposited on the fractionated alumina directly, in order to increase the catalyst surface area (See Figure 4 and Table 2). Some of the full extrudates were kept in their original shape in order to characterize them by SEM-microprobe and EDS.

Catalytic tests were performed by means of a tubular high-pressure reactor with n-heptane solutions of the reactants as feed. Catalysts were loaded as 600–850 μm granulates diluted with glass microbeads. In order to ensure that samples were fully sulfided before the catalytic test, *in situ* sulfidation was made for 4 h at 350 °C by means of a 2.5% solution of dimethyldisulfide (DMDS) in n-heptane and with $p(H_2)$ = 42 atm. Under these conditions DMDS decomposes readily to generate H_2S[4].

RESULTS AND DISCUSSION

I. ALD coating of the full extrudates

Thin films of $CoMoO_4$ and multilayered films of Co_3O_4 and MoO_3 were deposited on Al_2O_3 extrudates before to be grained into 600–850 μm granulates (Figure 1). The main goal was to investigate the catalytic activity of the coated carriers as function of the thickness of the films and the oxides order in the multilayers; therefore the thickness and order were the varying parameters for the Co_3O_4, MoO_3 and $CoMoO_4$ films depositions. All the obtained films are listed in Table 1.
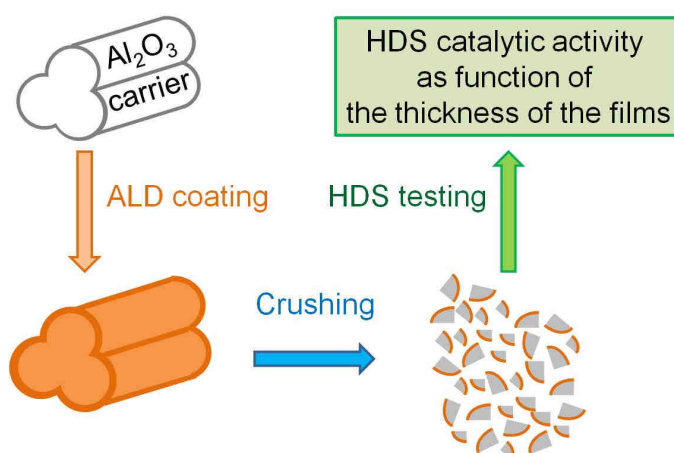

Figure 1: Schematic representation of the processed alumina carriers first coated by ALD and crushed into 600–850 μm granulates for the HDS catalytic activity testing.
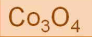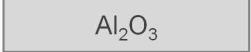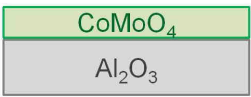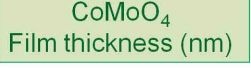
	Film thickness (nm)		
MoO_3 / Co_3O_4 / Al_2O_3	Co_3O_4	MoO_3	
	5	10	20
	10	10	20
Co_3O_4 / MoO_3 / Al_2O_3	2.5 5 10	10	
	2.5 5 10	20	
$CoMoO_4$ / Al_2O_3	$CoMoO_4$ Film thickness (nm)		
	20	40	80

Table1: Building of the multilayered films and the CoMoO₄ films deposited by ALD on the Al₂O₃ carriers and crushed into 600–850 µm granulates for the HDS catalytic activity testing.

1) Catalytic testing

The catalytic activity of the films in the hydrodesulfurization process was tested. The obtained activity was very low with a HDS conversion found to be about 1.7 (±0.1) % for all the tested materials.

2) Characterization of the coated extrudates

a) BET investigation of the surface area of the coated extrudates

Single point BET measurements have been performed on the granulates showing the surface area to be about 286 (±1) m^2/g. The surface area is about the same as for the uncoated granulates.

b) SEM-Microprobe investigation of the coated extrudates

The content of molybdenum and cobalt in the extrudates cross-section was investigated by SEM-Microprobe. The obtained results for the 3 combinations of films a) Co_3O_4 on top of MoO_3, b) MoO_3 on top of Co_3O_4 and c) $CoMoO_4$, are represented Figure 2. In all the configurations, the directions of the content measurements are indicated in order to show the variations from one direction to an other. These variations are due to an inhomogeneous coating of the substrates caused by the flow type deposition (See Figure 3). The 3

combinations show the molybdenum content close to the edge (about 2μm from the edge of the extrudate) to be about 0.5 to 2 % in weight, depending on the direction of the measurement. But molybdenum is not present further into the cross-section. Cobalt is not detected in the cross-section when deposited directly on the alumina extrudate (Figure 2 b), but is present to a very small amount (about 0.1 wt. %) at one edge of the carrier coated first with molybdenum. However, it is detected from 0.2 to 0.5 wt. % at the carriers edges coated with the $CoMoO_4$ film, and even present to a 0.1 wt. % content in the whole extrudate in one direction (Figure 2 c). It seems here that molybdenum penetrates better into the alumina pores structure when deposited directly on the carriers. The cobalt on the other hand is unable to enter the porous structure as deposited directly on alumina, but is helped as deposited simultaneously with molybdenum. The same phenomena were seen and verified by EDS mapping.
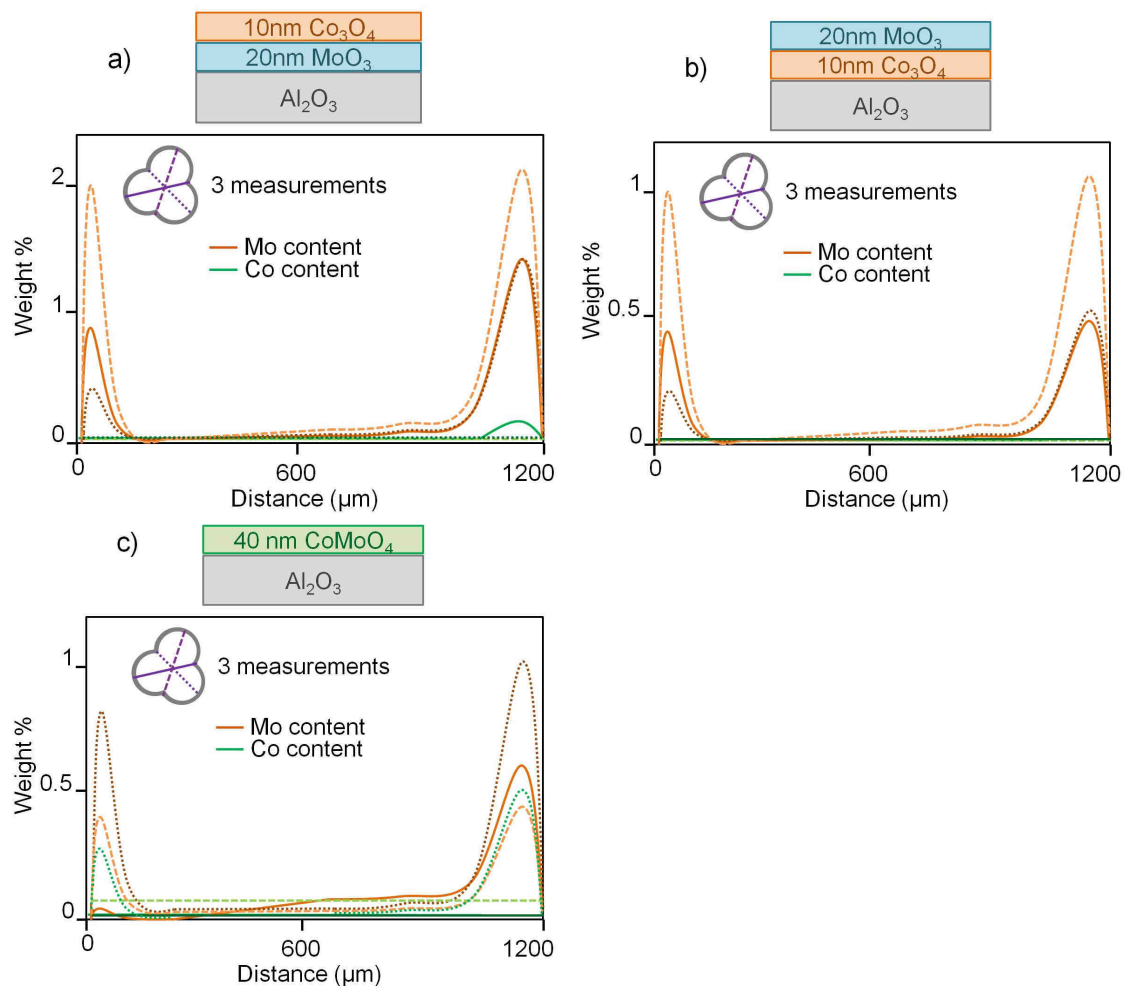

Figure 2: SEM-Microprobe investigation of molybdenum and cobalt contents in the extrudates cross-section. The obtained results are for the 3 films combinations: a) Co_3O_4 on top of MoO_3, b) MoO_3 on top of Co_3O_4 and c) $CoMoO_4$.
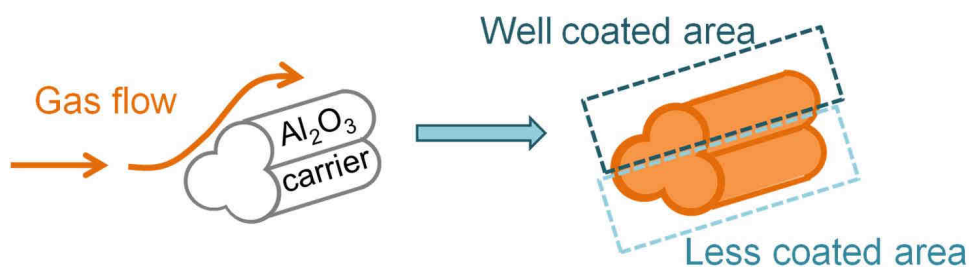
Figure 3: Schematic representation of the gas flow in the ALD reaction chamber, and the variation in the thickness of the coating of 3D structures.

3) Discussion

The HDS catalytic activity investigation of the coated alumina carriers was prevented by the low activity of the materials. This low activity was caused by a low content of molybdenum and cobalt inside the alumina porous structure. The average pore diameter of the alumina structure (about 40 Å) was too small to be coated by ALD. Therefore the next idea was to coat directly the granulates in order to increase the amount of metal in the alumina carriers. This study is presented in the following chapter.

II. ALD coating of the granulates

Thin films of $CoMoO_4$ and multilayered films of Co_3O_4 and MoO_3 were deposited directly on Al_2O_3 granulates about 600–850 µm large (Figure 4). The main goal was to increase the amount of cobalt and molybdenum on the tested granulates. The HDS catalytic activity of the obtained coated granulates was investigated as function of the thickness of the films and the oxides order in the multilayers; therefore the thickness and order were the varying parameters for the Co_3O_4, MoO_3 and $CoMoO_4$ films depositions. All the obtained films are listed in Table 2.
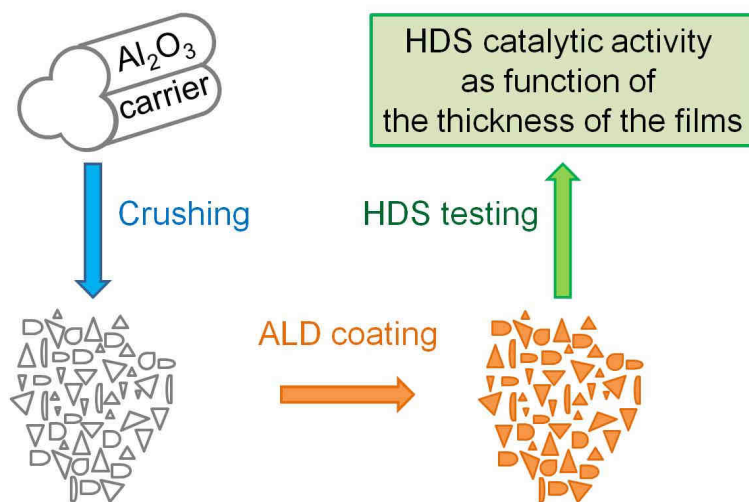
Figure 4: Schematic representation of the processed alumina carriers first crushed into 600–850 µm granulates and then coated by ALD for HDS catalytic activity testing.

A)		Film thickness (nm)	
Co_3O_4 MoO_3 Co_3O_4 Al_2O_3		Co_3O_4	MoO_3
		Top layer: 2 Bottom layer: 20	20, 30, 40, 50, 60
		Top layer: 10, 20 Bottom layer: 20	20
B)			
Al_2O_3		Top layer: 2 Other layers: 10	10
C)		$CoMoO_4$ Film thickness (nm)	
$CoMoO_4$ Al_2O_3		10 40 65 100	

Table 2: Building of the multilayered films and CoMoO$_4$ films deposited by ALD on the Al$_2$O$_3$ granulates for HDS catalytic activity testing.

1) Catalytic testing

The catalytic activity of the films in the hydrodesulfurization process were tested; the results are represented Figure 5. The obtained HDS conversion was studied as function of the thickness of the molybdenum oxide film in the configuration **A**, as function of the top Co_3O_4 layer thickness in configuration **A** and as function of the $CoMoO_4$ thickness in configuration

C. The HDS conversion was also measured for the multilayered film in configuration **B** and is represented on the right of the plot. The overall measured catalytic activity was low, but some trends are clearly seen. The HDS conversion over the CoMo monolayer films appear to be very stable about 2.55 % independently on the thickness of the films. However, for the films in configuration **A**, the catalytic activity increases with the thickness of the Co_3O_4 top layer from 2.2 to 3.2 % conversion for film thicknesses varying from 2 to 20 nm. The HDS conversion increases also with the MoO_3 thickness up to 3.3 % for a 50 nm thick film, but decreases drastically to 2.2% of conversion for the 60 nm thick film. The sudden drop of activity can be explained here by the fact that thicker films decrease the surface area of the catalyst by leveling the surface as described Figure 6.
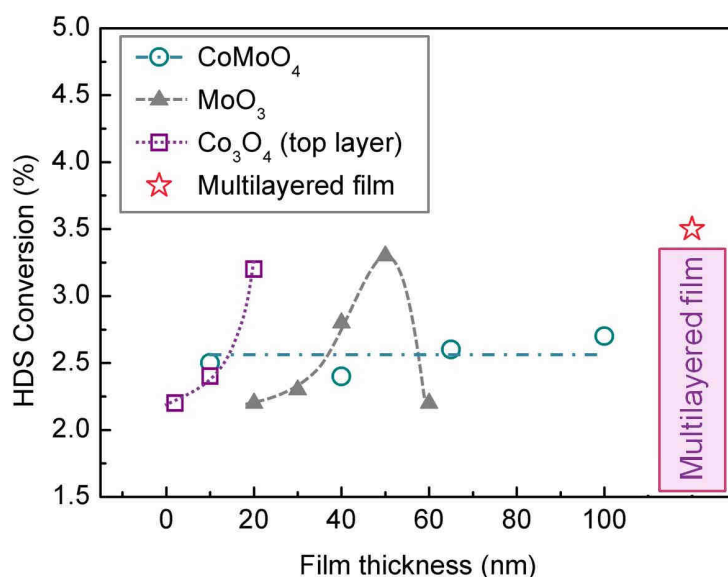

Figure 5: HDS conversion over the different catalysts as function of the thickness of the films.
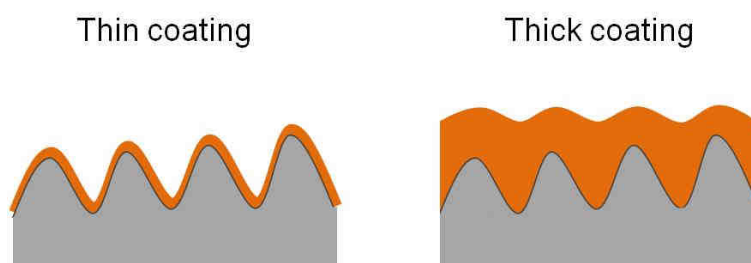

Figure 6: Schematic representation of the leveling effect of a coating with a thick amorphous film.

7

2) Characterization of the extrudates

a) BET investigation of the surface area of the coated extrudates

Single point BET measurements have been performed on the granulates showing the surface area to be about 244.5($\pm$1.5) m^2/g. The surface area is lower than for the first configuration, proving the content of catalyst to be higher on the granulate surface.

b) SEM-Microprobe investigation of the coated extrudates

All the films deposited on the granulates were deposited at the same time on full extrudates in order to perform SEM-microprobe investigations on the coated extrudates cross-sections. Granulated material cannot be characterized by the SEM-microprobe equipment used. The results from the SEM-Microprobe investigation are represented Figure 7. The trends are very similar to the trends obtained in the previous chapter, but for the overall very low cobalt content. However the results are not significative for our catalysts as they are representative of the films deposited on the full extrudates and not on the granulates. In order to characterize our catalyst content in the porous alumina, SEM-microprobe investigations should be performed on the coated granulates cross sections.
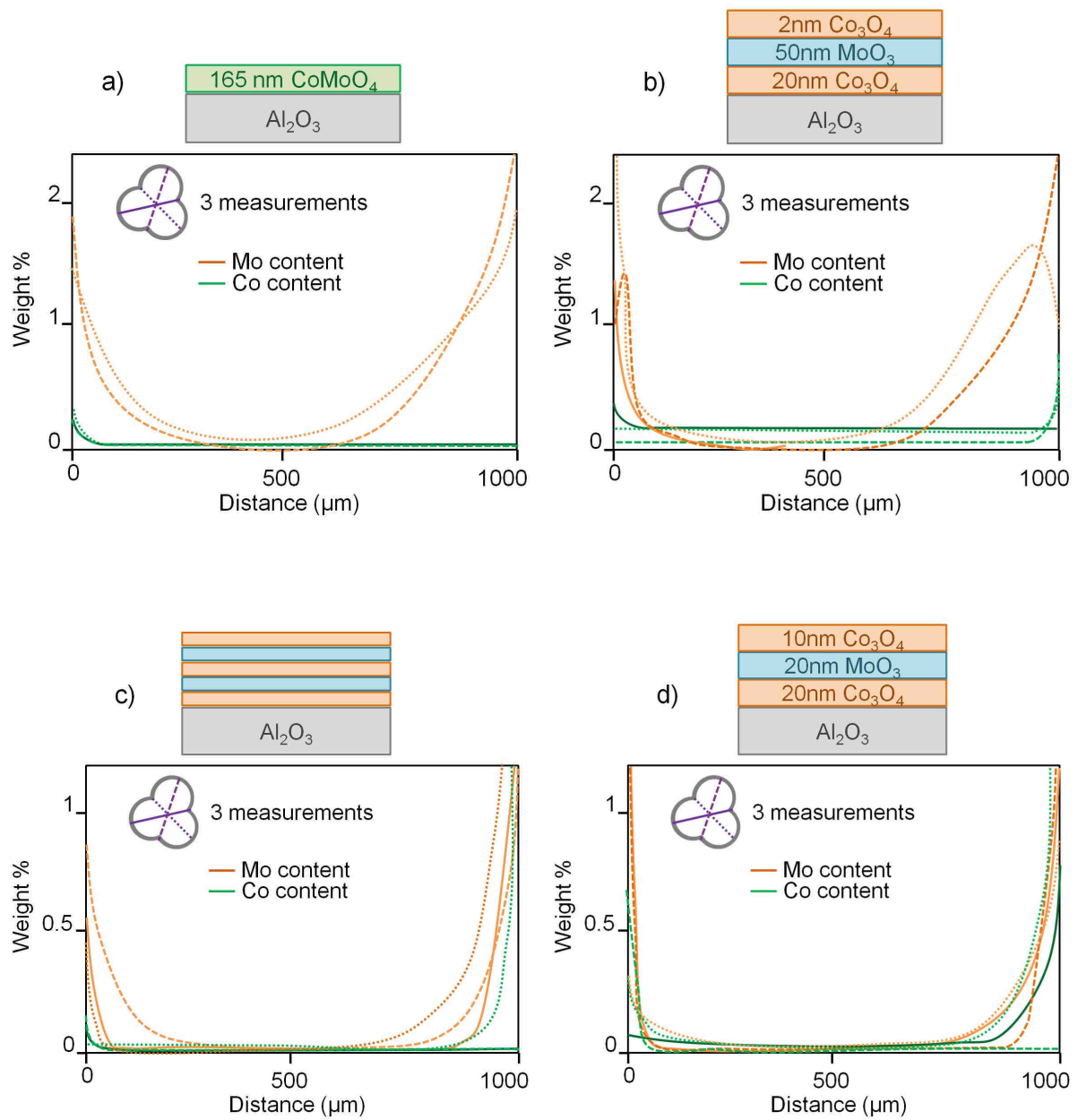
Figure 7: SEM-Microprobe investigation of the content of molybdenum and cobalt in the extrudates cross-section. The obtained results are for the 3 combinations of films a) CoMoO₄, b) and d) MoO₃ in between two layers of Co₃O₄ and c) the multilayered film.

DISCUSSION AND CONCLUSION

The alumina substrates pores were too narrow to enable ALD coating of the porous structure. The pores were only coated with molybdenum about 2 µm close to the edge. The better penetration of the molybdenum than cobalt is assumed to be due to a higher reactivity of the carbonyls compared to the cyclopentadienyl reactivity when adsorbing on the alumina surface. However, the alumina porous structure might be coated deeper and more homogneously for the coated granulates, as the smaller size of the granulates facilitates the diffusion of the precursors into the pores. Furthermore, investigations of the catalytic activity in the HDS process showed a higher conversion rate in the hydrodesulfurization process for the coated granulates than for the coated extrudates. This study proved the catalysts made of cobalt and molybdenum oxides multilayers to be more active than the catalysts made of a $CoMoO_4$ single phase coating (which has a constant activity independently on the thickness of the coating). Finally, the HDS conversion study as function of the thickness of the cobalt oxide and molybdenum oxide films showed an increase of the conversion as function of the thickness of the films, followed by a drop of the conversion due to leveling of the surface area for a thick coating.

FURTHER WORK

In order to explain the better activity of the multilayered films compared to the $CoMoO_4$ films, further investigations of the materials are requested such as *in situ* TEM characterization of the sulfidation of the films and SEM-microprobe investigation of the metal content in the coated granulates cross-section. The ALD coating of the mesoporous alumina can be improved by depositing oxides in a close type reactor, forcing the precursors to enter the porous structure and adsorb on the surface. Finally, it would be interesting to substitute the substrate with an alumina carrier with larger pores in order to be able to vary the thickness of the deposited films inside the porous structure and study the catalytic activity as function of the thickness of the films.

REFERENCES

1. Henrik Topsøe, B.S.C., Franklin E. Massoth, *Hydrotreating catalysis Science and Technology.* Catalysis Science and Technology, 1996. **11**.
2. Diskus, M., O. Nilsen, and H. Fjellvåg, *Thin Films of Cobalt Oxide Deposited on High Aspect Ratio Supports by Atomic Layer Deposition.* Chemical Vapor Deposition, 2011. **17**(4-6): p. 135-140.
3. Diskus, M., O. Nilsen, and H. Fjellvaag, *Growth of thin films of molybdenum oxide by atomic layer deposition.* J. Mater. Chem., 2011. **21**(Copyright (C) 2011 American Chemical Society (ACS). All Rights Reserved.): p. 705-710.
4. Hermann, N., M. Brorson, and H. Topsøe, *Activities of unsupported second transition series metal sulfides for hydrodesulfurization of sterically hindered 4,6-dimethyldibenzothiophene and of unsubstituted dibenzothiophene.* Catalysis Letters, 2000. **65**(4): p. 169-174.

Unpublished results II

"*Ex situ* and *in situ* Transmission Electron Microscopy imaging investigation of copper, zinc and aluminum oxides multilayered thin films obtained by ALD"

Madeleine Diskus, Stig Helveg, Jens Sehested and H. Fjellvåg.

Ex situ and *in situ* Transmission Electron Microscopy imaging of multilayered copper, zinc and aluminum oxide thin films deposited by ALD

Madeleine Diskus[a], Stig Helveg[b], Jens Sehested[b] and Helmer Fjellvåg[a]

[a] University of Oslo, Department of Chemistry, Innovative Natural Gas Processes and Products, Centre for Material Science and Nanotechnology, P.O.Box 1033 Blindern, N-0315 Oslo, Norway

[b] Haldor Topsøe, Nymøllevej 55, DK-2800 Kgs, Lyngby, Denmark

madeleine.diskus@kjemi.uio.no

INTRODUCTION

Cu/ZnO-based industrial catalysts are inter alia used in methanol synthesis. The morphology and state of these catalysts is strongly influenced by their environment during the methanol synthesis process. It is hence of high interest to perform *in situ* studies of the morphology of copper nanoparticles on a zinc oxide matrix in order to understand the effect of various gases on Cu particles and how this influences the activity of the Cu/ZnO-based catalysts [1]. However, the very similar size and mass-thickness contrast of the Cu and ZnO nanoparticles prevent the distinction between the two types of particles when investigated by transmission electron microscopy. Furthermore, the rather heterogeneous characteristics of an industrial catalyst makes TEM imaging studies cumbersome. Therefore the interest in designing model materials as close to the real catalyst as possible has nowadays drastically increased. Thin film model materials are often used as they represent both bulk and surface characteristics of the materials. A suitable technique to deposit and control the growth of oxide thin films is atomic layer deposition (ALD) [2]. In this work, ALD is used to build up multilayered thin films of copper oxide, zinc oxide and alumina. *In situ* TEM imaging is performed on the samples in order to investigate the changes in morphology during the reduction of CuO to metallic Cu.

EXPERIMENTAL DETAILS

Thin films of copper and zinc oxides were deposited by ALD in a F-120 Sat reactor (ASM Microchemistry Ltd.) using respectively ozone and $Cu(acac)_2$ (as solid) [3] and Diethyl Zinc (DEZ) (in a bubbler using nitrogen as carrier gas) and water as precursors. All the films were deposited on Si_3N_4 windows designed specifically for TEM investigations (see scheme in Figure 1). All the films were coating the windows uniformly and homogeneously. The thicknesses of the films were investigated by ellipsometry, using an α-SE^{TM} ellipsometer from J.A. Woollman Co., Inc. Initially, the films were deposited at 175°C. The TEM imaging investigations were performed using a Titan 80–300 transmission electron microscope (FEI Company) equipped with a gas mixing unit and a mass spectrometer to control and determine the gas composition at the specimen. It was either operated at standard high vacuum conditions of approx. 10^{-6} mbar (used for standard *ex situ* TEM investigations) or at *in situ* conditions (with gas as specified below).

For a second set of samples, the copper and zinc oxides films where obtained at 150 and 125°C respectively and alumina films were obtained by ALD at 225°C using TMA and ozone as precursors. The TEM imaging experiments were carried out using a Philips CM300 ST FEG-TEM instrument used, either *ex situ* or *in situ* as specified below.
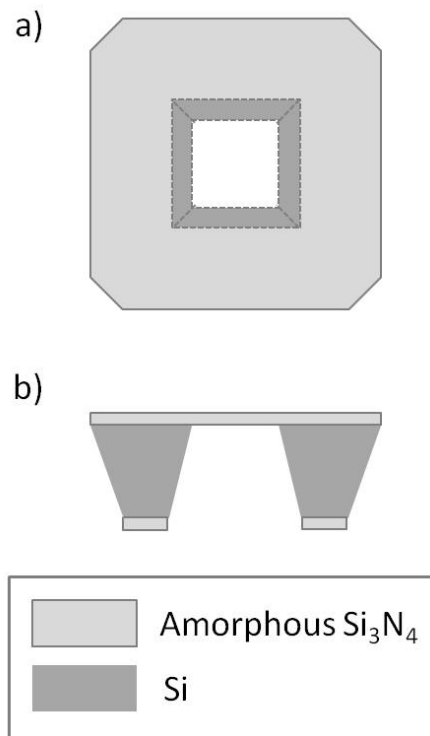

Figure 1: Schematics of a Si_3N_4 window used as substrate to investigate ALD thin films, a) Top view and b) Front view.

RESULTS AND DISCUSSION

I. TEM imaging of ZnO and CuO thin films deposited at 175°C by ALD

A 14 nm thick ZnO film and a 0.4 nm CuO / 10 nm ZnO multilayered film were prepared by ALD, deposited on two separate Si_3N_4 windows at 175°C. The top view *ex situ* TEM images of the films at low magnification are represented Figure 2 a) and b). The topographies and the grain size (about 5 nm) of both films are very similar. The roughness of the ZnO film is too high to make it feasible to distinguish CuO from ZnO on the multilayered film, furthermore the content of CuO in the multilayered film is very low. A close up of the films at higher magnification shows well distributed crystalline grains, about 5 nm large, each grain exhibiting a specific crystalline plane orientation (Figures 3 a and b). Again no distinctions are evident between the two films. The fringes spacing range varies largely from 0.18 to 0.29 nm (d_1 to d_6) [4], covering both ZnO and CuO interplanar spacing (see Table 1). It is therefore difficult to distinguish CuO from polycrystalline ZnO in the multilayered film. In order to be able to distinguish CuO on a ZnO thin film, a first idea was to flatten the ZnO film by hydroxylation under steaming before CuO coating by ALD. The 14 nm ZnO thin film was therefore annealed up to 250 °C under steam at 1.7 mbar for 20 minutes. The *in situ* heating in H_2O at 250 °C did not affect the morphology and size of the ZnO grains, therefore the temperature and pressure were increased up to 270 °C and 2.3 mbar. However the morphology and size of the ZnO grains remained unchanged, being about 5 nm large. The pressure and temperature were too low to affect the ZnO thin film morphology.

A second approach towards identifying copper in the CuO/ZnO film was to reduce copper oxide to metallic Cu, and benefit from the different interplanar spacings of metallic Cu. A lattice spacing of 0.18 nm corresponds to the Cu(220) lattice planes and the spacing associated with the Cu(111) planes is about 0.21 nm[5]. Cu clusters would therefore be seen if they aggregate to particles. The CuO/ZnO film was thus annealed at 250 °C under hydrogen. *In situ* TEM imaging of the film was recorded under H_2 at 250 °C at low magnification and high magnification (Figure 4). The picture taken at low magnification shows the morphology and crystallinity of the film remaining unchanged after reduction of CuO (Figure 4 a). The grains as seen at high magnification kept the same size (about 5 nm of diameter) and the fringes spacings (marked in yellow) covered the ZnO fringes spacing range from 0.18 up to 0.29 nm. Copper remained consequently undistinguished from ZnO and it is concluded that the copper content is too low to be noticeable with Cu-atoms likely

being finely dispersed over the surface. In order to locate both CuO and ZnO, one should investigate the film with more advanced TEM techniques such as dark field imaging and energy filtered imaging. As the post ALD deposition treatments of the films were ineffective to allow copper imaging on a zinc oxide surface, a last approach was to change the parameters of the films deposition in order to grow amorphous and smooth zinc oxide films, thereafter coated with copper oxide by ALD.
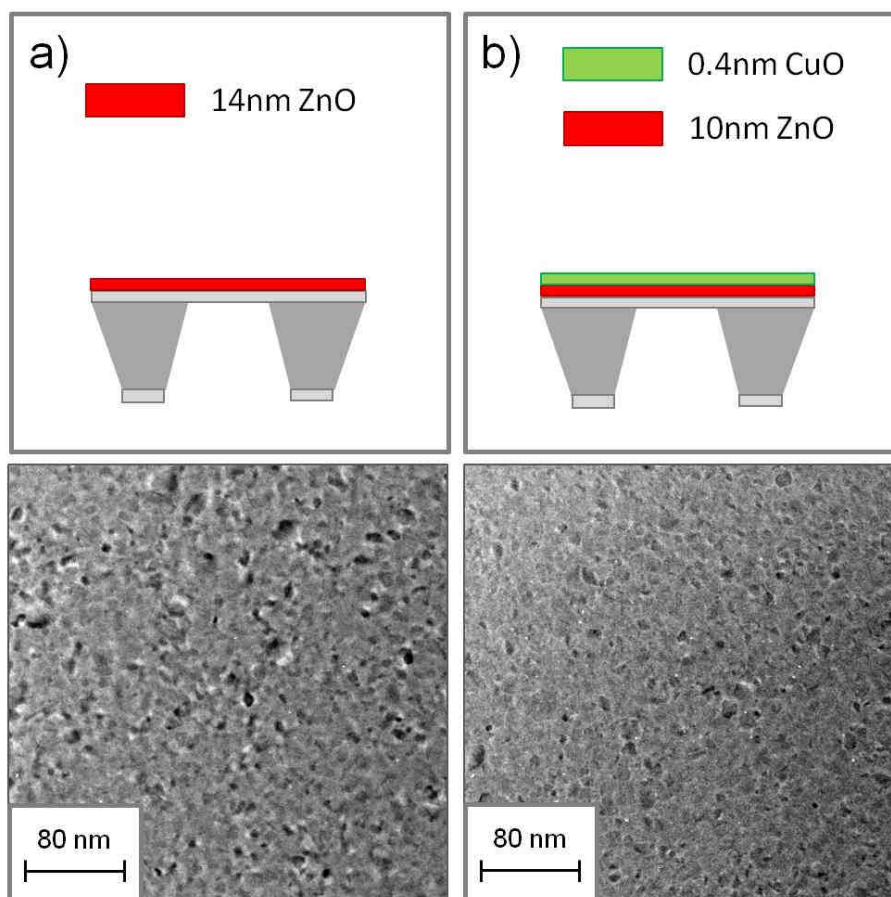

Figure 2: Top view *ex situ* TEM imaging of a) 14 nm thick ZnO film and b) 0.4 nm thick CuO film on top of 10 nm thick ZnO film deposited by ALD at 175°C. The pictures were taken at low magnification to highlight similarities and high roughness of the films.
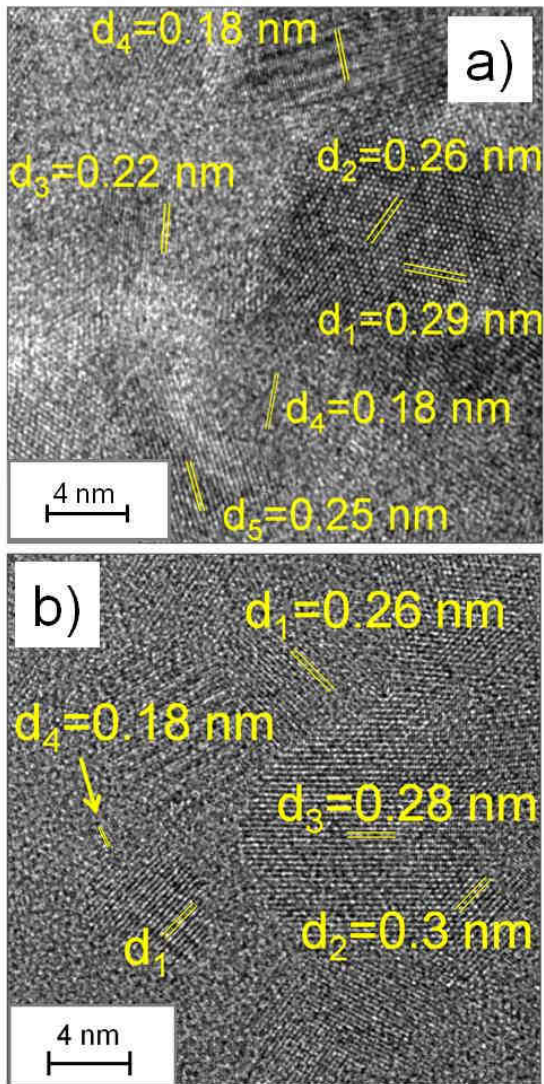
Figure 3: *Ex situ* TEM imaging of a) 14 nm thick ZnO film and b) 0.4 nm thick CuO film on top of 10 nm thick ZnO film, at high magnification. The wide ranges of fringes spacing for the two materials are indicated by the numerous distances in yellow and associated interplanar distances.
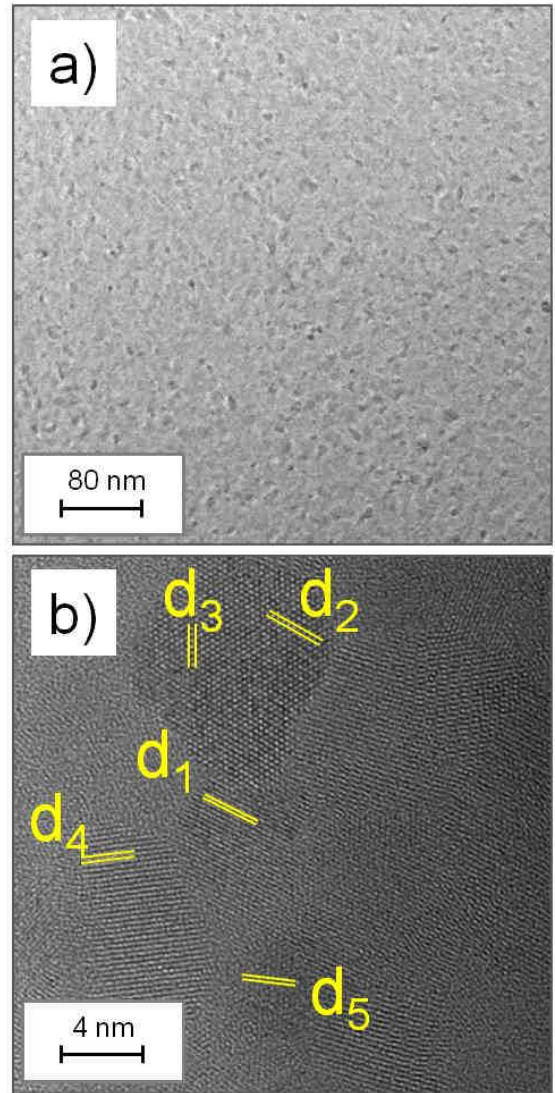

Figure 4: *In situ* TEM imaging of a 0.4 nm thick CuO film on top of a 10 nm thick ZnO film annealed under H_2 at 250 °C a) at low magnification and b) at high magnification where the fringes spacings are marked in yellow.

	(HKL)		
d (nm)	ZnO	CuO	Cu
0.16	(110)		
0.18			(002)
0.19	(012)	$(\bar{1}12)$	
0.21			(111)
0.22	(001)		
0.23		(111)	
0.24	(101)		
0.25	(011)	(002)	
0.27	(100)	(110)	

Table 1: Interplanar spacings for ZnO, CuO and Cu (0.16 nm < d < 0.27 nm)[4-9].

II. TEM imaging of Al_2O_3, ZnO and CuO thin films deposited at 125 and 150 °C by ALD

Since the crystallinity of ALD grown films of ZnO increases with temperature of deposition, the first step was to deposit ZnO at lower temperature and investigate the morphology of the film. A 13 nm thick ZnO film was deposited at 125 °C by ALD on a Si_3N_4 window. The *ex situ* TEM images of the films obtained at different magnifications are represented Figure 5. The pictures taken at low magnification reveal a very uneven film with darker agglomerations of grains and some large grains, about 10 nm in size, all over the surface. At higher magnification, some fringes in the bright contrast feature are seen, characteristic of crystalline particles[9]. Although the morphology of the ZnO film was not more smooth or uniform after deposition at lower temperature, the overall crystallinity was less. In order to improve the morphology and achieve amorphous ZnO films, a thin layer of alumina was added between the Si_3N_4 substrate and the ZnO film. Al_2O_3 films were deposited by ALD at 225 °C on the silicon chips. A 5.4 nm thick Al_2O_3 film was investigated by ex situ TEM imaging at low and high magnifications (Figure 6). The lack of lattice fringes at high magnifications and lack of domains at different contrast at low magnification prove a very uniform, smooth and amorphous coating of the Si_3N_4 window. The picture at lower magnification represents the bottom left corner of the window, illustrating the very homogeneous nature of the film on the window. A 7 nm thick ZnO film was deposited by ALD at 125 °C on top of the Al_2O_3 film. The ZnO/Al_2O_3 multilayered film *ex situ* TEM images are represented Figure 7. The film appears very homogeneous and uniform, the zinc oxide is forming grains on top of alumina but the overall roughness of the ZnO film surface is more smooth than for ZnO film deposited directly on Si_3N_4. At high magnification a start of

crystallization is seen but no well defined crystal planes are noticeable. The overall ZnO film morphology is now considered more suitable to support copper oxide nanoparticles. Hence, a 7 nm CuO thin film was deposited by ALD on top of these ZnO/Al₂O₃ films. CuO was deposited at low temperature (150 °C) in order to avoid crystallization of the ZnO film. The CuO/ZnO/Al₂O₃ multilayered film was imaged *ex situ* by TEM and pictures obtained at low and high magnification are presented in Figure 8. The overall morphology of the multilayered film is similar to the ZnO/Al₂O₃ multilayered film, but darker crystalline grains are seen at high magnification and fringes located on the grains have distances of 0.27 nm. This particular interplanar spacing is characteristic of CuO(110) [9] but also corresponds to the ZnO (002) interspace [10] (See Table 1). As no fringes are seen on the ZnO/Al₂O₃ multilayered film, it is more likely to consider the fringes in CuO/ZnO/Al₂O₃ multilayered film to reflect crystalline CuO grains. Further investigation of the ZnO/Al₂O₃ and CuO/ZnO/Al₂O₃ multilayered films are requested in order to confirm the only copper oxide to be crystalline, for instance by acquiring diffraction patterns of the two samples.
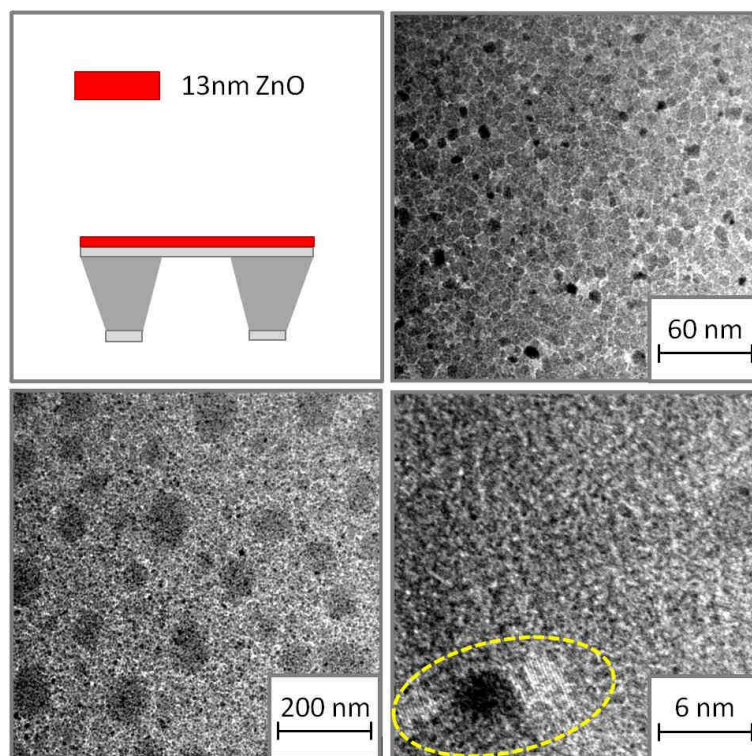

Figure 5: Top view *ex situ* TEM imaging of a 13 nm thick ZnO film deposited by ALD at 125 °C. The pictures were taken at low magnification in order to image the inhomogeneity of the films. For the picture at high magnification, fringes spacing is marked in yellow.
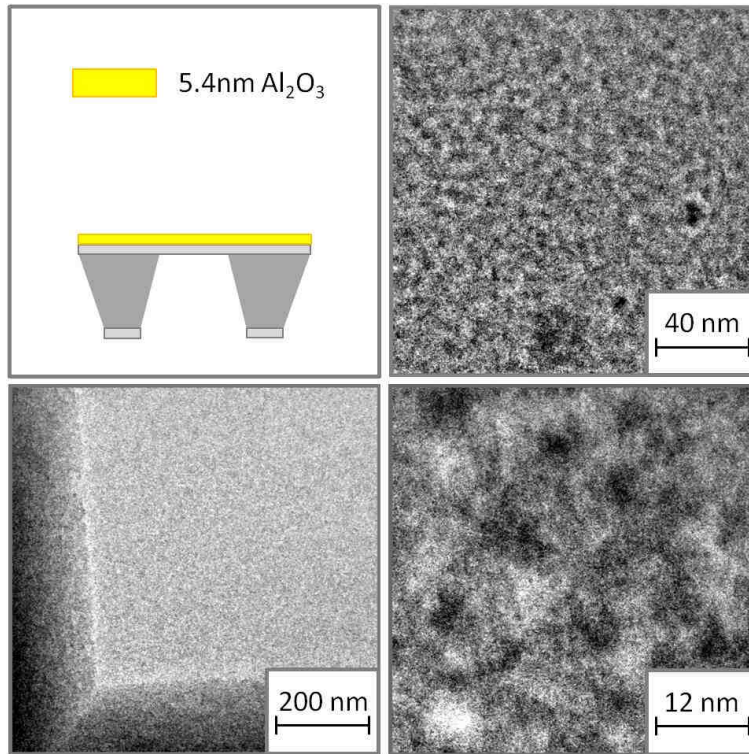
Figure 6: Top view TEM imaging of a 5.4 nm thick Al_2O_3 film deposited by ALD at 225 °C. The pictures were taken at low and high magnification in order to show the very even homogeneity and smoothness of the films.
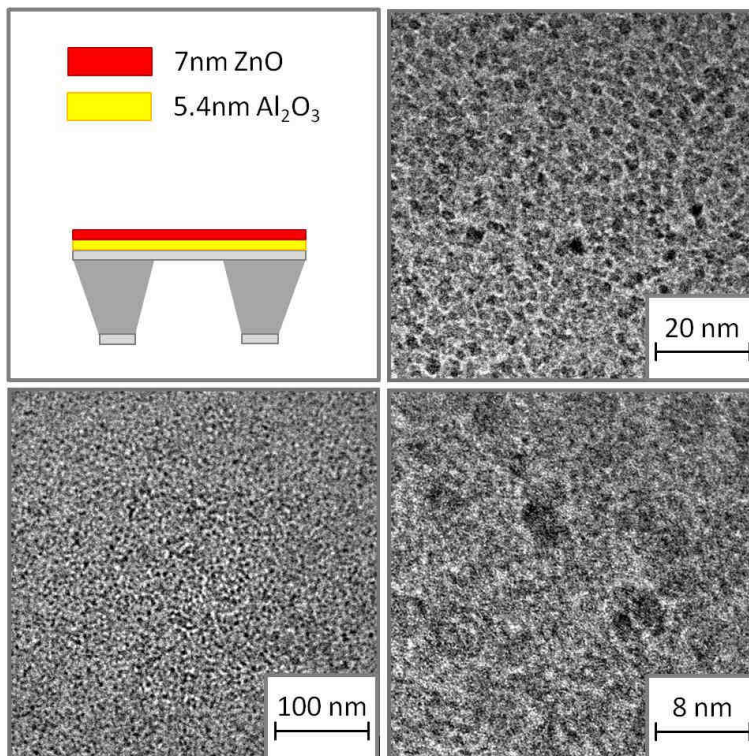

Figure 7: Top view TEM imaging at low and high magnification of a multilayered film made of a 7 nm thick ZnO film on top of a 5.4 nm thick Al_2O_3 film deposited by ALD.
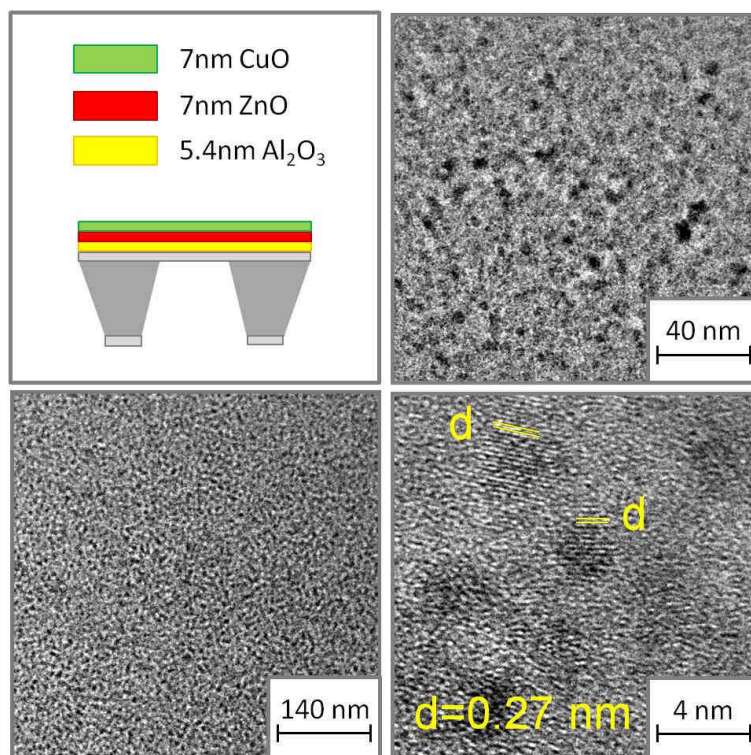
Figure 8: Top view TEM imaging at low and high magnification of the CuO/ZnO/Al$_2$O$_3$ multilayered ALD film. The fringes spacing is marked in yellow.

In situ TEM imaging of the CuO reduction to metallic Cu under hydrogen (at P=1.3 mbar) at 250 °C were performed on the CuO/ZnO/Al$_2$O$_3$ multilayered film. The pictures taken during each steps are shown in Figure 9: when H$_2$ was introduced at room temperature (a), during ramping of temperature (b), at stabilized temperature of 250 °C (c) and back at room temperature (d). The morphology of the multilayered film did not change on introduction of hydrogen in the chamber, the grains remained about 5 nm in size. However, during temperature ramping the grains evolved to better defined shapes, crystallized and the grain size increased up to 15 nm until the temperature reached 250 °C. Back at room temperature, the surface was again quite smooth, but the grains remained crystalline about 15 nm large. During the ramp of temperature, the particles growth could be either induced by the heating itself or due to a long exposure to the beam during recording of the images. However, the TEM images of the Cu/ZnO/Al$_2$O$_3$ multilayered film acquired when the temperature was stabilized at 250 °C were recorded at different areas all over the film; selected images are presented Figure 10. The pictures taken at different magnification are shown in the left column and the images of random particles seen at high magnification are presented in the right column. Dark particles about 10 to 15 nm large have appeared on the surface of the multilayered film, some of them are particularly edgy. These particles are most likely of the reduced Cu phase. Fringes are seen all over the film, overlapping the light

surface and the particles. Most of the fringes spacing are about 0.24 and 0.22 nm (d_1 and d_3) and are interpreted as crystalline plans from ZnO as the oxide crystallizes at 250 °C. Larger interplanar spacings are seen in the particles (d_2 = 0.6 nm) as well as Moiré patterns as known as an effect of overlapping of diverse fringes, which could indicate the superposition of the fringes from the ZnO film above and from the Cu crystalline particle on the top. A reason why the particles disappears after cooling to room temperature could be reoxidation in the microscope (the water background level about 10^{-4} mbar is sufficient for reoxidation). But further investigation of the sample are needed to confirm it. If the disappearance is due to reoxidation, it would corroborate with that the discussed particles are indeed Cu metal.
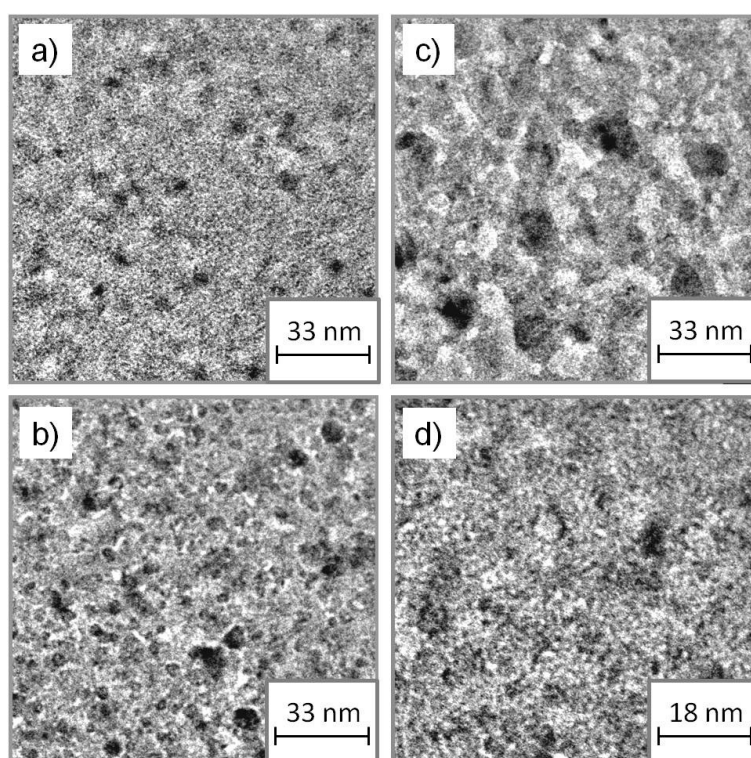

Figure 9: *In situ* TEM imaging of the CuO/ZnO/Al$_2$O$_3$ multilayered film: a) H$_2$ introduced at room temperature, b) under H$_2$ during the ramp of temperature, c) under H$_2$ stabilized at 250 °C, d) under H$_2$ cooled to room temperature and stabilized.
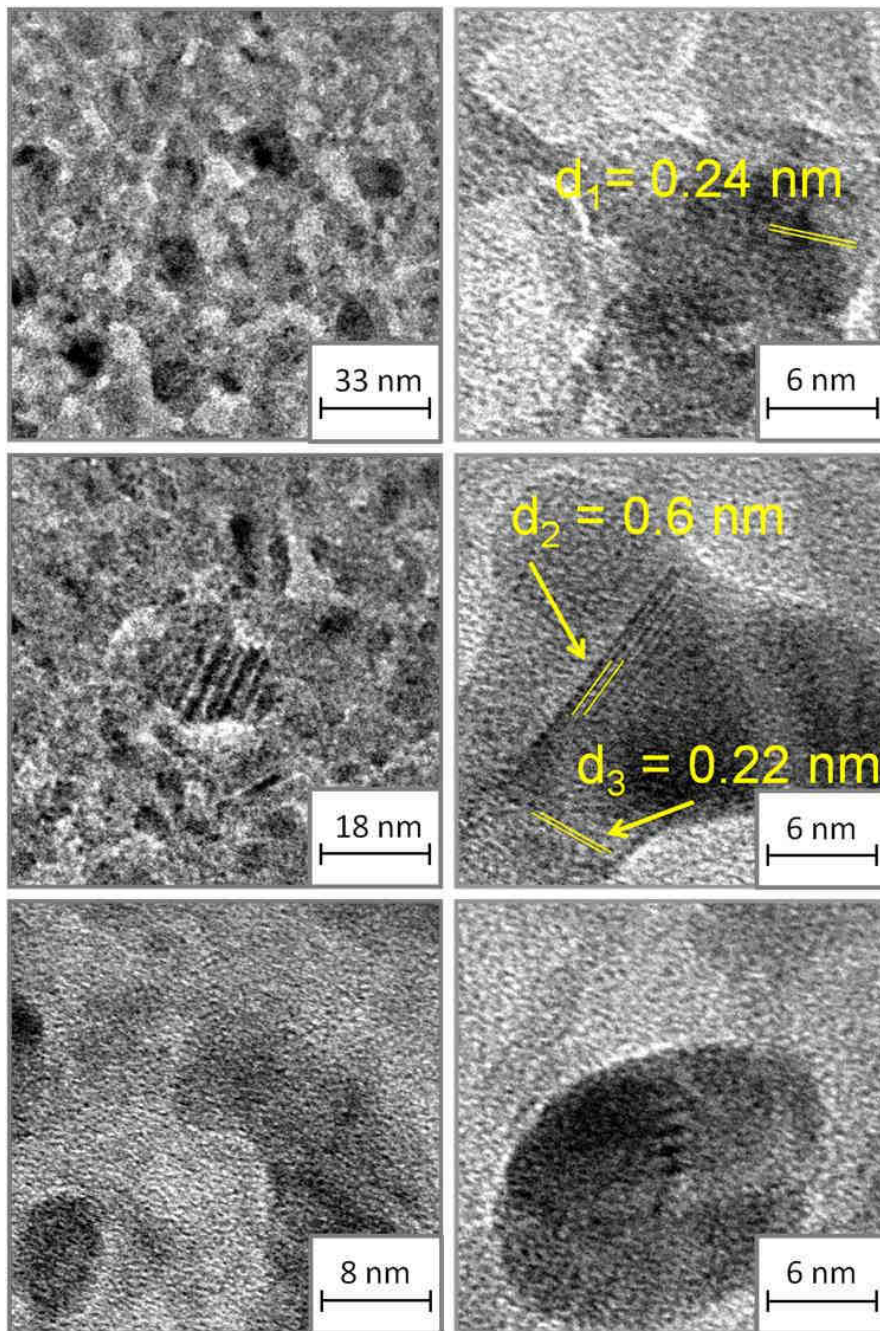
Figure 10: TEM imaging of the Cu/ZnO/Al$_2$O$_3$ multilayered film under H$_2$ stabilized at 250 °C, at different magnitudes (left column) and of different particles seen at high magnitude (right column).

CONCLUSION

TEM imaging characterization of copper and copper oxide particles on top of a zinc oxide film has been achieved by first depositing an underlayer of Al_2O_3 on a Si_3N_4 window, thereafter coated with zinc oxide and copper oxide thin films by ALD at low temperatures. *In situ* TEM imaging of the multilayered film at 250 °C under H_2 shows crystallization of the ZnO grains and formation of 10 nm large Cu particles.

REFERENCES

1.   Vesborg, P.C.K., et al., *Transient behavior of Cu/ZnO-based methanol synthesis catalysts.* Journal of Catalysis, 2009. **262**(1): p. 65-72.
2.   Ritala, M. and M. Leskelä, *Atomic layer deposition*, in *Handbook of Thin Films*, N. Hari Singh, M.Sc, and Ph.D, Editors. 2002, Academic Press: Burlington. p. 103-159.
3.   Mari Alnes, O.N., Helmer Fjellvåg, *Unpublished results.*
4.   Rataboul, F., et al., *Synthesis and characterization of monodisperse zinc and zinc oxide nanoparticles from the organometallic precursor [Zn(C6H11)2].* Journal of Organometallic Chemistry, 2002. **643-644**: p. 307-312.
5.   Long, N.J. and A.K. Petford-Long, *In-situ electron-beam-induced reduction of CuO: A study of phase transformations in cupric oxide.* Ultramicroscopy, 1986. **20**(1-2): p. 151-159.
6.   Prabakar, K., et al., *TiO$_2$ thin film encapsulated ZnO nanorod and nanoflower dye sensitized solar cells.* Materials Chemistry and Physics, 2011. **125**(1-2): p. 12-14.
7.   Limaye, M.V., et al., *Room temperature ferromagnetism in undoped and Fe doped ZnO nanorods: Microwave-assisted synthesis.* Journal of Solid State Chemistry, 2011. **184**(2): p. 391-400.
8.   Ju, M., Q. Li, and E. Wang, *Facile template-free fabrication of olive-like ZnO nanoparticles and their photoluminescence properties.* Materials Letters, 2011. **65**(3): p. 507-509.
9.   Lv, Y.Z., et al., *Temperature-dependent photoluminescence of ZnO nanorods prepared by a simple solution route.* Journal of Luminescence. **122-123**: p. 816-818.
10.   Yan, S., et al., *Solution-based synthesis of ZnO nanoparticle/CdS nanowire heterostructure.* Journal of Alloys and Compounds, 2011. **509**(24): p. L239-L243.